UNIVERSITÀ
DI PARMA

DOTTORATO DI RICERCA IN
SCIENZE DEL FARMACO

CICLO XXXVI

Colonoids and Cytokines: an *in vitro* model of drug absorption in the inflamed gut

Coordinatore:
Chiar.mo Prof. Marco Mor

Tutore:
Chiar.ma Prof.ssa Simona Bertoni

Dottoranda: Inês Araújo Parente

Anni Accademici 2020/2021 – 2023/2024

A vida é a hesitação entre uma exclamação e uma interrogação.
Na dúvida, há um ponto final.

Life is the hesitation between an exclamation and an interrogation.
In doubt, there is a final point.

Fernando Pessoa.

ABSTRACT

Introduction and Aim

Despite advances in the diagnosis and treatment of inflammatory bowel diseases (IBD), the incidence and prevalence continue to grow. Given the lack of human preclinical studies, reliable models that mimic the inflamed intestinal epithelium are increasingly explored. Patient-derived colonoids are a powerful tool that recapitulate many physiological features of the human colon *in vitro*. The aim of the present work was to establish an IBD *in vitro* model based on human colonoid-derived monolayers.

Methods

Colonic crypts, isolated from biopsies of healthy volunteers, were embedded in 70% Matrigel® and grown for 5-7 days. IntestiCult™ Organoid Growth Medium (OGM) was used to generate cystic-like colonoids, further expanded in suspension cultures. After dissociation, cells were seeded at $7.5x10^5$ cells·cm^{-2} onto 24-well inserts coated with Matrigel® (1:50). The integrity of the epithelial barriers was monitored through transepithelial electrical resistance (TEER) measurements. When confluence was reached (TEER $\geq$ 100 Ω·cm^2), IntestiCult™ OGM was switched to Organoid Differentiation Medium. Differentiated colonoid-derived monolayers (CDMs) were exposed for 24 hours to 25 ng·mL^{-1} TNF-α and 25 ng·mL^{-1} IFN-γ. Changes in cell morphology and viability, IL-8, CCL20, and NF-κB p65 levels, and FITC-D4 apparent permeability (P_{app}) were evaluated. The P_{app} values of conventional compounds were determined.

Results

Over 5-15 days, CDMs showed increasing TEER values, confirming the gradual development of epithelial barriers and the strengthening of tight junctions. Immunocytochemical (ICC) staining for villin and MUC2 showed that the cells were polarised and differentiated. Exposure to TNF-α and IFN-γ, although heterogeneously, impaired significantly the barrier integrity of CDMs and increased the secretion of IL-8 and CCL20. When the barrier damage was more severe, FITC-D4 P_{app} and NF-κB p65 levels were also increased, while cell viability was reduced. ICC images showed a large number of apoptotic cells near the basal side, and a decrease in the expression of villin and MUC2, suggesting that cell polarity and differentiation were impaired. While the steady-state flux and the P_{app} of atenolol increased significantly under inflammatory conditions, the transport of propranolol and budesonide was not affected.

Conclusions

Exposure of CDMs to an inflammatory milieu altered cell morphology, compromised the epithelial barrier integrity, and increased chemotactic cytokine secretion, although to different extents in different patients. Inflammatory conditions significantly increased the paracellular transport of low permeable compounds, highlighting their damaging effect on intercellular proteins.

Keywords: Intestinal epithelium; *in vitro* models; organoids; inflammatory bowel diseases; inflammation; drug permeability.

TABLE OF CONTENTS

ABSTRACT ..... **I**

CHAPTER I. INTRODUCTION **1**

I.1. *What?* The human intestinal epithelium. 1

I.1.1. Structural and functional subsets 1

I.1.2. Intestinal epithelial cells 2

I.1.2.1. Intestinal stem cells and the stem cell niche 3

I.1.2.2. Intestinal cell differentiation 6

I.1.3. Intestinal stroma 7

I.2. *Why?* Inflammatory bowel diseases 8

I.2.1. Mucosal immunity in the healthy state 9

I.2.2. Mucosal immunity in IBD 10

I.2.3. Therapeutic approaches 12

I.3. *How?* Preclinical *in vitro* models of intestinal inflammation 14

I.3.1. Immortalised cell lines 15

I.3.2. Primary cells 15

OBJECTIVES AND SCOPE OF THE THESIS **19**

CHAPTER II. MATERIALS AND METHODS **20**

II.1. Materials 20

II.2. Methods 21

II.2.1. Establishment of human colonoid cultures 21

II.2.1.1. Human tissue collection 21

II.2.1.2. Isolation of human colonic crypts from fresh biopsies 21

II.2.1.3. Dome culture 22

II.2.1.4. Suspension culture 23

II.3. Establishment of colonoid-derived monolayers (CDMs) 24

II.3.1. CDMs exposed to TNF-α and IFN-γ 24

II.3.2. CDMs exposed to IFN-γ 24

II.4. Immunocytochemistry (ICC) 24

II.4.1. Cystic-like colonoids (3D colonoids) 24

II.4.2. Colonoid-derived monolayers 25

II.5. Evaluation of the epithelial barrier integrity 26

II.5.1. Transepithelial electrical resistance (TEER) 26

II.5.1.1. CDMs cultured in 24-well inserts 26

II.5.1.2. CDMs cultured in 96-well inserts 26

II.5.2. FITC-D4 apparent permeability 26

II.6. Evaluation of cytotoxic effects and cell viability 27

II.6.1. Lactate dehydrogenase (LDH) assay 27

II.6.2. MTT assay 27

II.7. Quantification of NF-κB p65 levels 28

II.8. Quantification of cytokine and chemokine secretion 28

II.9. Drug permeability studies 28
II.9.1. Drug transport across CDMs exposed to TNF-α and IFN-γ 28
II.9.1.1. HPLC-MS/MS conditions for compound quantification 29
II.9.2. Drug transport across CDMs exposed to IFN-γ 29
II.10. Statistical analysis 30

CHAPTER III. RESULTS AND DISCUSSION 31
III.1. Establishment of human colonoid cultures 31
III.1.1. Optimization of culture conditions 31
III.1.2. Human colonoid culture 33
III.2. Establishment of human colonoid-derived monolayers 36
III.3. Functional and morphological characterization of colonoid-derived monolayers exposed to TNF-α and IFN-γ 38
III.3.1. Cell differentiation and morphology 38
III.3.2. Barrier integrity 40
III.3.3. Cytotoxicity and cell metabolic activity 41
III.3.4. NF-κB p65 activation 42
III.3.5. Cytokine and chemokine secretion 43
III.3.6. Drug permeability studies 44
III.4. Transepithelial transport across colonoid-derived monolayers exposed to IFN-γ 45

CHAPTER IV. CONCLUSIONS AND FUTURE PERSPECTIVES 48

REFERENCES 50

SUPPLEMENTARY DATA 57

TABLE OF FIGURES

Figure 1. Schematic representation of the **small intestinal (A) and colonic epithelium (B)**. Based on Allaire *et al.*, 2018[1]. Created with BioRender.com. 2

Figure 2. Structure of the intestinal epithelium. (A) In the small intestine, one villus is surrounded by multiple crypts. (B, C) A continuous stream of cells migrates upwards the crypt towards the tip of the villi, in the small intestine, or the top of the crypt, in the colon, before undergoing apoptosis and being replaced by advancing cells. Crypt base columnar (CBC) cells are located at the bottom of the crypts, at the stem cell zone, in +1 to +3 positions wedged between Paneth cells (in the small intestine). Intestinal crypts are divided into different areas: the mature cell area, the transit-amplifying zone, and the stem cell zone at the very bottom. (D) Above the stem cell zone, lineage-committed progenitor cells sit at the transit-amplifying zone and fuel the intestinal cell turnover. From Gehart & Clevers, 2019[9]. 3

Figure 3. Intestinal cell population: epithelial and stromal cells. Based on Beumer & Clevers, 2021[8]. Created with BioRender.com. 4

Figure 4. Signalling pathways governing the stem cell niche. (A) Gradient of Wnt, BMP and EGF along the crypt axis. **(B)** Representation of the stem cell niche. Lgr5+ CBC cells are in direct contact with Paneth cells. **(C)** Signalling pathways in the stem cell niche. Wnt, Notch and EGF are essential signals for intestinal epithelial stemness, whereas BMP negatively regulates stemness. Sufficient Wnt activation always requires R-spondin signals to be present. From Sato & Clevers, 2013[13]. 5

Figure 5. Cell lineages in the intestinal epithelium. As crypt base columnar (CBC) cells ascend the crypt axis and exit the stem cell niche, Notch signalling determines their differentiation into either absorptive (Notch on) or secretory (Notch off) lineages. Absorptive progenitors can differentiate into enterocytes or M cells, whereas secretory progenitors have the potential to become goblet, Paneth, enteroendocrine or tuft cells. Dashed lines indicate pathways or signals that are not yet fully defined. From Gehart & Clevers, 2019[9]. 7

Figure 6. Mucosal immune system in the healthy state. The intestinal epithelium works in tandem with the immune system to protect the integrity of the mucosal barrier. From Chang, 2020[16]..... 10

Figure 7. Mucosal immune system in inflammatory bowel diseases (IBD). The tightly controlled balance of the immune system is disrupted. From Chang, 2020[16]. 11

Figure 8. Schematic representation of the step-up and top-down drugs **therapeutic approaches** adopted in inflammatory bowel diseases (IBD). Created with BioRender.com. 12

Figure 9. Patient on a dish: workflow for the use of patient-derived organoids (PDOs) in disease modelling, precision medicine and regenerative medicine. **1)** Tissues (healthy and non-healthy) are collected and PDOs established from the isolated crypts. Simultaneously, blood and stool samples can be collected from the same patient for the isolation of peripheral blood mononuclear cells (PBMCs) and the isolation and expansion of microbiota. **2)** After some expansion, healthy and non-healthy PDOs can be obtained. **3)** PDO biobanks can also be created for later use. Tight quality control measures are in place to ensure there are no alterations in the phenotype after sample collection, PDO expansion and when stocks are retrieved from the biobank. **4)** Non-healthy PDOs can be applied as platforms for modelling patient's response to drug treatments and for precision medicine. Complex models can also be established by co-culturing non-healthy PDOs with autologous immune cells and microbiota. Healthy PDOs can be transplanted endoscopically to promote tissue repair in damaged areas. Created with BioRender.com. 17

Figure 10. **Isolation of human colonic crypts from freshly isolated biopsies.** (1) Collected biopsies in 1.5 mL tubes. (2) Crypts isolated from the tissue that lays at the bottom of a 15 mL tube. (3) Bright-field microscopy images of human colonic crypts. 22

Figure 11. Establishment of colonoid suspension cultures. First, human colonoids are generated from freshly isolated crypts, in domes. After reaching maturity, colonoids are dissociated, suspended in Matrigel® and seeded on the centre of a 6-well plate pre-filled with 3 mL of warm IntestiCult™ Organoid Growth Medium (OGM). Colonoids expanded in suspension can grow for 7-10 days. 23

Figure 12. Establishment of colonoid-derived monolayers. Colonoids were harvested and dissociated after growing for 7 to 10 days in suspension. Cells were seeded at $7.5x10^5$ or $3.57x10^5$ cells·cm^{-2} into 24-well or 96-well inserts, respectively, coated with Matrigel® (1:50). Media was switched from IntestiCult™ Organoid Growth Media (OGM) to IntestiCult™ Organoid Differentiation Media (ODM) when transepithelial electrical resistance (TEER) values reached 100-200 Ω·cm^2. Differentiated monolayers were exposed for 24h to 25 ng·mL^{-1} TNF-α and 25 ng·mL^{-1} IFN-γ, in the apical and basal sides. 25

Figure 13. Optical microscopy images of colonoids obtained from single cells (A, B) and crypt fragments (C, D) in expansion media produced in-house and IntestiCult™ Organoid Growth Medium (OGM). Colonoid yield is higher with IntestiCult™ OGM. 32

Figure 14. Establishment of human colonoids in dome cultures. A) Schematic representation of the establishment of dome cultures. **B)** Crypts isolated from human colonic biopsies #43 (HCB43) embedded in Matrigel®, at day 0. **C)** Swollen crypts, at day 2. **D)** Human colonoids with mixed morphologies, at day 5. Colonoids with crypt-like structures highlighted with white arrows and a cystic-like colonoid highlighted with a blue arrow. **E)** Colonoid with crypt-like structures in detail. 33

Figure 15. Optical microscopy images of cystic-like colonoids derived from human colonic biopsies #43 (HCB43). **A)** Colonoids at passage 2 after 7 days in culture. **B)** Colonoids at passage 4 after 7 days in culture. 34

Figure 16. Confocal images of a cystic-like human colonoid. Cells were stained for F-actin (phalloidin, green) and nucleus (DAPI, blue). Proliferative cells were marked with anti-Ki67 (red). Images show the overall 3D structure of colonoids and their basal-out polarity. Colonoids were mainly delimited by proliferative cells and their centre was depleted of cells. 34

Figure 17. Dome vs Suspension culture. Human colonoids derived from human colonic biopsies #37 (HCB37) culture in (**A**) dome and (**B**) suspension. 35

Figure 18. Optical microscopy images throughout the establishment of colonoid-derived monolayers (CDMs) from human colonic biopsies #25 (HCB25). 37

Figure 19. **Growth profile of colonoid-derived monolayers (CDMs).** Transepithelial electrical resistance (TEER) values increased over time. The days in which monolayers reached confluence (TEER $\geq$ 100 $\Omega \cdot cm^2$), and consequently medium was switched from IntestiCult™ organoid growth media (OGM) to organoid differentiation media (ODM), is highlighted by empty symbols. Values show mean $\pm$ standard deviation. HCB: human colonic biopsies. 37

Figure 20. Confocal microscopy images of colonoid-derived monolayers (CDMs) in the absence (control) (A, C) and presence of 25 ng·mL^{-1} TNF-α and 25 ng·mL^{-1} IFN-γ (cytokines) (B, D) on the apical and basolateral sides for 24h. Cells were stained for F-actin (Phalloidin, green) and the nucleus (DAPI, blue). Microvilli were marked with anti-Villin (red). Goblet cells and mucus were stained with anti-MUC2 (magenta). White arrows show examples of chromosome condensation and fragmentation. CDMs obtained from human colonic biopsies #43 (HCB43). 39

Figure 21. Transepithelial electrical resistance (TEER) values of colonoid-derived monolayers (CDMs) after 24h exposure to vehicle (CTR) or to 25 ng·mL^{-1} TNF-α and 25 ng·mL^{-1} IFN-γ (CYT). **A)** TEER values ($\Omega \cdot cm^2$) at 0h and 24h. **B)** TEER relative (%) to the timepoint 0h. Values are reported as mean ± standard deviation. The Shapiro-Wilk test was used to verify if the data followed a normal distribution. *p* values were determined using a two-way analysis of variance (ANOVA) followed by Sídák's multiple comparison post-test (**$p \leq 0.01$; ***$p \leq 0.001$). HCB: human colonic biopsies. 40

Figure 22. FITC-D4 apparent permeability of colonoid-derived monolayers (CDMs) in the absence (CTR) and presence of 25 ng·mL^{-1} TNF-α and 25 ng·mL^{-1} IFN-γ, for 24h (CYT). Results are reported as mean ± standard deviation. The Shapiro-Wilk test was used to verify if the data followed a normal distribution. *p* values were determined using a two-way analysis of variance (ANOVA) followed by Bonferroni's multiple comparison post-test (***$p \leq 0.001$). HCB: human colonic biopsies. 41

Figure 23. Lactate dehydrogenase (LDH) release (%) of colonoid-derived monolayers (CDMs) when exposed to 25 ng·mL^{-1} TNF-α and 25 ng·mL^{-1} IFN-γ, for 24h. Values obtained in the absence of cytokines were used as a baseline while 100% represents the LDH release after cell lysis. The cytotoxic threshold was set at 20%. Values are reported as mean ± standard deviation. The Shapiro-Wilk test was used to verify if the data followed a normal distribution. *p* values were determined using one-way analysis of variance (ANOVA) followed by Tukey's multiple comparison post-test (**$p \leq 0.01$). HCB: human colonic biopsies. 41

Figure 24. **Cellular metabolic activity** (%) of colonoid-derived monolayers (CDMs) exposed to vehicle (CTR) or to 25 ng·mL^{-1} TNF-α and 25 ng·mL^{-1} IFN-γ, for 24h (CYT). Values are reported as mean ± standard deviation. The Shapiro-Wilk test was used to verify if the data followed a normal distribution. *p* values were determined using two-way analysis of variance (ANOVA) followed by Sídák's multiple comparison post-test (***$p \leq 0.001$). HCB: human colonic biopsies. 42

Figure 25. NF-κB p65 levels of colonoid-derived monolayers (CDMs) in the absence (CTR) and in the presence of 25 ng·mL^{-1} TNF-α and 25 ng·mL^{-1} IFN-γ, for 24h (CYT). Values are reported as mean ± standard deviation. The Shapiro-Wilk test was used to verify if the data followed a normal distribution. *p* values were determined using two-way analysis of variance (ANOVA) followed by Sídák's multiple comparison post-test. HCB: human colonic biopsies. 42

Figure 26. Secretion of human (A) IL-8 and **(B) CCL20** by colonoid-derived monolayers (CDMs) after 24h exposure to vehicle (CTR) or to 25 ng·mL^{-1} TNF-α and 25 ng·mL^{-1} IFN-γ, for 24h (CYT). Values are reported as mean ± standard deviation. The Shapiro-Wilk test was used to verify if the data followed a normal distribution. *p* values were determined using two-way analysis of variance (ANOVA) followed by Tukey's multiple comparison post-test for the comparison between patients (**$p \leq 0.01$; ***$p \leq 0.001$), and by Sídák's multiple comparison post-test for the comparison between CTR and CYT ($^{\#}p \leq 0.05$; $^{\#\#\#}p \leq 0.001$). HCB: human colonic biopsies. 43

Figure 27. Transepithelial transport of (A) atenolol, (B) propranolol, (C) budesonide and (D) celecoxib across colonoid-derived monolayers (CDMs) exposed to vehicle (CTR) or to 25 ng·mL^{-1} TNF-α and 25 ng·mL^{-1} IFN-γ for 24h (CYT). Apparent permeability (Papp) was determined from the apical to the basolateral direction (A→B). Results are reported as mean ± standard deviation. The Shapiro-Wilk test was used to verify if the data followed a normal distribution. *p* values were determined by means of two-way analysis of variance (ANOVA) followed by Sídák's multiple comparison post-test ((*$p \leq 0.05$; **,##$p \leq 0.01$; ***,###$p \leq 0.001$). HCB: human colonic biopsies. 44

Figure 28. Transepithelial electrical resistance (TEER) **of colonoid-derived monolayers** (CDMs) **throughout growth and 24h after exposure to 25 ng·mL^{-1} IFN-γ**. Monolayers were derived from commercial organoid lines of the ascending colon (A) and sigmoid colon (B). C) TEER values relative (%) to the timepoint 0h. Results are reported as mean ± standard deviation. The Shapiro-Wilk test was used to verify if the data followed a normal distribution. *p* values were determined using a two-tailed Student's t-test (***$p \leq 0.001$). 46

Figure 29. Transepithelial transport of (B) **propranolol,** (C) **atenolol,** (D, E) **digoxin, and** (F) **cimetidine across colonoid-derived monolayers** (CDMs) **from the ascending and sigmoid colon treated with 25 ng·mL^{-1} IFN-γ** for 24h (CYT). Vehicle-treated CDMs were used as controls (CTR). Apparent permeability (Papp) was determined from the apical to basolateral direction. (D) 5 μM elacridar was used as a P-gp inhibitor. (A) Mannitol was used as a leakage marker. Results are reported as mean ± standard deviation. The Shapiro-Wilk test was used to verify if the data followed a normal distribution. *p* values were determined using a using two-way analysis of variance (ANOVA) with Sídák's multiple comparison test (*,#$p \leq 0.05$; **$p \leq 0.01$). 47

CHAPTER I. INTRODUCTION

A Doctor of Philosophy (PhD) is the highest academic degree a student can obtain. The term 'philosophy' itself derives from the Greek for 'love of wisdom', a pursuit that seeks to understand the fundamental laws of nature. Earning this title requires one to dig into the essential questions concerning a chosen research topic.

Every research project, especially one that may culminate in a PhD degree, begins by addressing the core questions: *What are we studying? Why are we studying it? How will we study it?* These fundamental questions form the basis of all scientific endeavours and are crucial in determining the aims and methods of our research. This thesis seeks to explore these questions within the context of gastrointestinal health and disease, focusing particularly on inflammatory bowel diseases (IBD).

I.1. *What?* The human intestinal epithelium.

The focus of this research is the human intestinal epithelium, a critical barrier and interface between the body and the external environment within the gastrointestinal tract. This epithelial layer is highly specialised, composed by multiple cell types each contributing to its unique functions in nutrient absorption, immune defence, and microbial interactions.

I.1.1. Structural and functional subsets

Consisting of a single layer of cells, the intestinal epithelium plays an essential role in maintaining intestinal homeostasis. It acts both as a physical barrier and as a coordinating centre for immune response and crosstalk between microbes and immune cells. The architectural structure and cellular composition of the epithelium are closely aligned with the specific functions it must perform in each region of the gastrointestinal tract, as shown in **Fig. 1**. In the small intestine, the mucosa extends into structures known as villi that project into the lumen[1]. Along with circular folds and microvilli, these villi significantly increase the surface area of the intestine, thereby enhancing digestion and nutrient absorption, which are the primary functions of the small intestine[2]. In contrast, the colon lacks villi, resulting in a relatively flat epithelium that helps minimize potential damage caused by stool transit. Microvilli, however, are present on the surface of epithelial cells in both regions of the intestine. Supported by actin-based microfilaments, these plasma membrane protrusions form the so-called brush border. This specialized protective barrier is essential for efficient digestion and nutrient transport[3].

The intestinal tract hosts a complex and diverse population of microorganisms, collectively known as the microbiota[4,5]. These microorganisms maintain a mutualistic relationship with their host, aiding in the degradation of complex carbohydrates, in drug metabolism, and in the maturation of the immune system. Although the gut microbiota is generally beneficial, the vast number of microbial cells poses a constant threat to the host. Consequently, the gut mucosa is protected by a mucus layer that prevents the translocation of microbiota into underlying tissues. In the small intestine, a single mucus layer covers the villi. In contrast, the colon features two distinct mucus layers: an inner layer that is virtually free of microbial cells, and a more permeable outer layer[6].

In both the small intestine and the colon, the intestinal epithelium is organized not as a flat surface, but in invaginations known as 'crypts of Lieberkühn'. These crypts, facing away from the intestinal lumen, connect to the mucosa through small openings between densely packed cells. The microenvironment within the crypts is further shielded from the digestive process by the mucus layer, making them a highly protected site. This is crucial as crypts house the regenerative compartment of the intestine. Located at the base of the crypts, this portion comprises a stem cell zone at the very bottom and a transit-amplifying area just above it (**Fig. 2**).

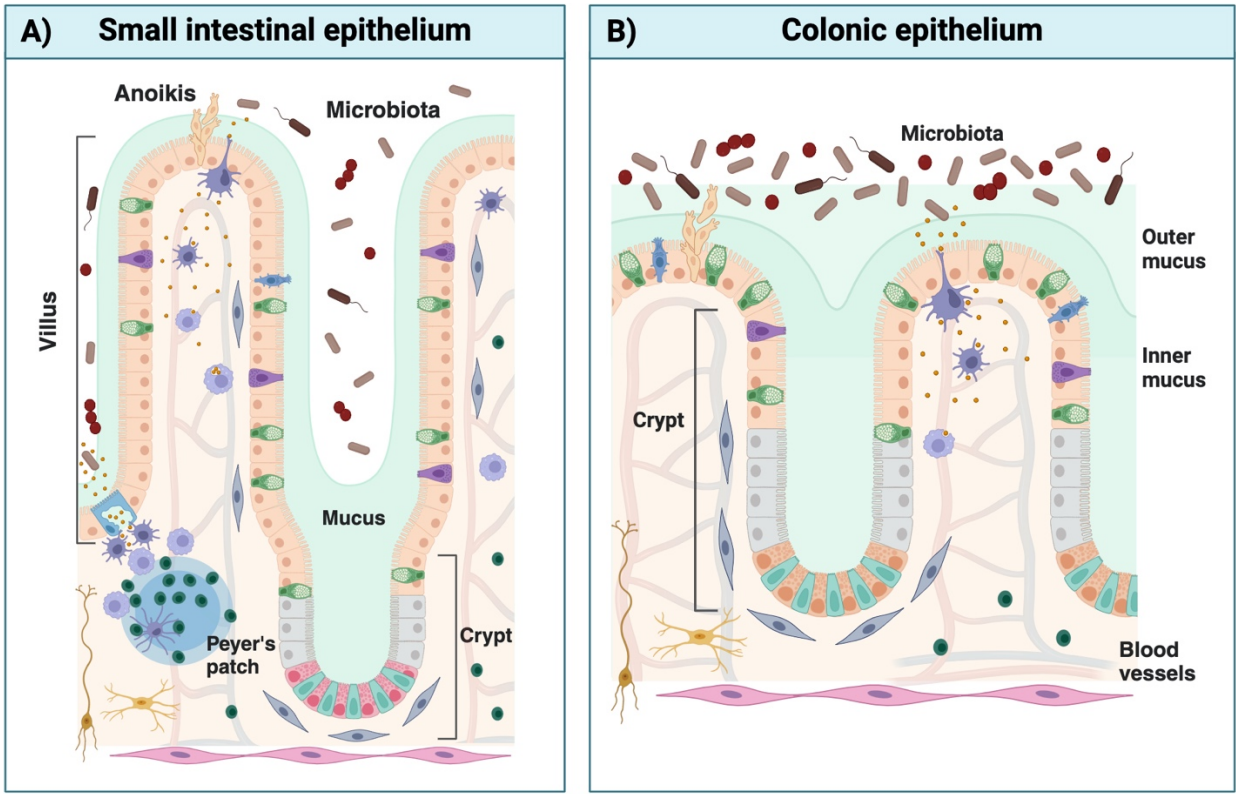

Figure 1. Schematic representation of the **small intestinal (A) and colonic epithelium (B)**. Based on Allaire *et al.*, 2018[1]. Created with BioRender.com.

Intestinal stem cells give rise to transit-amplifying cells that differentiate as they move upwards through the epithelium. Paneth cells are the only cell type that differentiate by migrating downwards to the stem cell zone. The intestinal epithelium is in a state of constant renewal, undergoing regular cycles of cell replenishment and, under homeostatic conditions, being completely replaced every 4 to 5 days[1,7]. Most mature cells live for only a few days before being shed from the top of the crypts or the tip of the villi (anoikis). Paneth cells are again the exception as they can live for 1-2 months at the crypt base before being cleared by infiltrating macrophages[8].

I.1.2. Intestinal epithelial cells

Different subtypes of epithelial and stromal cells are found within the gut mucosa, each carrying out specific functions (**Fig. 3**). The distribution of these cell types also differs between the small intestine and the colon[1]. Epithelial cell lineages can be divided into two broad categories: cells that absorb luminal contents (absorptive cells) and secretory cells. Enterocytes make up 80-90% of all differentiated cells and are responsible for nutrient and water absorption. Microfold cells (M cells) are responsible for sampling luminal contents and presenting antigens to the underlying immune cells that make up the Peyer's patches, thereby regulating immune responses. Secretory cells include mucus-secreting goblet cells, hormone-producing enteroendocrine cells, chemosensory tuft cells that mediate immune responses, and Paneth cells that produce niche factors and antimicrobial peptides (AMP) to protect the stem cell zone[8].

Most cell types that constitute the colonic epithelium are also found in the small intestine with exception of Paneth cells, which are absent in the colon. Instead, the colon contains deep secretory cells that are intercalated between stem cells. These cells presumably fulfil functions similar to those of Paneth cells by secreting epidermal growth factor (EGF) and Notch ligands, but they do not produce Wnt ligands, which exclusively derive from the colonic stroma[8].

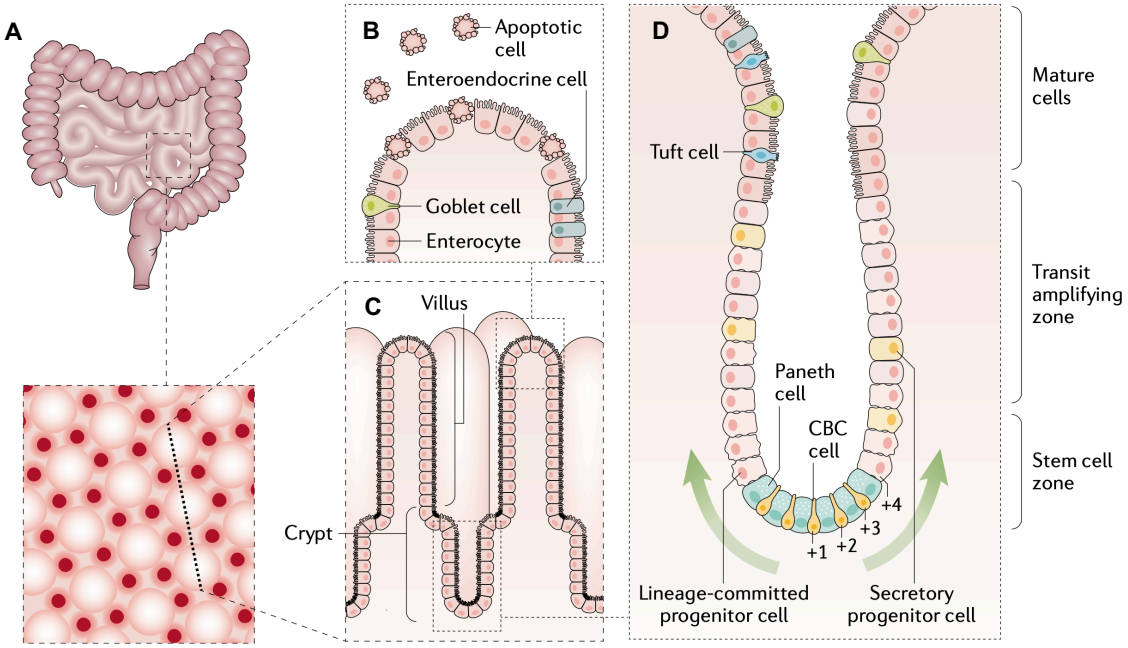

Figure 2. Structure of the intestinal epithelium. (A) In the small intestine, one villus is surrounded by multiple crypts. (B, C) A continuous stream of cells migrates upwards the crypt towards the tip of the villi, in the small intestine, or the top of the crypt, in the colon, before undergoing apoptosis and being replaced by advancing cells. Crypt base columnar (CBC) cells are located at the bottom of the crypts, at the stem cell zone, in +1 to +3 positions wedged between Paneth cells (in the small intestine). Intestinal crypts are divided into different areas: the mature cell area, the transit-amplifying zone, and the stem cell zone at the very bottom. (D) Above the stem cell zone, lineage-committed progenitor cells sit at the transit-amplifying zone and fuel the intestinal cell turnover. From Gehart & Clevers, 2019[9].

I.1.2.1. Intestinal stem cells and the stem cell niche

Intestinal stem cells, located at the base of crypts, divide continuously to fuel epithelial renewal. Two distinct populations of intestinal stem cells have been described: crypt base columnar (CBC) cells and +4 cells, also known as label-retaining cells (LRCs). CBC cells are slender cells wedged between Paneth cells (in the small intestine), while +4 cells, as their name suggests, are located approximately four cell diameters from the crypt base, directly above Paneth cells (in the small intestine)[10]. In 2007, lineage-tracing experiments demonstrated that leucine rich repeat containing G protein-coupled receptor 5 (Lgr5) is a CBC-specific marker[11]. Lgr5$^+$ cells can generate all epithelial cell types in the intestine and establish long-term *ex vivo* organoid cultures that recapitulate the structure and function of the intestine[12]. Thus, Lgr5$^+$ cells fulfil both criteria of stemness: generation of multiple cell lines and long-term self-renewal. In addition to CBC cells, +4 stem cells have been described and intensively debated as another stem cell population. Although the contribution to tissue homeostasis is still discussed, +4 stem cells are considered a reserve stem cell with high resistance to radiation that replenish the pool of CBC cells when required. However, reports on plasticity in the intestinal epithelium call the concept of dedicated reserve stem cells into question. Tracing undifferentiated, non-dividing cells at the crypt base revealed that LRCs during homeostasis are precursors of Paneth cells and enteroendocrine cells that do not contribute to homeostatic tissue renewal [9].

CBCs are highly susceptible to damage from radiation and chemotherapy. However, recent findings have uncovered alternative sources of CBCs during such insults. These include lineage-restricted progenitors such as LRCs, Delta Like Canonical Notch Ligand 1 (DLL1$^+$) secretory progenitors and progenitors destined to differentiate into enterocytes. There is also evidence that mature enteroendocrine cells (often located at the +4 position), Paneth cells, and keratin 20 (KRT20$^+$) colonocytes in the colon also have the ability to “acquire stemness”. This broad stem cell potential of crypt cells is facilitated by a permissive open chromatin state in differentiated cells[8].

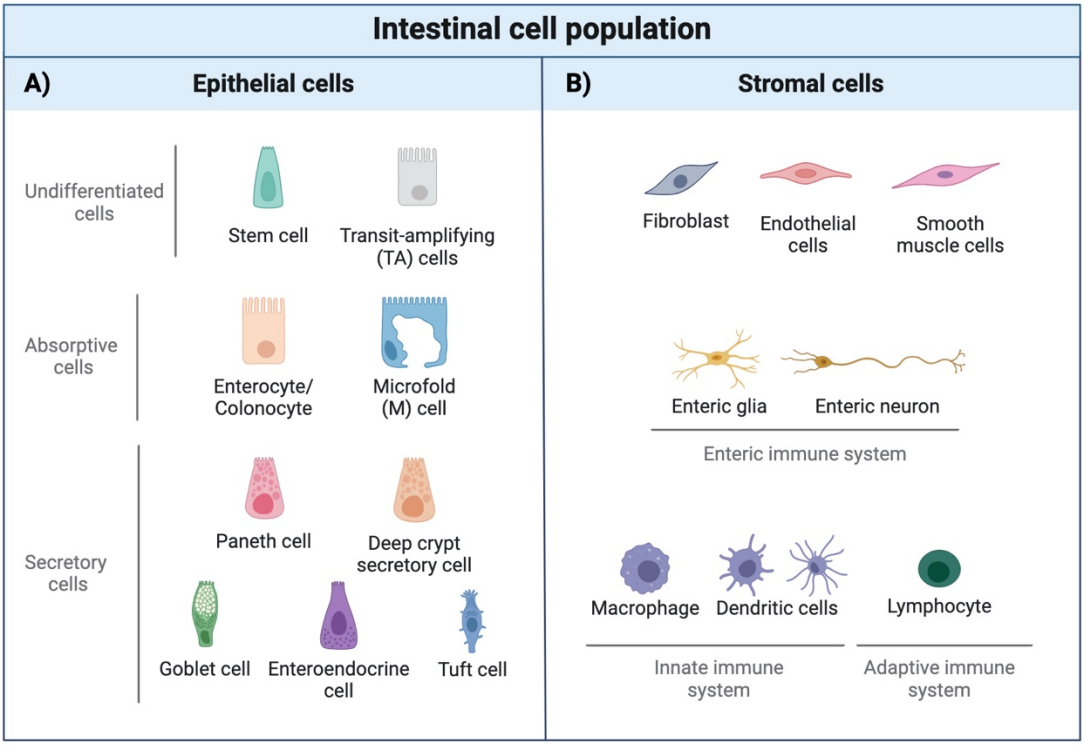

Figure 3. Intestinal cell population: epithelial and stromal cells. Based on Beumer & Clevers, 2021[8]. Created with BioRender.com.

Stem cell maintenance and the precise regulation of differentiation into different cell lineages are governed by the microenvironment of the stem cell niche (**Fig. 4A**, **B**). Competition for limited niche space ensures tight control over stem cell numbers. Both epithelial and stromal cells contribute to the maintenance of this microenvironment by producing essential signalling molecules[8,10]. Signalling pathways, including Wnt, Notch and EGF, regulate CBC cell fate. Bone morphogenetic protein (BMP) pathway negatively regulates stemness and is responsible for controlling lineage commitment (**Fig. 4C**). Gradients of secreted factors confine stem cells to the crypt base and stimulate division among transit-amplifying cells within the crypt (**Fig.4A**)[13].

The canonical Wnt pathway is crucial for the proliferation and maintenance of intestinal stem cells[10]. Interestingly, Wnt also drives terminal differentiation of Paneth cells, that are in direct contact with stem cells[13]. Wnt ligands bind to the Frizzled–LRP5–LRP6 receptor complex, which inhibits continuous destruction of β-catenin. The accumulation of β-catenin leads to its translocation to the nucleus where it binds to T cell factors and activates Wnt target gene expression that supports stemness[9]. Both the canonical and non-canonical pathway are activated by Wnt ligands secreted at the surrounding niche by both epithelial and stromal cells. The epithelial source of Wnt are Paneth cells that produce short-range Wnt3[10]. Wnt ligand range is limited by its poor solubility. As a result, the majority of the signal is transferred by direct cell-to-cell contact[9]. $Fox11^+$ telocytes as well as $Gli1^+$ and $CD34^+$ subepithelial mesenchymal cells have been identified as the main stromal source of Wnt[9,10].

Although Wnt ligands are abundant at the base of the crypts, their ability to activate the Wnt pathway relies on R-spondins. R-spondin enhances Wnt signalling, primarily by acting through the Lgr family of receptors. This interaction effectively nullifies a negative feedback loop within the Wnt pathway. Wnt pathway activity sufficient for stem cell maintenance always requires R-spondin signals and cannot be achieved with high Wnt ligand levels alone[8]. Among the four members of the R-spondin family, R-spondin2 and R-spondin3 are crucial for $Lgr5^+$ stem cell maintenance[10].

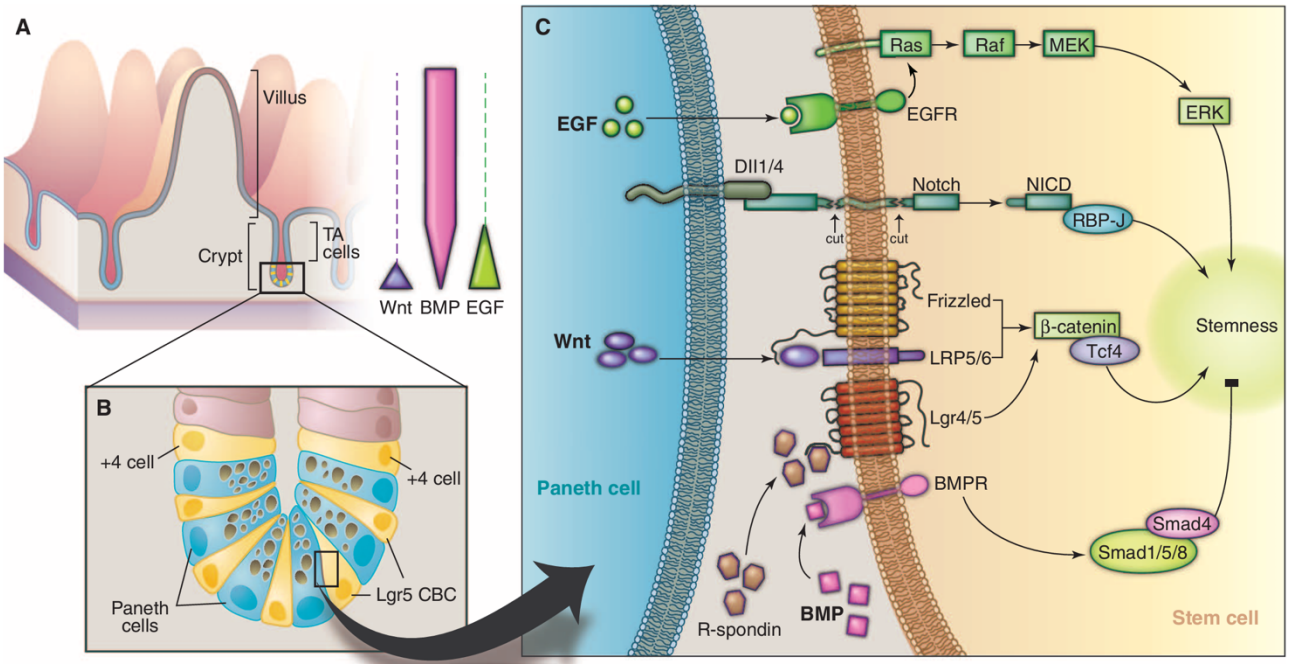

Figure 4. Signalling pathways governing the stem cell niche. (A) Gradient of Wnt, BMP and EGF along the crypt axis. **(B)** Representation of the stem cell niche. Lgr5+ CBC cells are in direct contact with Paneth cells. **(C)** Signalling pathways in the stem cell niche. Wnt, Notch and EGF are essential signals for intestinal epithelial stemness, whereas BMP negatively regulates stemness. Sufficient Wnt activation always requires R-spondin signals to be present. From Sato & Clevers, 2013[13].

Notch signalling is essential for the maintenance of the stem cell population, whereas inhibition of Notch leads to a reduction in the number and proliferation of Lgr5^{+} cells. Notch signalling requires direct physical contact between cells, where the interaction between them triggers the signalling that releases the intracellular domain of the receptor. Notch ligands are mainly presented by neighbouring Paneth cells[8].

EGF is another critical factor required for stem cell proliferation. The EGF receptor, ERBB1, a tyrosine kinase receptor, is highly expressed by CBC cells. Similar to Wnt3, ligands that activate the receptor, such as EGF and transforming growth factor α, are secreted by Paneth cells and likely also by mesenchymal cells. Because overactive EGF signalling can lead to neoplastic growth and eventually cancer, the activity of the signalling pathway is tightly regulated by the co-expression of ERBB receptors with their negative regulator, Lrig1. Although EGF signalling influences the division rate of intestinal stem cells, it is not essential for maintaining stem cell identity. This distinguishes EGF from Wnt or Notch signalling, both of which are essential for maintaining stem cell identity[9].

BMP signalling plays a crucial role in intestinal cell differentiation by creating a gradient that opposes Wnt signalling along the crypt/villus axis. The opposing gradients of BMP and Wnt are essential for maintaining intestinal homeostasis: Wnt promotes stemness at the crypt base, while BMP inhibits proliferation and promotes differentiation[10]. The primary BMPs in the gut, including BMP2 and BMP4, which are recognised by the type 1 receptor BMPR1A, are produced by mesenchymal cells. Surrounding the crypt base, stromal cells, such as myofibroblasts and smooth muscle cells, secrete BMP inhibitors, including noggin, chordins and gremlins. Binding of BMP2/BMP4 to BMPR1A promotes interaction with the type 2 receptor BMPR2, which initiates downstream signalling through phosphorylation and activation of SMAD proteins. These proteins then regulate the transcription of target genes and recruit histone deacetylases to repress stem cell signature genes, thereby confining the stem cell zone to the bottom of the crypt[8].

I.1.2.2. Intestinal cell differentiation

The fate of CBC daughter cells is determined as they leave the stem cell niche. The first fate decision is between absorptive and secretory cell linage specification (**Fig. 5**). Cell fate depends on the presence or absence of Notch signals. Active Notch signalling in a low Wnt environment promotes absorptive specification whereas lack of Notch signals and activation of transcription factor ATOH1 determines the secretory fate[9]. The cell ratio entering each differentiation path is determined by lateral inhibition which strongly favours the absorptive lineage. Lateral inhibition consists in the production of Notch ligands by progenitors of the secretory lineage which induce absorptive fate in the surrounding progenitor cells[7].

At the base of the crypts, Paneth cells play a crucial role in protecting and nurturing stem cells. Paneth cell differentiation depends on the presence of Wnt signalling and the expression of the Wnt target gene Sox9. Essentially, a cell in a high Wnt environment that lacks Notch signalling will differentiate into a Paneth cell. Interestingly, in the absence of Paneth cells, stem cells lose their source of Notch signals and can differentiate into Paneth cells themselves. This transformation allows them to provide Notch signals to neighbouring cells, thereby maintaining stem cell features within the niche[9].

However, Paneth cells are absent in the colon, where their role is thought to be fulfilled by deep secretory cells identified by REG4 expression. These cells express Notch ligands (DLL1 and DLL4) but not Wnt ligands, which are thought to be expressed by stromal cells[8].

Among the different types of secretory cells, mucus-secreting goblet cells are the most abundant. Unlike Paneth cells, the differentiation of goblet cells requires the inhibition of the Wnt pathway. Therefore, progenitor cells that lack Notch signals and do not receive Wnt signals are destined to differentiate into goblet cells[8].

Enteroendocrine cells, which release hormones into the bloodstream upon stimulation, make up less than 1% of the epithelium. These cells are categorized into five different lineages, collectively producing over 20 hormones. The specification mechanisms for this cell type are not fully understood, but it is known that neurogenin 3 (Neurog3) is a crucial driver of enteroendocrine progenitors, and its expression is repressed by the Notch target HES1[8]. *In vitro*, enteroendocrine cells are typically generated by inhibiting Notch signalling to encourage secretory differentiation, blocking Wnt signalling to prevent Paneth cell differentiation, and inhibiting MEK to avoid goblet cell fate[9].

Tuft cells are even rarer than enteroendocrine cells, comprising approximately 0.4% of all intestinal epithelial cells. Like enteroendocrine cells, tuft cells are chemosensory and trigger type II immune responses upon detecting parasites[7]. Although these cells originate from DLL+ progenitors, their classification as secretory cells is debated. Unlike all other secretory cells, tuft cells do not rely on ATOH1 or the major secretory transcription factors Neurog3 or Sox9. Interestingly, tuft cell numbers are regulated in response to helminth infections by interleukin (IL)-4 and IL-13, which not only increase tuft cell proliferation but also bias stem cell differentiation towards tuft and goblet cell lineages[9].

The default differentiation pathway of the absorptive lineage leads to enterocytes. Enterocyte differentiation primarily depends on Notch signalling. As stem cells exit their niche, they move away from a high Wnt environment, yet continue to receive Notch signals from their DLL^+ neighbouring cells, which makes them transition into absorptive transit-amplifying cells. In turn, these cells are locked out of the secretory lineage due to Notch-dependent repression of ATOH1. Subsequently, as they move along an increasing gradient of BMP, these cells undergo several divisions within the transit-amplifying zone before fully differentiating into enterocytes[9].

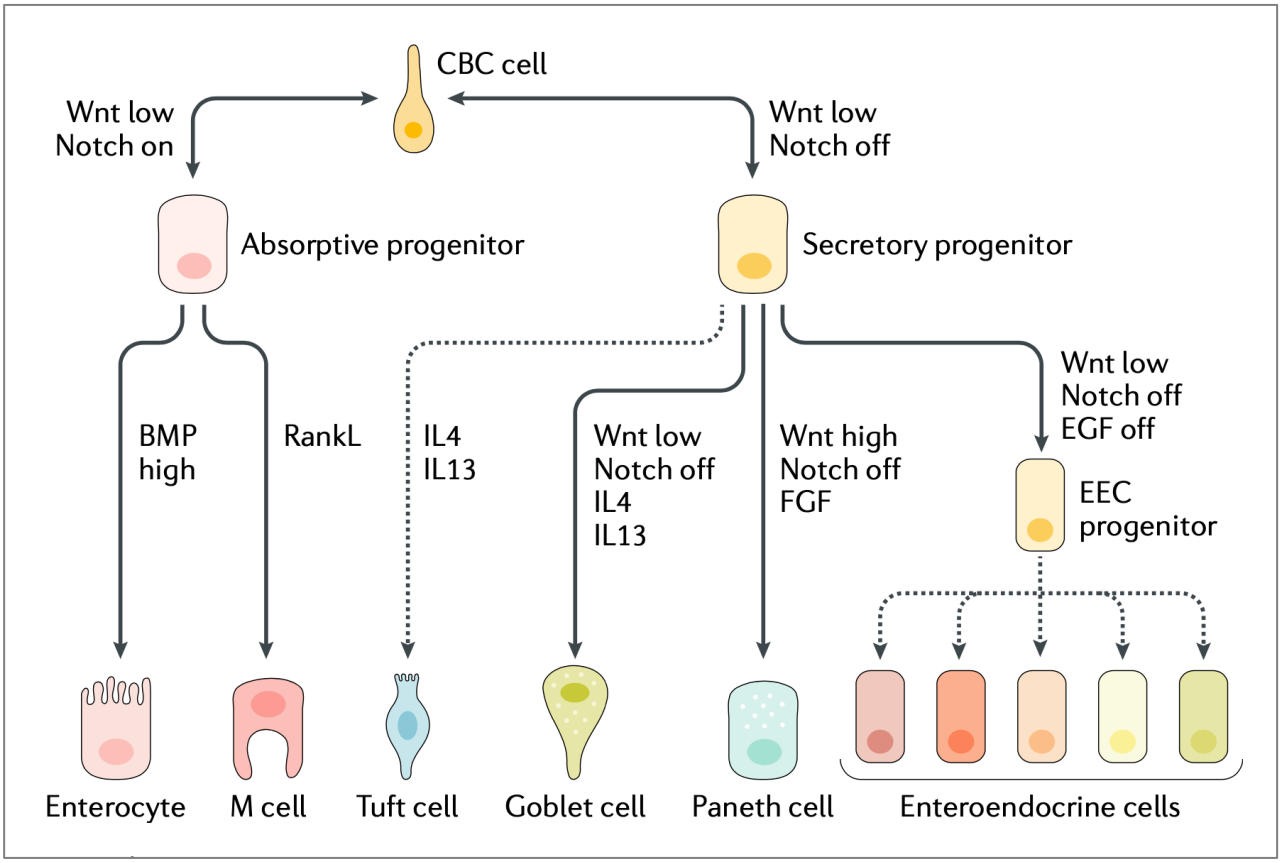

Figure 5. Cell lineages in the intestinal epithelium. As crypt base columnar (CBC) cells ascend the crypt axis and exit the stem cell niche, Notch signalling determines their differentiation into either absorptive (Notch on) or secretory (Notch off) lineages. Absorptive progenitors can differentiate into enterocytes or M cells, whereas secretory progenitors have the potential to become goblet, Paneth, enteroendocrine or tuft cells. Dashed lines indicate pathways or signals that are not yet fully defined. From Gehart & Clevers, 2019[9].

M cells are not evenly distributed across the intestinal epithelium but, instead, are concentrated above Peyer's patches, lymphoid follicles that contain primarily B and T cells[7]. Contrary to all other cell types, the fate of M cells is not immediately determined after exiting the stem cell niche. When absorptive progenitor cells or enterocytes encounter receptor activator of nuclear factor κ-B (RANK) ligand (RANKL) presented by subepithelial stromal cells that cover Peyer's patches, they differentiate to M cells[9].

I.1.3. Intestinal stroma

Beneath the intestinal epithelial layer lies a subepithelial compartment where the stroma supports epithelial function. Intestinal stromal cells include fibroblasts, myofibroblasts, pericytes, telocytes, endothelial cells, neural cells and immune cells. These stromal cell populations provide structural support and multiple signalling molecules, depending on their position across the crypt axis. Near the crypt base, stromal cells produce mainly Wnt ligands, R-spondins and BMP inhibitors. Cells located upwards in the crypt axis produce increasing amounts of BMP creating a gradient that induces the maturation of progenitor cells [7].

Additionally, stromal cells contribute to the regulation of innate immunity by producing cytokines such as IL-6 and chemokines that recruit neutrophils (e.g., IL-8), monocytes (e.g., C-C motif chemokine ligand (CCL)-2), and T cells (e.g., CCL-5). When the equilibrium among these cells and the epithelium is disrupted, stromal cells can also become involved in the pathogenesis of multiple diseases, including IBD, fibrosis, and ultimately cancer[14,15]. By occupying a privileged position between the epithelium and the immune compartment, stromal cells are key players in regulating intestinal homeostasis.

In terms of physiological function, interstitial cells of Cajal, along with myocytes, regulate motility and provide mechanical support in the colon. Meanwhile, pericytes, which encircle the capillary vasculature, are crucial for regulating vascular stretching and permeability[15].

I.2. *Why?* Inflammatory bowel diseases

The intestinal epithelium is instrumental in maintaining overall gastrointestinal health, but its homeostasis is often compromised which can lead to a number of disorders, particularly IBD. Understanding the functional and structural integrity of this epithelium is critical to unravelling the complex pathogenesis of IBD and other related diseases.

IBD are chronic relapsing disorders characterized by a progressive inflammation of the gastrointestinal tract. Ulcerative colitis (UC) and Crohn's disease (CD) are the two main forms of IBD[16]. UC is a non-transmural IBD that is confined to the colon and is typically characterised by symptoms such as bloody diarrhoea, passage of pus, mucus and abdominal cramping during bowel movements. CD, on the other hand, is a transmural IBD that can affect any part of the gastrointestinal tract, from the mouth to the anus. Patients with CD often have discontinuous segments of inflamed tissue and may develop complications such as strictures, abscesses, or fistulas[17].

Although the mortality rate associated with IBD is low, the condition significantly affects the quality of life of its patients, resulting in substantial health and economic burdens[18]. In 2020, the incidence and prevalence of IBD continued to rise worldwide, affecting 0.2% of the European population[19]. In Europe, CD affects more women than men, whereas UC is believed to be evenly distributed among males and females of all ages and across all regions of the world[20]. Traditionally, IBD has mainly affected Western European countries. In recent decades, however, the prevalence of IBD has increased worldwide in tandem with industrialisation and the adoption of western diets and lifestyles. By 2030, it is estimated that the prevalence of IBD could be as high as 1% in many western regions, owing to the advancing age of the population[21].

The aetiology of IBD is not fully understood, but it is thought to be influenced by dysregulation of the immune system and microbiota, triggered by genetic risk factors and environmental insults. Numerous studies have demonstrated that both forms of IBD are associated with reductions in the abundance, diversity, and richness of the microbiota - dysbiosis. To date, over 200 risk loci have been identified that contribute to IBD, with genetic factors playing a stronger role in CD than in UC. Genes most strongly associated with the diseases are involved in immune responses against microbes, including microbial product recognition (e.g., NOD2 or TLR4), inflammatory responses to microbes (IL23R), and autophagy (ATG16L1). However, the heritability risk remains low[16,18,22,23].

Regarding environmental risk factors, many have been studied, but none fully explain the pathogenesis of IBD. Smoking, a risk factor for Crohn's disease, may contribute to IBD development by inducing dysbiosis. Urbanization is also thought to play a role, as children in more urban environments have reduced microbial exposure, potentially leading to abnormal immune responses later in life. Additionally, dietary factors, such as low-fibre and high-fat diets, are associated with IBD[18,22].

Despite the fact that genetic and environmental risk factors have been linked to IBD, it remains difficult to pinpoint the exact causes. The prevailing hypothesis suggests a scenario in which individuals genetically susceptible to IBD are exposed to environmental triggers that lead to an aberrant immune response. This response targets the gut microbiota inappropriately, causing mucosal damage and triggering further recruitment of immune cells. To better understand the role of this exacerbated immune response in IBD, it is

important to first understand the delicate balance that regulates the intestinal epithelium under healthy conditions.

I.2.1. Mucosal immunity in the healthy state

Ensuring intestinal homeostasis depends primarily on the maintenance of the structural epithelial integrity, and therefore its rapid turnover. Serving as the first line of defence for the immune system, the epithelial barrier is critical. In an environment that is constantly exposed to food antigens and harbours the largest microbial community in the body, immune cells must discriminate between what is a threat and what is harmless to the host.

Epithelial cells work closely with immune cells to protect the intestinal barrier (**Fig. 6**). For example, the mucus layer produced by goblet cells reduces the exposure of epithelial cells to microbiota. As mentioned above, Paneth cells secrete AMPs such as alpha-defensins, lysozyme and secretory phospholipase A2, which protect not only the stem cell niche but also the wider epithelial barrier. Enterocytes throughout the small intestine and colon can also produce AMPs, including the C-type lectin regenerating islet-derived protein IIIγ (REGIIIγ). In addition, plasma cells secrete immunoglobulin A (IgA), which binds to mucus and neutralises toxins and pathogens without causing inflammation. This process helps prevent pathogen invasion and maintains a balance between the host and commensal microbiota. Both epithelial and immune cells recognise elements of the microbiota through pattern recognition receptors (PRRs) such as toll-like receptors (TLRs)[16,24].

Distinct cells belonging to the innate and adaptive immune systems are found in the intestinal stroma. Innate immune cells including macrophages, innate lymphoid cells (ILCs), dendritic cells, and granulocytes express invariant receptors that detect microbial products or patterns. Adaptive immune cells, including B and T cells, express highly variable receptors that recognize specific antigens. Macrophages ingest and degrade microorganisms and dead cells, producing mediators that drive epithelial renewal. Innate lymphoid cells regulate tissue homeostasis, repair and microbial defence and subsets of these cells can be defined by their cytokine production. Dendritic cells work as a link between the innate and adaptive immune systems. These cells can either sample the gut luminal content or acquire antigens from M cells and then mediate tolerance to food antigens and the microbiota. Once activated, dendritic cells migrate to the mesenteric lymph nodes and gut-associated lymphoid tissue (GALT), such as the Peyer's patches, where they present antigens to naïve T cells. These cells also control the balanced differentiation of naïve T cells into effector T cells (Th1, Th2, Th17) or regulatory T cells (Treg), can trigger an innate immune response, and promote B cell differentiation into IgA^+ plasma cells [16,24].

Intestinal homeostasis is maintained by a complex cytokine network that mediates interactions between epithelial and immune cells. Signal transducer and activator of transcription 3 (STAT3)-inducing cytokines, such as IL-6, IL-22 and IL-17, are critical for promoting epithelial cell survival and antimicrobial defence. Cytokine production stimulated by microbial activity and metabolites, in particular IL-10 and transforming growth factor β1 (TGF-β1), play an essential role in promoting tolerance through interactions between mononuclear phagocytes and Treg. IL-10 promotes anti-inflammatory responses and tolerance in mononuclear phagocytes, which in turn can support the development of forkhead box $P3^+$ ($Foxp3^+$) Treg. The dynamic interaction between mononuclear phagocytes, Treg and B cells is a critical host adaptation to microbial stimuli, and its dysregulation can lead to IBD[25].

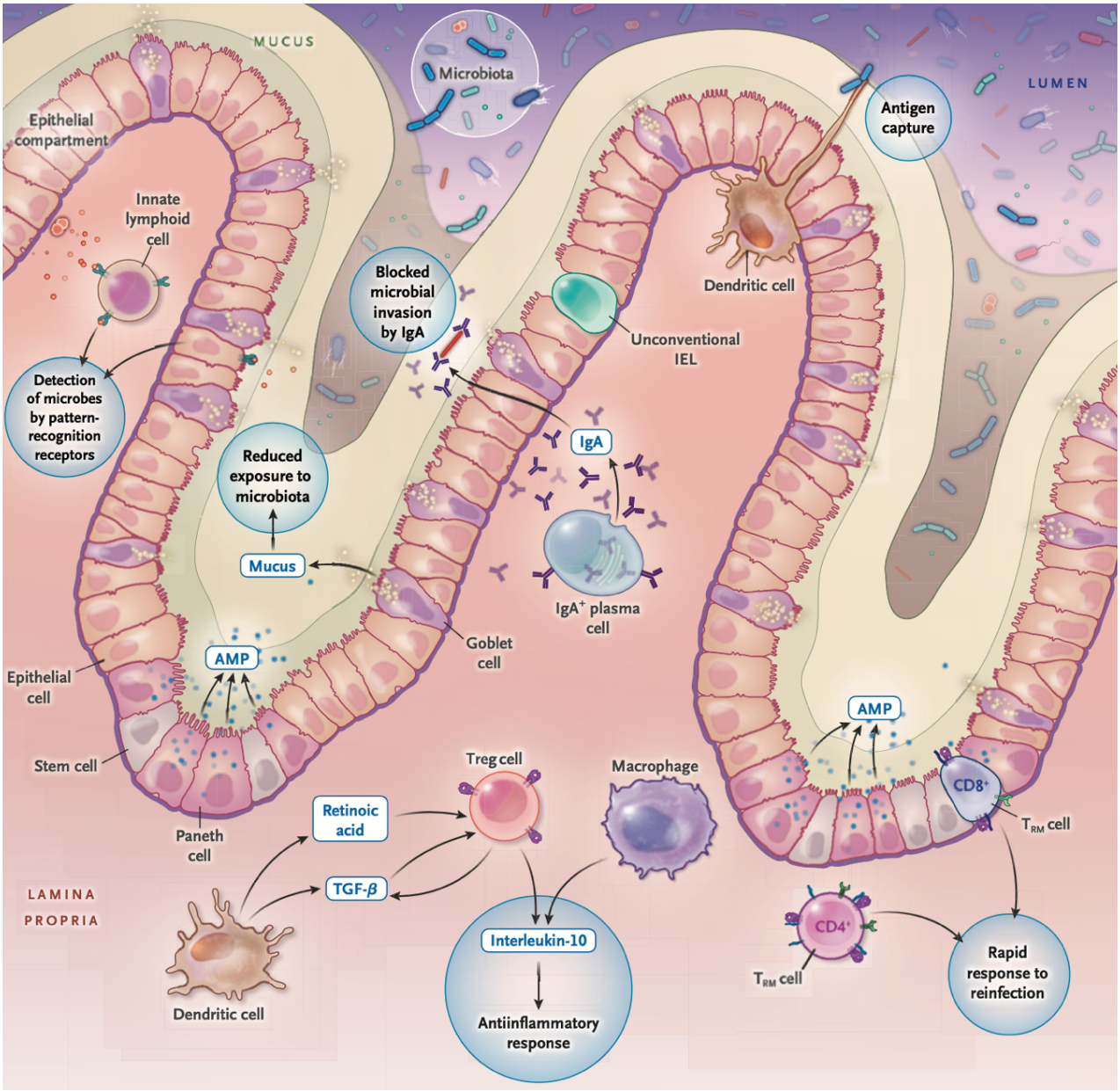

Figure 6. Mucosal immune system in the healthy state. The intestinal epithelium works in tandem with the immune system to protect the integrity of the mucosal barrier. From Chang, 2020[16].

I.2.2. Mucosal immunity in IBD

Inflammation is a critical element of the immune system, serving primarily as a protective mechanism and promoter of repair and regeneration in response to injury or infection. Under normal circumstances, this inflammatory response is tightly regulated, ensuring that it fades as soon as the threat is neutralised. The problem arises when the inflammatory response becomes chronic. In diseases such as IBD, this regulation fails. Instead of aiding tissue repair, persistent inflammation leads to an exacerbated response that not only fails to resolve, but also perpetuates tissue damage and dysfunction (**Fig. 7**). This chronic, uncontrolled inflammation drives the progressive nature of IBD, making it critical to understand the triggers and mechanisms that lead to its dysregulation.

While it is uncertain whether it is a cause or a consequence, IBD is characterised by dysbiosis, compromised barrier integrity and significant mucosal infiltration by both innate and adaptive immune cells[25]. The loss of mucosal integrity, caused by disruption of tight junction proteins and the mucus layer, leads to increased intestinal permeability and translocation of microbiota and their mediators. This prompts the

activation of innate immune cells, resulting in the production of cytokines and chemokines. Subsequently, additional immune cells are recruited, and the adaptive immune system is activated. The immune cells and the cytokines they produce further damage the epithelial cells, impairing barrier function and ultimately perpetuating gut inflammation[16,22].

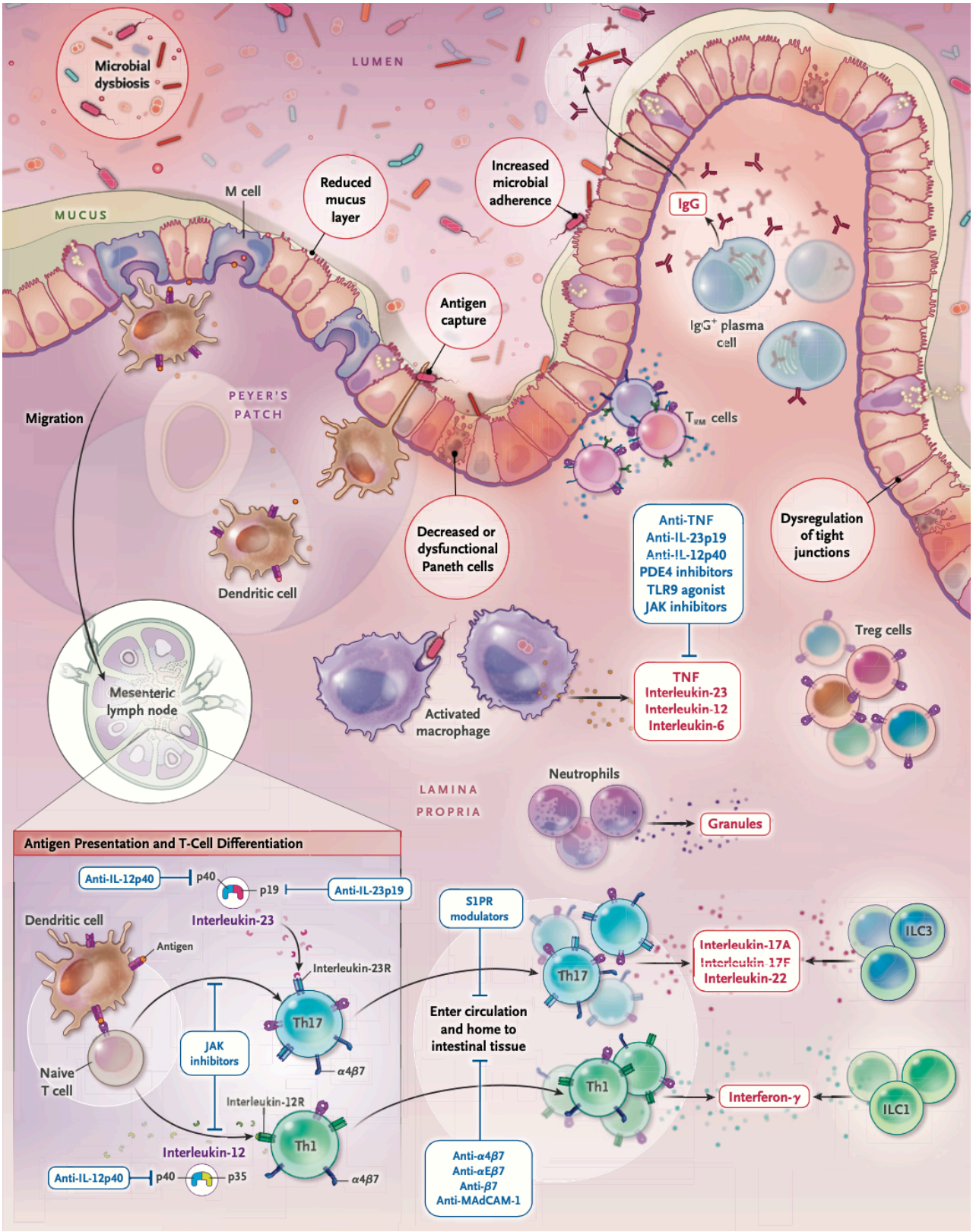

Figure 7. Mucosal immune system in inflammatory bowel diseases (IBD). The tightly controlled balance of the immune system is disrupted. From Chang, 2020[16].

Following an increase in intestinal permeability, macrophages recognise pathogen/damage-associated molecular patterns via PRRs and become activated. This activation induces phagocytosis and triggers the production of high levels of pro-inflammatory cytokines such as tumour necrosis factor α (TNF-α), IL-1β, IL-6, IL-23 and IL-12, which further promote inflammation. Dendritic cells present antigens to naïve T cells, which then proliferate and differentiate into natural killer T cells, Th1 cells and Th17 cells. Natural killer cells produce IL-13 and IL-5, which further compromise the epithelial barrier. Th1 and Th17 cells upregulate chemokine receptors and integrins, allowing them to enter the systemic circulation and migrate to the intestinal tissue. In the inflamed tissue, Th1 cells produce interferon-γ (IFN-γ), while Th17 cells secrete IL-17A, IL-17F and IL-22. At the same time, there is an increase in the number of IFN-γ-producing ILC1, IL-17A-producing ILC3 and IgG-secreting plasma B cells[26].

The extensive knowledge gathered over the years on the complex immune pathways and onset of IBD has improved our ability to accurately predict disease progression and identify effective therapeutic treatments.

I.2.3. Therapeutic approaches

In the past, the standard of care for patients with IBD focused primarily on symptom management. However, it is now recognised that the absence of symptoms does not necessarily indicate the absence of inflammation and that more specific treatment goals need to be established. Mucosal healing has become an important goal in the treatment of both UC and CD. Position papers recently published by the European Crohn's and Colitis Organisation (ECCO) define the absence of intra-epithelial neutrophils, erosion and ulceration as the minimum criteria for histological remission[27,28].

The type of treatment given to IBD patients is closely related to the severity of the disease. A step-up approach, in which the intensity of drug treatment progressively increases with disease severity, is commonly used, as shown in the treatment pyramid in **Fig. 8**. Alternatively, a top-down approach entails the early use of highly effective and potent treatments to prevent disease progression[29].

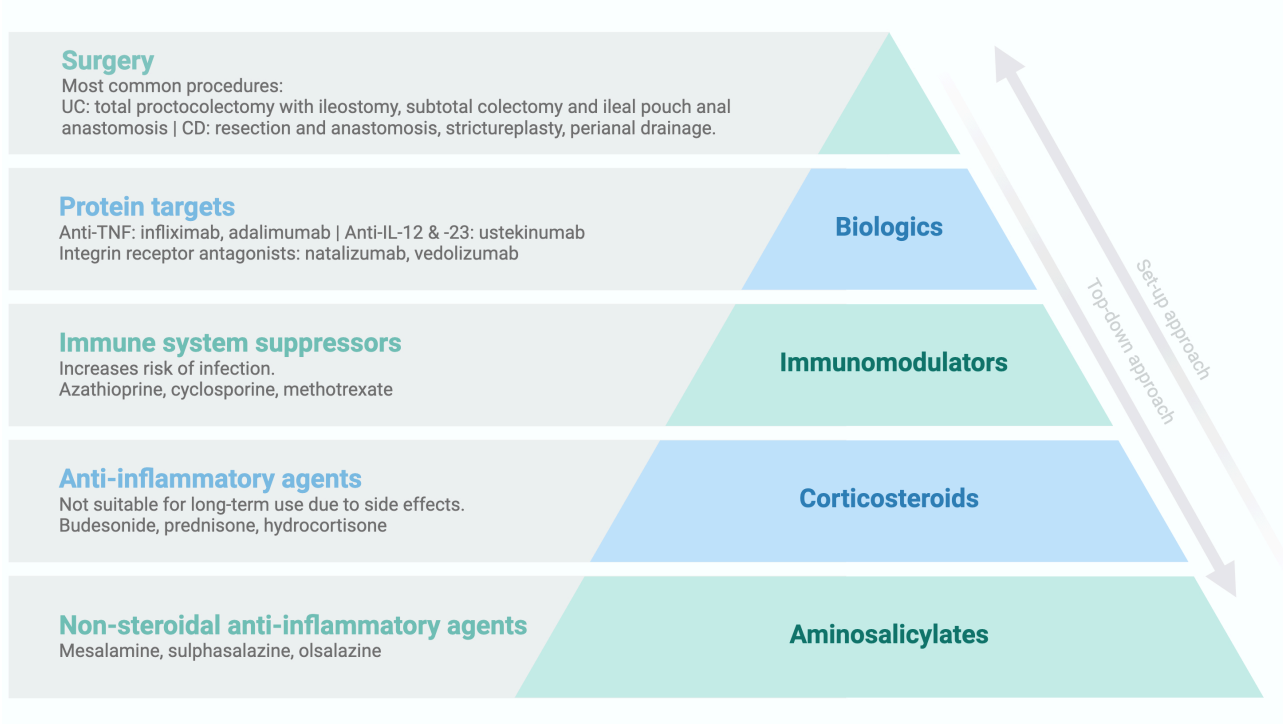

Figure 8. Schematic representation of the step-up and top-down drugs **therapeutic approaches** adopted in inflammatory bowel diseases (IBD). Created with BioRender.com.

5-aminosalicylic acid (5-ASA), commonly known as mesalamine, and its derivatives remain the primary anti-inflammatory treatment for IBD and are particularly effective in the management of mild to moderate UC. 5-ASA reduces the production of prostaglandins and proinflammatory cytokines and inhibits neutrophil chemotaxis and mast cell activation[30].

Corticosteroids are effective in inducing remission in IBD, but they are unable to maintain it and are associated with a variety of side effects. Glucocorticoids, such as budesonide, bind to cytosolic receptors and form a steroid receptor complex that translocate to the nucleus. There, it reduces the transcription of nuclear factor kappa-light-chain-enhancer of activated B cells (NF-κB) and activator protein 1 (AP1), thereby suppressing the production of inflammatory mediators[31].

Immunomodulators such as azathioprine, 6-mercaptopurine, methotrexate, cyclosporine A or tacrolimus can also be used in IBD, but they have numerous side effects that may limit their use, including nausea, vomiting, headaches and they can also show hepatotoxicity[32].

With many patients either refractory or intolerant to the mentioned treatments, there was an urgent need to develop more specific therapeutic approaches. In this context, anti-TNF agents, including infliximab, adalimumab, golimumab and certolizumab pegol, have been introduced into IBD therapy. TNF is produced by various immune and non-immune cells in the inflamed bowel, including epithelial cells, macrophages, T cells, dendritic cells, fibroblasts and adipocytes. This cytokine induces neo-angiogenesis, activates macrophages to produce other cytokines, favours Paneth cell death by necroptosis, promotes intestinal epithelial cell apoptosis, and regulates T-cell apoptosis. Thus, anti-TNF antibodies may suppress intestinal inflammation in IBD through multiple mechanisms (**Fig. 7**)[32,33]. Despite the success of anti-TNF treatment, up to 40% of IBD patients are non-responders, representing a major unmet need in the management of IBD. Recently, this non-responsiveness has been linked to the activation of alternative cytokine pathways, in particular IL-23 and the IL-6 family member oncostatin M[25].

Targeting the IL-23 axis is already used in clinical practice for CD patients with Ustekinumab, a treatment that neutralises the IL-12 p40 subunit, which is shared by both IL-12 and IL-23 (**Fig. 7**)[25,33].

Another class of biologic agents approved for IBD consists of anti-α4 integrin agents, such as natalizumab and vedolizumab, that reduce leukocyte migration to the inflammation site by blocking integrins, transmembrane receptors that mediate cells adhesion and migration. Another important development in the context of immune cell trafficking in IBD relates to sphingosine 1-phosphate (S1P) signalling (**Fig. 7**). Ozanimod was approved for the treatment of UC patients with moderately to severely active disease and intolerant to either conventional therapy or biological agents. Ozanimod induces the internalization of the S1P receptor, reducing the lymphocyte migration towards the inflamed areas[32,33].

Over the last few years, Janus kinase (JAK) inhibitors have gained a lot of attention. JAK are intracellular tyrosine kinases, activated by IFN-γ and other cytokines, that allow the transcription of effector proteins leading to inflammatory processes (**Fig. 7**). Tofacitinib, a JAK inhibitor upstream of STAT signalling used by many cytokines, is approved for use in UC patients but has not shown efficacy in CD patients, which may reflect differing cytokine profiles between UC and CD. Filgotinib, a more selective JAK inhibitor that shows a clinical response in CD patients, impairs signalling downstream of IL-6, IL-10, and IFN family cytokines by inhibiting JAK1[25].

Although several drugs are available for the treatment of IBD, a significant number of patients either do not respond or lose their responsiveness over time. The development of predictive preclinical models and the

careful planning and execution of clinical trials are crucial to discover more effective and personalized treatment alternatives for IBD.

I.3. *How?* Preclinical *in vitro* models of intestinal inflammation

By studying the intestinal epithelium under inflammatory conditions, new insights could be uncovered into its role in disease progression and response to treatments, which could lead to more effective therapies and diagnostic tools. Preclinical models are powerful instruments that help to investigate the properties and behaviour of the intestinal epithelium under various conditions. These models provide a controlled environment to closely study the biological processes and interactions at play, simulating conditions without the ethical and technical complexities associated with *in vivo* studies.

For decades, animal models have been invaluable in elucidating disease mechanisms and providing proof of concept for therapeutic approaches in many diseases, including IBD. Whole organisms offer the opportunity to study systemic interactions, immune responses, disease progression and the effects of therapies. These models mimic complex tissue interactions, microbiota-host dynamics and genetic factors that are difficult to replicate *in vitro*, providing critical insights into the pathogenesis and treatment of IBD. Each *in vivo* model has its own strengths and weaknesses, and the key to robust scientific research is to select the most appropriate model for the specific scientific question at hand.

The most commonly used species to simulate IBD are mice and rats, although pigs and dogs are also used. Mouse models of IBD are extremely diverse and include chemically induced colitis models (e.g. dextran sodium sulphate or trinitrobenzene sulphonic acid models), genetic models (e.g. IL-10 knockout mice), and models induced by manipulation of the immune response (adoptive transfer models) or introduction of specific bacteria (e.g. adherent invasive *E. coli* or salmonella). However, accurate modelling of the complex interactions between host genetics and environmental factors in the gastrointestinal system poses significant challenges in surrogate species. In addition, even well-established models of colitis often face problems of reproducibility between laboratories, in part due to variations in the microbiota present in different research facilities [34].

Bridging the gap between experimental protocols and *in vivo* testing, *in vitro* models have facilitated the study of cellular responses to inflammatory stimuli. These models bypass the ethical and logistical complexities associated with animal testing, providing researchers with a more accessible and affordable alternative. *In vitro* systems allow the detailed study of multiple treatments on disease-specific cellular activities, with the possibility of conducting high-throughput studies. However, while these models are invaluable tools, they must be selected and interpreted with caution, as they do not fully replicate the biological context of a living organism or its systemic responses.

Ideally, an *in vitro* model of IBD should closely mimic the key pathophysiological features of the disease. These include: i) a compromised intestinal epithelial barrier, ii) a reduced mucus layer, iii) increased expression of inflammatory mediators, cytokines and chemokines[35]. To effectively recreate these conditions, inflammatory responses can be induced by exposing epithelial cells to well-characterised IBD-related pro-inflammatory cytokines or immunostimulatory microbial components. Alternatively, the complex epithelial-immune crosstalk inherent to IBD can be simulated by co-culturing epithelial cells with immune cells. In this setup, inflammation is induced by targeted activation of immune cells, closely mimicking the inflammatory milieu seen in IBD. However, this approach is technically demanding and adds significant complexity to the model, posing challenges both in terms of experimental design and interpretation[36].

Initially, *in vitro* models of intestinal inflammation were quite simple, typically based on single cell cultures. Subsequently, the introduction of cell culture inserts provided a straightforward solution for *in vitro* studies, allowing assessment of barrier function and intestinal permeability by providing access to both the apical and basolateral sides of polarised cell monolayers. The knowledge gained from these initial approaches revolutionised several physiological concepts and laid the foundation for the development of more sophisticated models.

I.3.1. Immortalised cell lines

Immortalised intestinal cell lines are the most commonly used models to reconstitute the human intestinal epithelium *in vitro*, typically relying on Caco-2 and HT29-MTX cells to mimic enterocytes and goblet cells respectively. These models are highly reproducible, and their unlimited lifespan is considered their main strength[36,37].

Caco-2 cells, derived from human colorectal adenocarcinoma, form a polarised monolayer with an apical brush border. These cells are responsive to cytokines such as IL-1β, TNF-α and INF-γ. For example, TNF-α can increase the permeability of Caco-2 monolayers by activating NF-κB, which leads to the downregulation of ZO-1. A similar downregulation is observed with an increase in myosin light chain kinase activity [36,37].

HT-29 cells are also derived from human colorectal adenocarcinoma and express properties of both enterocytes and secretory cells. When exposed to high concentrations of methotrexate, these cells adapted and developed the stable clone HT29-MTX, which differentiates spontaneously into goblet-like mucus-producing cells. HT29-MTX also secrete growth factors (platelet derived growth factor AA, TGF-α, and TGF-β), cytokines (TNF-α, IL-1β, and IL-6), immune-modulatory cytokines (IL-3 and G- and GM-granulocyte colony-stimulating factor), and chemokines (fractalkine, IL-8, monocyte chemoattractant protein-1, and IFN-γ-induced protein 10) in similar levels to those found *in vivo*. HT29-MTX cells have been widely used in coculture with Caco-2 cells supplementing their lack of mucus production and decreasing overall barrier tightness [36,37].

A variety of cell lines have been used as alternative immune cells in intestinal *in vitro* models. However, THP-1, a human monocytic leukaemia cell line, is the most used. THP-1 cells can be differentiated into macrophages using phorbol 12-myristate 13-acetate (PMA) but there is a lack of consistency regarding the conditions of the PMA stimulus. When THP-1 are exposed to PMA for longer and/or at higher concentrations, they will likely elicit a stronger immune response and a dose-dependent increase in the secretion of IL-8 and TNF-α is observed. Raji B is a B lymphocyte cell line that is used to promote the differentiation of Caco-2 into M-like cells [36,37].

While cell lines are precious for high-throughput screening and basic cellular studies, there are considerable limitations that need to be addressed. Firstly, many cell lines suffer from genetic drift over time, which can alter their phenotype and reduce the relevance of findings to the original tissue type or disease state. Additionally, the use of immortalised cell lines can sometimes lead to misleading results due to their altered metabolic and growth characteristics, which differ significantly from normal cells [36,37].

I.3.2. Primary cells

In contrast to immortalised cell lines, primary cells offer greater physiological relevance and the opportunity to establish *in vitro-in vivo* correlations. Derived directly from donor tissues, these cells retain many of the genetic, phenotypic and functional characteristics of their source, making them priceless instruments for more accurate *in vitro* modelling.

However, while primary cells may fill some of the gaps left by cell lines, they come with their own set of challenges, including inter-donor variability, limited lifespan in culture and the logistical complexities of tissue procurement and handling. The limitations associated with the lifespan of primary cells can be overcome to some extent by using stem cell-based models. Organoids are three-dimensional (3D) tissue-engineered models that closely mimic many aspects of the complex structure and function of the corresponding *in vivo* tissue. These clusters are physiologically more relevant than standardized cell lines, for they can differentiate into all epithelial cell types and self-organize into hierarchical, polarized structures, with a hollow lumen and crypt domains[38].

Organoids can be derived from two types of stem cells: i) organ-restricted adult stem cells (ASCs) and ii) pluripotent stem cells (PSCs), including both induced (iPSCs) and embryonic stem cells (ESCs). ASCs, located at the base of intestinal crypts, can be isolated from surgical resections or biopsy samples. Once isolated, these cells can be expanded either within the whole crypt or as single cells to form organoids composed primarily of epithelial layers. In contrast, PSC-derived organoids are capable of generating not only epithelial cells but also a mesenchyme. PSCs from the same patient can also be differentiated into other resident cell populations including enteric neurons[39,40], vascular endothelial cells[41], and adipocytes[42]. This setup allows the study of the complex crosstalk between different cell types, which is particularly valuable for personalised medicine approaches. However, while PSC-derived organoids could provide a more complex system, their expansion and differentiation are time-consuming and technically challenging. This complexity often requires sophisticated protocols and can lead to variability in the resulting organoids[43].

When working with human organoids, ethical concerns and regulatory frameworks must be addressed. In the EU, the use of organoids in research, particularly when human cells or tissues are involved, must follow the broad framework of EU regulations related to human tissues, medical research and ethical considerations. In the case of intestinal organoids originated from biopsies or resected tissues, the general data protection regulation must be followed to ensure the privacy and data protection of each donor[44]. The quality and safety of each donation as well as their procurement, testing, processing, preservation, storage, and distribution should meet the standards set on directive 2004/23/EC of the European parliament[45], recently amended on standards of quality and safety for substances of human origin intended for human application and mandatory up to now only for human tissues and cells intended for clinical use[46].

In addition to EU regulations, many EU countries have their own specific legislation that regulates the use of human tissues and cells in research. Compliance with this legislation is ensured by national ethical committees that need to approve ethical agreements ahead of each project's beginning. All these requirements then come to life in a document that each patient must sign informing of their consented donation.

Patient-derived organoids (PDOs) offer a unique opportunity in disease modelling, precision medicine and regenerative medicine (**Fig. 9**). In the context of IBD modelling, ASCs derived from patient-specific inflamed tissues can potentially represent the specific cellular and molecular characteristics of IBD, offering unprecedented insights into individual disease mechanisms and responses to treatment[47–52]. For example, colon organoids derived from IBD patients have shown persistent inflammatory features, such as decreased expression of specific tight junction proteins (e.g., ZO-1, occludin, and claudin-1) and upregulation of antigen presentation genes, alongside slower growth and altered polarization, unlike control organoids[49–52]. However, there is an ongoing discussion regarding the use of IBD patient-derived organoids.

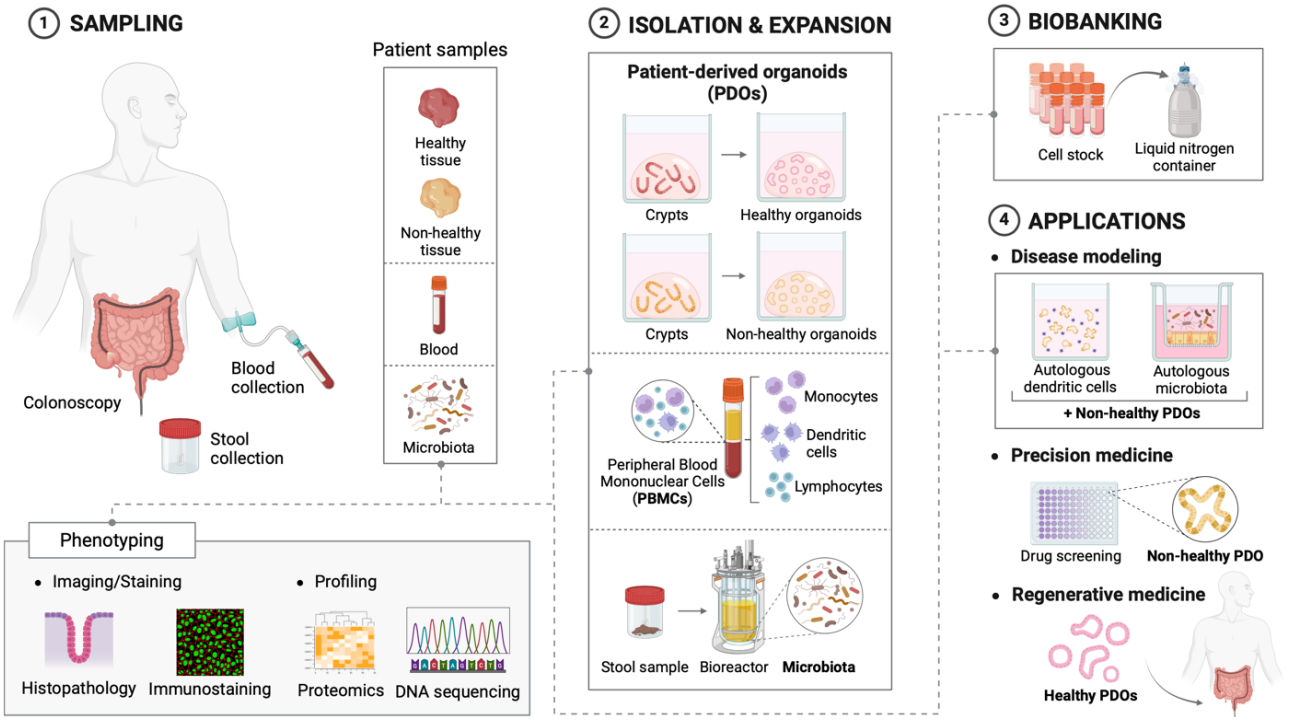

Figure 9. Patient on a dish: workflow for the use of patient-derived organoids (PDOs) in disease modelling, precision medicine and regenerative medicine. **1)** Tissues (healthy and non-healthy) are collected and PDOs established from the isolated crypts. Simultaneously, blood and stool samples can be collected from the same patient for the isolation of peripheral blood mononuclear cells (PBMCs) and the isolation and expansion of microbiota. **2)** After some expansion, healthy and non-healthy PDOs can be obtained. **3)** PDO biobanks can also be created for later use. Tight quality control measures are in place to ensure there are no alterations in the phenotype after sample collection, PDO expansion and when stocks are retrieved from the biobank. **4)** Non-healthy PDOs can be applied as platforms for modelling patient's response to drug treatments and for precision medicine. Complex models can also be established by co-culturing non-healthy PDOs with autologous immune cells and microbiota. Healthy PDOs can be transplanted endoscopically to promote tissue repair in damaged areas. Created with BioRender.com.

One significant concern is whether these organoids maintain their diseased phenotype over time. There is evidence suggesting that as patient-derived organoids are passaged, they may lose some of the inflammatory cues, reverting to a more 'normal' phenotype[47,53,54]. This phenotypic drift can potentially limit their utility for long-term studies or affect the reproducibility of experimental results. Additionally, other studies have reported difficulties in generating long-term cultures with organoids from active inflamed regions[55,56].

To culture organoids, isolated cells are typically embedded in an extracellular matrix and propagated using a well-defined culture media that ensures the right growth-factor environment to generate epithelial cell clusters. The enclosed sphere-like structure of these systems, however, prevents direct access to the apical side of the cells. Recently, protocols were developed to invert cell polarity and convert organoids from basal-out to apical-out[57]. Another alternative, especially useful for pharmacological studies, involves the establishment of organoid-derived monolayers. Both 3D and 2D systems have been used as IBD models, and when derived from healthy tissue or PSCs, the inflammatory stimuli frequently used are cytokines and/or immunostimulatory microbial components. The most commonly used cytokines are TNF-α and IFN-γ, either alone or in combination with other stimuli, in concentrations that range between 0.2 and 100 ng·mL^{-1}. Exposure to these inflammatory stimuli invariably results in increased cytokine and chemokine secretion, disruption of tight junction proteins, enhanced paracellular permeability, and a reduction in cell viability, villin, and mucin-2 (MUC2) production[49,53–55,58–66].

Organoids have also been co-cultured with primary immune cells to develop a more pathophysiological relevant model. Several immune cell subsets have been used in these studies, including monocytes[67], macrophages[68,69], polymorphonuclear leukocytes[70–72], autologous T cells[73–75] and dendritic cells[76]. However,

this approach faces several technical and biological challenges. First, maintaining the viability and functionality of primary immune cells in culture alongside organoids requires highly optimised culture conditions that can support both cell types without compromising their natural behaviour. In addition, the physical integration of these cells must be carefully managed to ensure realistic cell-cell interactions, an aspect aggravated by the fact that the inherent variability of primary immune cells from different donors can introduce inconsistencies that complicate the interpretation of results and the reproducibility of the model. This could be avoided by using autologous immune cells, but it adds to the technical complexity of the model and potentially increases the burden to the donors, as it would require a blood donation and an intestinal biopsy.

The lack of standardised protocols for obtaining *in vitro* models of intestinal inflammation is not due to a lack of research in this area. Rather, it is due to the extensive but inconsistent literature on key variables. These inconsistencies include the number and types of cells used, the inflammatory stimuli (such as type, concentration and site of application) and even the outcomes measured.

OBJECTIVES AND SCOPE OF THE THESIS

Considering the increasing medical and societal concern regarding colonic diseases, the EU H2020 MSCA-ITN COLOTAN project, which supports the PhD research highlighted in this dissertation, aims to improve colon targeting of drugs to efficiently treat diseases of the large intestine. In order to reach this goal, a major challenge in drug development must be addressed: the need for predictive tools and models of the human colon.

The primary goal of this work is to establish a physiologically relevant model capable of reliably predicting drug transport through the inflamed human colon, possibly contributing to understand the impact of colonic inflammation on oral drug disposition.

To this end, an *in vitro* intestinal model based on human colonoid-derived monolayers exposed to the inflammatory cytokines TNF-α and IFN-γ was developed and validated. The morphological, cytochemical and functional changes induced by the inflammatory milieu on the barrier integrity, cell viability, and release of inflammatory mediators was investigated. In the last part, preliminary data obtained in Parma and during the secondment at Johnson & Johnson Innovative Medicine are presented, focusing on the colonic permeability of six conventional drugs of different biopharmaceutical classification system (BCS) levels.

CHAPTER II. MATERIALS AND METHODS

II.1. Materials

Caco-2 cell line (HTB-37™) kindly provided by prof. Annalisa Bianchera, Department of Food and Drug, University of Parma was bought from **American Type Culture Collection** (Manassas, VA, USA). Advanced Dulbecco's Modified Eagle Medium/nutrient mixture F12 (Advanced DMEM/F12), trypsin-EDTA (0.25% (v/v) trypsin/0.53 mM EDTA), TrypLe™ Express Enzyme 1x and GlutaMAX™ supplement 100x were bought from **Gibco™** (Walthalm, MA, USA). Fetal Bovine Serum (FBS) from **EuroClone** (Milan, Italy) was used. 10000 $IU \cdot mL^{-1}$ Penicillin/ 10 $mg \cdot ml^{-1}$ Streptomycin (P/S) 100x, trypan blue, Matrigel® matrix basement membrane (growth factor reduced; phenol-red free), Costar® 6-well ultra-low attachment plates and HTS Transwell®-96 Permeable Support with 0.4 µm PET Membrane were purchased from **Corning®** (NY, USA). Recombinant Human TNF-α and IFN-γ were bought from **PeproTech** (London, UK). Anti-villin polyclonal antibody, and anti-MUC2 polyclonal antibody purchased from **Proteintech** (Rosemont, IL, USA), iFluor™ 594 goat anti-rabbit IgG and Phalloidin-iFluor™ 488 Conjugate from **AAT Bioquest** (Sunnyvale, CA, USA), rabbit anti-Ki67 monoclonal antibody from Abcam (Cambridge, UK), VECTASHIELD® Antifade Mounting Medium with DAPI (4′,6-diamidino-2-phenylindole) from **Vector Laboratories** (Burlingame, CA, USA) were used. Paraformaldehyde (PFA), Triton™ X-100, ethylenediaminetetraacetic acid (EDTA) disodium salt dihydrate, [(3-(4,5-dimethylthiazol-2-yl)-2,5-diphenyltetrazolium bromide] (MTT), fluorescein isothiocyanate-dextran 4 kDa (FITC-D4), propranolol, atenolol, elacridar, Human IL-8/CXCL8 and Human IL-6 ELISA Kit were bought from **Sigma-Aldrich** (St. Louis, MO, USA). NF-κB p65 (Total/Phospho) Human InstantOne™ ELISA Kit and MIP-3α/CCL20 Human ELISA Kit was purchased from **Invitrogen** (Waltham, MA, EUA). Bovine Serum Albumin (BSA) lyophilized powder was bought from **AppliChem** (Darmstadt, Germany). Budesonide, celecoxib, and Rho-kinase inhibitor (Rho-KI; Y27632 dihydrochloride) was bought from **MedChemExpress** (Monmouth Junction, NJ, USA). Dimethyl sulfoxide (DMSO) from **VWR Chemicals** (Milan, Italy) was used. Dithiothreitol (DTT) was purchased from USB corporation (Cleveland, OH, USA). From **STEMCELL™ Technologies** (Vancouver, Canada), IntestiCult™ Organoid Growth Medium (OGM) human basal medium, IntestiCult™ Organoid Differentiation Medium (ODM) human basal medium and organoid supplement were used. Phosphate Buffered Saline (PBS, w/o Ca^{2+} and Mg^{2+}) and Hanks' Balanced Salt Solution (HBSS) were produced in house. To sterilize buffers, 0.22 µm filters from **Sarstedt** (Newton, NC, USA) were used. Transparent PET inserts for 24 well-plates with 0.4 µm pores, were bought from Sarstedt (Newton, NC, USA). CytoTox® 96 Non-Radioactive Cytotoxicity Assay kit was purchased from **Promega** (Madison, WI, USA). [^{14}C]-mannitol was bought from **Revvity** (Waltham, MA, EUA). [^{3}H]-atenolol was purchased from **Moravek Inc.** (Brea, CA, USA). [^{3}H]-Propranolol and [^{3}H]-digoxin and Ultima Gold™ were obtained from **PerkinElmer** (Waltham, MA, USA). [^{3}H]-cimetidine was provided by **American Radiolabelled Chemicals, Inc.** (St. Louis, MO, USA).

II.2. Methods

II.2.1. Establishment of human colonoid cultures

II.2.1.1. Human tissue collection

Colonic biopsies were obtained from healthy patients undergoing routine colonoscopy at Parma's University Hospital who gave their informed consent prior to sample collection and processing. The protocol was approved by the regional ethics committee *Aziende Sanitarie/IRCCS dell'Area Vasta Emilia Nord* (Protocol ID: 57/2021/TESS/UNIPR COLOTAN).

Tissues were freshly collected from adult patients with ages ranging from 26 to 86 years old. Only non-IBD subjects, undergoing colonoscopy for mild gastrointestinal symptoms or screening for colorectal cancer, who had a normal mucosa were included. From each patient, 4 to 6 biopsies were collected from the descending colon, using EndoJaw FB-235 2.8 mm single-use oval-cup biopsy forceps (Olympus, Tokyo, Japan). Patients' demographics and sample characteristics of the tissues used to establish colonoid-derived monolayers (CDMs) are provided in **Table 1**.

Table 1. Patients' demographic data and characteristics of human colonic biopsies used to establish colonoid-derived monolayers.

Biopsies ID	Demographics		Resection region
	Sex	Age	
HCB25	Female	56	Descending colon
HCB29	Female	67	
HCB31	Female	60	
HCB37	Male	26	
HCB43	Male	56	
HCB48	Female	86	

HCB: Human colonic biopsy.

II.2.1.2. Isolation of human colonic crypts from fresh biopsies

Fresh colonic biopsies were collected in 1.5 mL tubes (**Fig. 10**) with Advanced DMEM/F12 supplemented with 10% (v/v) FBS, 1x P/S and 1x GlutaMAX™. Samples were kept in ice at all times. After three washes of 5 minutes each with 10 mL of ice-cold PBS with 1x P/S, samples were incubated in the same volume of ice-cold dissociation buffer (5 mM EDTA/5 mM DTT), for 30 minutes on the orbital shaker (200 rpm). Intestinal crypts were released by vigorously shaking the tissue fragments (**Fig. 10**). After allowing biopsies to settle by gravity, crypts were transferred into a fresh tube with 1 mL of ice-cold FBS. Biopsies were replenished with 10 mL of ice-cold dissociation buffer and the process was repeated 5x. Crypts were collected by centrifugation at 4ºC and 200 *g*, for 5 minutes and re-suspended in 1 mL of ice-cold Advanced DMEM/F12 with 1x P/S and 1% (w/v) BSA. The number of crypts was determined in each of the 5 tubes. The fractions with the highest number of crypts were combined and centrifuged at 4ºC and 200 *g,* for 5 minutes. Dome cultures were used to generate colonoids from the resulting crypts.

Figure 10. **Isolation of human colonic crypts from freshly isolated biopsies.** (1) Collected biopsies in 1.5 mL tubes. (2) Crypts isolated from the tissue that lays at the bottom of a 15 mL tube. (3) Bright-field microscopy images of human colonic crypts.

II.2.1.3. Dome culture

Establishment of colonoids from isolated crypts

Human colonic crypts were suspended in 70% (v/v) Matrigel® and 30% (v/v) ice-cold complete IntestiCult™ OGM. 20 µL domes were seeded in the centre of pre-warmed 48-well plate at a seeding density of approximately 50 crypts per well. For at least 20 minutes, plates were transferred upside down into the incubator at 37 ºC and 5% CO_2, to allow Matrigel® to polymerise. Colonoids were expanded in 200 µL per well of complete IntestiCult™ OGM supplemented with 1x P/S. 10 µM Rho-KI was added to the media only at the time of seeding. Media was changed every 2 to 3 days, and the culture was maintained at 37 °C and 5% CO_2, for 5 to 7 days.

For passaging, colonoids were harvested by flushing and scraping domes with 500 µL of ice-cold 5 mM EDTA. Colonoids from 8 to 12 wells of a 48-well plate were collected in a 15 mL tube. Colonoids were mechanically disrupted by pipetting up and down with a 10 µL tip attached to a 200 µL tip, in 200 µL of ice-cold Advanced DMEM/F12 with 1x P/S and 1% (w/v) BSA. Colonoid fragments were collected by centrifugation at 4 ºC and 200 *g,* for 5 minutes.

Establishment of colonoids from commercial lines

Information concerning two human colonoid lines acquired from HUB Organoids, during the secondment at Johnson & Johnson Innovative Medicine (Beerse, Belgium), is provided in **Table 2**. Human colonoid fragments, obtained through mechanical disruption, as above described, of commercial organoid lines purchased from HUB Organoids, were suspended in 70% (v/v) Matrigel® and 30% (v/v) ice-cold complete IntestiCult™ OGM. From 15 to 20 domes of 10 µL each were seeded in pre-warmed 6-well plates. Plates were transferred for at least 20 minutes into the incubator at 37 ºC and 5% CO_2, to allow Matrigel® to polymerise. Colonoids were expanded in 3 mL per well of complete IntestiCult™ OGM supplemented with 1x P/S. 10 µM Rho-KI was added to the media only at the time of seeding. Media was changed every 2 to 3 days, and the culture was maintained at 37 °C and 5% CO_2, for 5 to 7 days.

For passaging, colonoids were harvested by flushing and scraping domes with 1 mL of ice-cold wash medium (Advanced DMEM/F12 supplemented with 10 mM HEPES, 10% (v/v) FBS, 1x P/S, 1% (w/v) BSA and 1x GlutaMAX™) per well. Colonoids from 3 wells of a 6-well plate were collected per 15 mL tube, they were mechanically disrupted by pipetting up and down with a syringe, in 1 mL of ice-cold wash medium per tube. Colonoid fragments were then collected by centrifugation at 4 ºC and 200 *g,* for 5 minutes.

Table 2. Characteristics of commercial organoid lines purchased from HUB organoids.

Colonoid line ID	Demographics		Resection region	Clinical status	Tissue condition	Passage #
	Sex	Age				
HUB-02-A2-092	Male	56	Sigmoid colon	Cancer	Healthy	6
HUB-02-D2-089-I	Female	42	Ascending colon	Healthy	Healthy	11

II.2.1.4. Suspension culture

This protocol was described by STEMCELL™ Technologies on the product information sheet of IntestiCult™ Differentiation Medium.

Establishment from colonoid fragments

Colonoid expansion was scaled up thanks to a suspension culture, as illustrated in **Fig. 11**. To this end, colonoid fragments, obtained from dome cultures, were suspended in 500 µL Matrigel® and seeded in the centre of warmed 6-well plates pre-filled with 3 mL of complete IntestiCult™ OGM with 1x P/S and 10 µM Rho-KI. Half-media changes were performed every 2 to 3 days, and the culture was maintained at 37 °C and 5% CO_2, for 7 to 10 days.

Colonoid dissociation

For passaging, the Matrigel® cloud from each 6-well plate was disrupted by pipetting up and down and collected into a 15 mL tube. After centrifuging at 4 ºC and 200 *g,* for 5 minutes, colonoids were re-suspended in 10 mL of ice-cold 5 mM EDTA and incubated in ice for 50 minutes, on the orbital shaker (200 rpm). Colonoids were harvested by centrifugation at 4 ºC and 200 *g,* for 5 minutes, and mechanically disrupted by pipetting up and down with a 10 µL tip attached to a 200 µL tip, in 200 µL of ice-cold Advanced DMEM/F12 with 1x P/S and 1% (w/v) BSA. Colonoid fragments were collected by centrifugation at 4 ºC and 200 *g,* for 5 minutes.

To seed colonoid-derived monolayers, colonoid fragments were further dissociated into single cells using TrypLe™ express enzyme.

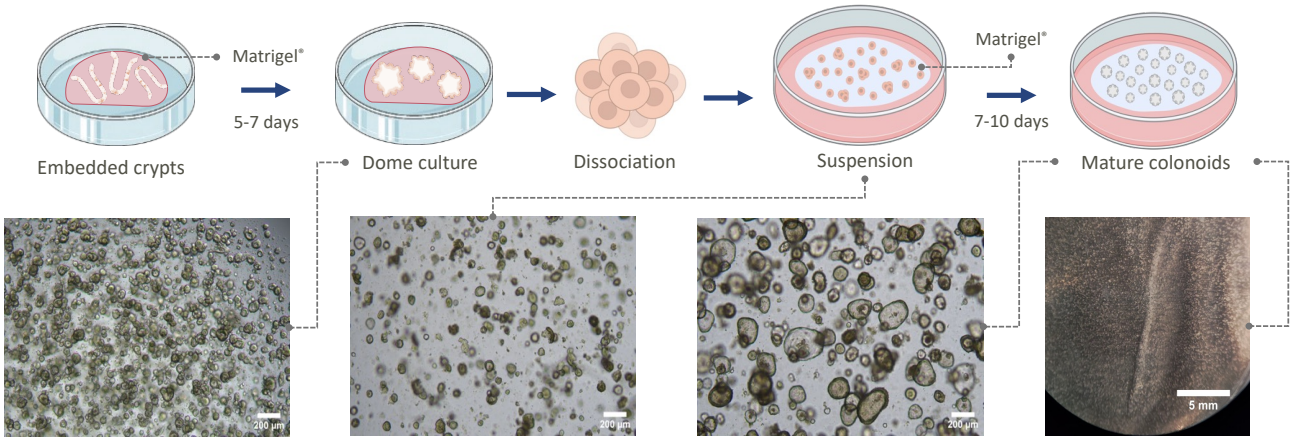

Figure 11. Establishment of colonoid suspension cultures. First, human colonoids are generated from freshly isolated crypts, in domes. After reaching maturity, colonoids are dissociated, suspended in Matrigel® and seeded on the centre of a 6-well plate pre-filled with 3 mL of warm IntestiCult™ Organoid Growth Medium (OGM). Colonoids expanded in suspension can grow for 7-10 days.

II.3. Establishment of colonoid-derived monolayers (CDMs)

Once sufficiently expanded, colonoids were dissociated into single cells as described in section II.2.1.4. and seeded into 24-well or 96-well transwell® systems allowing access to the apical and basolateral sides of the cells. A schematic representation of the workflow is shown in **Fig. 12**.

II.3.1. CDMs exposed to TNF-α and IFN-γ

24-well inserts were coated with Matrigel® diluted 50x in ice-cold PBS for at least 30 minutes at 37 ºC and 5% CO_2, before removing the residual PBS and washing twice. Colonoid-derived cells were seeded at $7.5x10^5$ cells·cm^{-2} in 100 µL of complete IntestiCult™ OGM with 1x P/S, in the apical side. 500 µL of complete IntestiCult™ OGM with 1x P/S were added to the basolateral side. 10 µM Rho-KI was added to the medium only at the time of seeding. Media was changed every 2-3 days, and plates were maintained at 37 °C and 5% CO_2, for 8 to 15 days. Monolayers were kept in IntestiCult™ OGM until transepithelial electrical resistance (TEER) values reached 100 to 200 Ω·cm^2, after which the medium was switched to complete IntestiCult™ ODM.

Differentiated colonoid-derived monolayers were exposed to 25 ng·mL^{-1} TNF-α and 25 ng·mL^{-1} IFN-γ for 24 h, in the apical and basolateral sides, to recreate inflammatory conditions.

II.3.2. CDMs exposed to IFN-γ

During the secondment at Johnson & Johnson, colonoid-derived cells were seeded into 96-well inserts, coated with Matrigel® diluted 50x in ice-cold PBS for at least 30 minutes at 37 ºC and 5% CO_2, before removing the residual PBS and washing twice. Cells were seeded at 3.57 x 10^5 cells·cm^{-2} in 100 µL of complete IntestiCult™ OGM with 1x P/S and 10 µM Rho-KI, in the apical side. 300 µL of complete IntestiCult™ OGM with 1x P/S and 10 µM Rho-KI were added to the basolateral side. Media was changed every 2-3 days, and plates were maintained at 37°C and 5% CO_2, for 8 to 15 days. Monolayers were kept in IntestiCult™ OGM until TEER values reached 100 to 200 Ω·cm^2, after which the medium was switched to complete IntestiCult™ ODM. Differentiated CDMs were exposed to 25 ng·mL^{-1} IFN-γ for 24 h, in the apical and basolateral sides, to recreate inflammatory conditions.

II.4. Immunocytochemistry (ICC)

Cell morphology, polarization and differentiation were evaluated through immunocytochemistry (ICC).

II.4.1. Cystic-like colonoids (3D colonoids)

In order to stain 3D colonoids, they were carefully released from Matrigel®. Cystic-like colonoids grown in domes were resuspended in ice-cold PBS and transferred into a pre-coated (PBS with 2% (w/v) BSA) 15 mL tube. After centrifuging at 4 °C for 5 minutes and 500 *g*, colonoids were washed three times with 1 mL of PBS using a precoated tip. Colonoids were harvested by centrifugation at 4 °C for 5 minutes and 500 *g*, resuspended in 1 mL of 4% (w/v) PFA, and transferred into a pre-coated 1.5 mL tube.

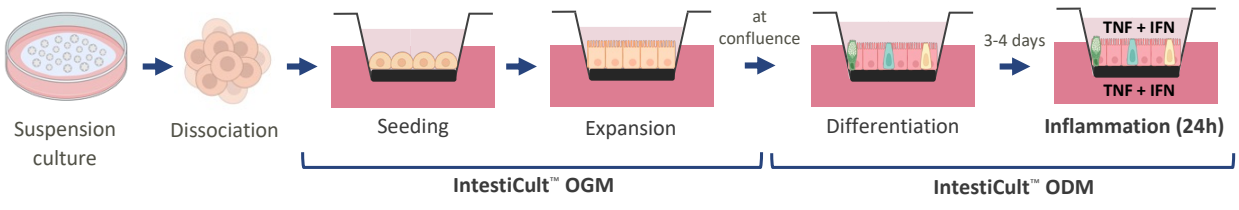

Figure 12. Establishment of colonoid-derived monolayers. Colonoids were harvested and dissociated after growing for 7 to 10 days in suspension. Cells were seeded at $7.5x10^5$ or $3.57x10^5$ cells·cm^{-2} into 24-well or 96-well inserts, respectively, coated with Matrigel® (1:50). Media was switched from IntestiCult™ Organoid Growth Media (OGM) to IntestiCult™ Organoid Differentiation Media (ODM) when transepithelial electrical resistance (TEER) values reached 100-200 Ω·cm^2. Differentiated monolayers were exposed for 24h to 25 ng·mL^{-1} TNF-α and 25 ng·mL^{-1} IFN-γ, in the apical and basal sides.

Following incubation at room temperature for 45 minutes on the orbital shaker (200 rpm), colonoids were centrifuged for 1 minute at 500 *g* and 4 °C, the supernatant was removed, and the pellet washed three times with PBS. Colonoids were then permeabilized with 1 mL of 0.2% (v/v) Triton™ X-100 solution and incubated with gentle horizontal agitation (50 rpm) for 30 minutes at room temperature. After settling by gravity, colonoids were washed three times with 1 mL of ice-cold PBS and spun at 500 *g* and 4 °C for 1 minute. 1 mL of blocking buffer (PBS with 2% (w/v) BSA) was added, and a 1-hour incubation followed. Colonoids were collected by centrifugation at 500 *g* and 4 °C for 1 minute and incubated with 1 mL of anti-Ki67 monoclonal antibody solution (1 µg·mL^{-1} in PBS with 0.5% (w/v) BSA), overnight with gentle horizontal agitation at room temperature.

The primary antibody solution was removed and colonoids were washed 3x with blocking buffer. 1 mL of iFluor™ 594 IgG antibody (4 µg·mL^{-1} in PBS with 0.5% (w/v) BSA) was added, incubating for 24 hours with gentle horizontal agitation, protecting the samples from light. Once the fluorochrome-labelled secondary antibody solution was removed, colonoids were washed three times with PBS. Then, phalloidin-iFluor™ 488 conjugate (in PBS with 1% (w/v) BSA) was added and colonoids incubated for 2 hours at room temperature.

Colonoids were spun for 1 minute at 500 *g* and 4 °C, washed three times with PBS and resuspended in 20 µL of VECTASHIELD™ mounting medium with DAPI. 10 µL of suspension were loaded in the centre of a glass slide, then sealed with varnish and stored at -20 °C protected from light.

Images were acquired using a Leica STELLARIS 5 confocal microscope and analysed using ImageJ.

II.4.2. Colonoid-derived monolayers

CDMs exposed to vehicle or to inflammatory cytokines were fixed with 4% (w/v) PFA for 15 minutes, at room temperature. PFA was removed and cells were washed three times with cold PBS. Then, 0.2% (v/v) Triton™ X-100 in PBS was added and the plate incubated for 10 minutes at 4 °C. After removing Triton™ X-100 and washing three times with cold PBS, blocking buffer (2% (w/v) BSA in PBS) was added and incubated for 1 hour at room temperature or at 4°C overnight. Blocking buffer was removed without washing and primary antibody solutions (6.67 µg·mL^{-1} anti-villin polyclonal antibody, 4.33 µg·mL^{-1} anti-MUC2 polyclonal antibody diluted in PBS with 0.5% (w/v) BSA) were added maintaining the plate in incubation for 1.5 hours at room temperature. Blocking buffer was removed, inserts washed three times with cold PBS and fluorochrome-labelled secondary antibody (4 µg·mL^{-1} iFluor™ 594 IgG in PBS with 0.5% (w/v) BSA) was added. The plate was incubated for 1 hour at room temperature, avoiding samples to be exposed to light. After removing the secondary antibody and rinsing three times with PBS, phalloidin-iFluor™ 488 conjugate working solution (in PBS with 1% (w/v) BSA) was added, incubating the plate at room temperature for 1 hour, protected from light. The solution was removed, and the inserts were washed three times with PBS.

The membranes were cut with a scalpel blade, placed onto glass slides and mounted using 20 µL VECTASHIELD™ mounting medium with DAPI. Glass slides were sealed with varnish and stored at -20 °C protected from light.

Images were acquired using a Leica STELLARIS 5 confocal microscope and analysed using ImageJ.

II.5. Evaluation of the epithelial barrier integrity

II.5.1. Transepithelial electrical resistance (TEER)

The integrity of epithelial barriers was assessed by transepithelial electrical resistance (TEER) monitoring.

II.5.1.1. CDMs cultured in 24-well inserts

TEER was measured using an EVOM3™ epithelial Volt/Ohm meter with STX2-PLUS electrodes from World Precision Instruments (Sarasota, FL, USA). TEER was measured in 200 µL PBS in the apical side of transwell systems, and 700 µL in the basolateral side at each medium change and after 24 hours of incubation with inflammatory cytokines.

II.5.1.2. CDMs cultured in 96-well inserts

TEER was measured using an EVOM2™ epithelial Volt/Ohm meter with STX2 electrodes from World Precision Instruments (Sarasota, FL, USA). TEER was measured in complete IntestiCult™ OGM at each medium change and after 24 hours of incubation with IFN-γ.

TEER ($\Omega \cdot cm^2$) is the resistance of a unit area of 1 cm^2, and values were calculated by subtracting the readings of cell-free inserts from cell-cultured inserts and multiplying it by the surface area of the membrane (0.33 cm^2 for 24-well inserts, 0.14 cm^2 for 96-well inserts), according to *Equation 1:*

$$TEER\ (\Omega \cdot cm^2) = (cell\ resistance - blank\ resistance) \times insert\ surface\ area \quad [1]$$

In order to better understand the effect of cytokine exposure on the epithelial barrier integrity, relative TEER (%) was calculated according to *Equation 2*. TEER values after 24 hours of exposure to cytokines were normalised with TEER values at 0 hours. Vehicle-treated monolayers were used as control. Relative TEER (%) was calculated for monolayers derived from the same human colonic biopsies (HCB) under control and inflammatory conditions. The comparison between the relative TEER of control and inflammatory conditions was plotted and analysed.

$$Relative\ TEER\ (\%) = \frac{TEER_{24h} - TEER_{0h}}{TEER_{0h}} \times 100 \quad [2]$$

II.5.2. FITC-D4 apparent permeability

Paracellular permeability, and indirectly the epithelial barrier integrity, was evaluated through the determination of FITC-D4 apparent permeability coefficient (P_{app}).

Inserts were moved into a new 24-well plate and cells were washed three times with warm HBSS. The plate was incubated at 37 ºC for 15 minutes. HBSS was then removed and 200 µL of 5 $mg \cdot mL^{-1}$ FITC-D4 in HBSS were added to the apical side and 700 µL of HBSS were added to the basolateral side of CDMs previously exposed to vehicle or to inflammatory cytokines. The plate was then incubated at 37 ºC and 5% CO_2, for 2 hours. Transport was measured from the apical to the basolateral side (A→B). Samples of 200 µL were collected from the basolateral side every 30 minutes and, after every sample collection, 200 µL of fresh HBSS were added to the basolateral side. After 2 hours, samples were collected from both the apical (100 µL) and basolateral sides (200 µL). 50 µL of collected samples were transferred into a 96-well plate and the

fluorescence intensity was measured with an excitation and emission wavelengths of 485 and 550 nm, respectively.

Standard curves were generated using fluorescence intensity values (550 nm) from FITC-D4 standards (0-12 mg·mL^{-1}). The amount of FITC-D4 in both the apical and the basolateral side was quantified by interpolation of fluorescence intensity values (550 nm) on the standard curves (**Suppl. Fig. 1**).

The P_{app} (cm·s^{-1}) was calculated according to *Equation 3:*

$$P_{app}\ (cm \cdot s^{-1}) = \frac{V_r \times \Delta C_r}{\Delta t} \times \frac{1}{A \times C_0} \quad [3]$$

where V_r is the volume of the basolateral compartment (mL), $\Delta C_r/\Delta t$ is the change in substance concentration over time in the basolateral compartment (mg·mL^{-1} s^{-1}), A is the surface area of the insert (cm^2) and C_0 is the initial FITC-D4 concentration in the apical compartment (mg·mL^{-1}). This equation can be applied when the concentration in the receiver chamber does not exceed 10% of the concentration in the donor chamber, referred to as 'sink conditions'[77].

II.6. Evaluation of cytotoxic effects and cell viability

II.6.1. Lactate dehydrogenase (LDH) assay

Cytotoxicity was evaluated through the lactate dehydrogenase (LDH) assay. LDH is a cytosolic enzyme that catalyses the oxidation of lactate to pyruvate, using NAD^+ as a coenzyme reduced to NADH. Upon cell lysis, LDH is released into the culture media and therefore its quantification is an indirect measure of cytotoxicity. The amount of LDH in culture media is measured through a coupled enzymatic assay which results in the NADH-dependent reduction of a tetrazolium salt (substrate) to a red formazan product[78]. The CytoTox 96® Non-Radioactive Cytotoxicity Assay kit was used.

The content of LDH was determined in the supernatant of cytokine-stimulated CDMs (experimental), in vehicle-treated cells (spontaneous release of LDH), in medium (blank), and in lysed cells (maximum LDH release).

Briefly, cell culture media was collected and centrifuged at 250 rpm for 5 minutes. 50 µL of each sample were transferred to a 96-well plate and then the same volume of the substrate mix was added to each well and incubated at room temperature for 30 minutes. Finally, 50 µL of the stop-reaction solution were added to each well and absorbance was measured at 490 nm, with a reference wavelength at 690 nm. The absorbance values were proportional to the percentage of dead cells, calculated according to *Equation 4*:

$$Cytotoxicity\ (\%) = \frac{Abs_{experimental} - Abs_{spontaneous} - Abs_{blank}}{Abs_{maximum} - Abs_{spontaneous} - Abs_{blank}} \times 100 \quad [4]$$

II.6.2. MTT assay

Cell metabolic activity was assessed through the 3-[4,5-dimethylthiazol-2-yl]-2,5 diphenyl tetrazolium bromide (MTT) assay. MTT is reduced by succinate dehydrogenases into violet formazan crystals. In principle, the mitochondrial activity of viable cells is constant and therefore the amount of formazan produced is directly proportional to the number of metabolically active cells[79].

After cytokine exposure, CDMs were washed three times with PBS. 100 µL of 1 mg·mL^{-1} MTT was added to each insert and the plate incubated for 2 hours at 37 ºC and 5% CO_2. The reagent was removed and DMSO

was added to dissolve formazan crystals. After pipetting up and down to homogenize, the content of each well was transferred into a 96-well plate. The absorbance (Abs) at 550 nm was determined, with a reference wavelength at 450 nm.

Vehicle-treated cells (control - 100% metabolic activity) and cells exposed to 40% (v/v) DMSO for 1 hour (0% metabolic activity) were considered as negative and positive controls, respectively. Cellular metabolic activity values were expressed as percentage of vehicle-treated cells and calculated according to *Equation 5*:

$$Cell\ metabolic\ activity\ (\%) = \frac{Abs_{experimental}}{Abs_{control}} \times 100 \quad [5]$$

II.7. Quantification of NF-κB p65 levels

The activation of the NF-κB pathway was determined using the NF-κB p65 (Total/Phospho) Human InstantOne™ ELISA Kit.

Briefly, differentiated CDMs derived from 3 patients, were exposed to 25 ng·mL^{-1} TNF-α and 25 ng·mL^{-1} IFN-γ, on the apical and basolateral sides. After 24 hours of incubation, cells were lysed, and the cell lysate was stored at -80 ºC for later detection. The absorbance of phosphorylated NF-κB p65 was determined in triplicate at 450 nm. Vehicle-treated cells were used as a negative control.

II.8. Quantification of cytokine and chemokine secretion

The secretion of CCL20, IL-6 and IL-8 was quantified using a MIP-3α/CCL20 Human ELISA kit, a Human IL-6 ELISA Kit, and a Human IL-8/CXCL8 ELISA Kit, respectively.

Briefly, differentiated CDMs derived from 3-4 patients, were exposed to 25 ng·mL^{-1} TNF-α and 25 ng·mL^{-1} IFN-γ, on the apical and basolateral sides. After 24 hours of incubation, samples were collected from the basal side and stored at -80 ºC for later detection. The concentration of human CCL20, IL-6 and IL-8 was determined in triplicate and calculated after interpolation of the samples' absorbance in the respective calibration curves (**Suppl. Fig. 2**). Vehicle-treated cells were used as a negative control.

II.9. Drug permeability studies

II.9.1. Drug transport across CDMs exposed to TNF-α and IFN-γ

Inserts were placed in a new 24-well plate and CDMs (previously exposed to vehicle or to 25 ng·mL^{-1} TNF-α and 25 ng·mL^{-1} IFN-γ) were washed twice with warm HBSS. Then, the plate was pre-incubated at 37 ºC for 15 minutes. After the pre-incubation, the buffer was removed and 200 µL of 10 µM atenolol, propranolol, budesonide or celecoxib (in HBSS 1% DMSO) were added to the apical side of the respective wells and 700 µL of HBSS were added to the basal side. The plate was then incubated at 37 ºC and 5% CO_2, for 2 hours. Transport was measured from the apical to the basolateral side (A→B). Samples of 200 µL were collected every 30 minutes from the basal side, and the same volume of fresh HBSS was immediately replaced. After 2 hours, samples were collected from both the apical (100 µL) and basal sides (200 µL). Collected samples were stored at -20 ºC for later detection by HPLC-MS/MS.

The P_{app} (cm·s^{-1}) of each compound was calculated according to *Equation 3* where V_r is the volume of the basolateral compartment (L), $\Delta C_r / \Delta t$ is the change in substance concentration over time in the basolateral compartment (nM·s^{-1}), A is the surface area of the insert (cm^2) and C_0 is the initial compound concentration in the apical compartment (nM).

II.9.1.1. HPLC-MS/MS conditions for compound quantification

Thanks to the collaboration with Professor Vacondio of the Medicinal Chemistry - Pharmaceutical Analysis group of the Department of Food and Drug, an Accela 1250 HPLC system (Thermo, USA) coupled with a TSQ Quantum Access Max Triple Quadrupole mass spectrometer (Thermo, USA), with a heated electrospray (H-ESI) ion source was used for compound quantification.

The HPLC column used was a Waters Xselect HSS T3 (100 x 2.1 mm, 3.5 µm; Waters, USA). Mobile phases A and B were acetonitrile and ultra-pure water, both containing 0.1% (v/v) formic acid. Different compounds were eluted employing a linear gradient: 0-1 minute: 5% A; 1-6 minutes: 5-100% A; 6-8 minutes: 100% A; 8.5 minutes: 100-5% A; 8.5-10 minutes: 5% A. Total run time: 10 minutes. For the elution of beclomethasone dipropionate and hydrolytic metabolites the following linear gradient was used: 0-1 minutes: 5% A; 1-6 minutes: 5-100% A; 6-8 minutes: 100% A; 8-8.5 minutes: 100-5% A; 8.5-10 minutes: 5% A. Flow rate: 0.22 mL/minute; injection volume: 10 µL.

Instrumental parameters were set as follows: ion source voltage: 4000 V (ESI^+); 3000 V (ESI^-); capillary temperature: 270 °C; vaporizer temperature: 250 °C; sheath gas (N_2): 35 psi; auxiliary gas (N_2): 15 psi; collision gas (Ar) pressure: 1.5 mtorr. Xcalibur software version 2.2 (Thermo, USA) was used for both data acquisition and processing.

Mass spectrometer operated both in positive ion (ESI^+) and in negative ion mode (ESI^-) and in Multiple Reaction Monitoring (MRM) acquisition. Tube lens (TL) and collision energies (CE) voltages were optimized for each compound by Flow Injection Analysis (FIA) starting from 10 µM solutions in MeOH. Atenolol: *m/z* = 267.2 $[M+H]^+ \rightarrow$ *m/z* = 225.1, 190.1, 145.2 (TL = 91 V; CE = 13, 16, 24 eV, respectively); budesonide: *m/z* = 431.2 $[M+H]^+ \rightarrow$ *m/z* = 413.3, 225.1, 147.2 (TL = 101 V; CE = 9, 22, 27 eV); celecoxib: *m/z* = 380.1 $[M-H]^- \rightarrow$ *m/z* = 316.2, 276.2, 179.1 (TL = 105 V; CE = 24, 30, 32 eV); propranolol: *m/z* = 260.1 $[M+H]^+ \rightarrow$ *m/z* = 183.1, 155.1, 116.2 (TL = 88 V; CE = 14, 15, 24 eV); corticosterone (internal standard): *m/z* = 347.1 $[M+H]^+ \rightarrow$ *m/z* = 329.1, 121.1, 105.1 (TL = 106 V; CE = 13, 24, 32 eV).

Calibration curves for each compound were prepared by spiking cell medium with standard solutions of each compound prepared in DMSO, maintaining a final DMSO content in samples of 1% (v/v). Calibration curves were set in the 10,000 nM-10 nM concentration range, spanning three orders of magnitude. Coefficients of determinations (R^2) were >0.99 for all regression lines. The accuracy of calibration standards was considered acceptable within ± 15% (± 20% at the LLOQ) of the nominal concentrations, while precision, expressed as percent relative standard deviation (%RSD), had to be <15% (<20% at the LLOQ). Examples of calibration curves and related linear regression equations for the four tested reference compounds are reported in **Suppl. Fig. 3**.

II.9.2. Drug transport across CDMs exposed to IFN-γ

CDMs, previously exposed to vehicle or to 25 $ng \cdot mL^{-1}$ IFN-γ, were washed three times with HBSS supplemented with 10 mM HEPES. Cells were pre-incubated with transport medium containing 5 µM elacridar, P glycoprotein (P-gp) inhibitor, and/or 0.5% (v/v) DMSO, for 30 minutes. The transport medium was then removed and 150 µL of 1 µM [^{3}H]-atenolol, [^{3}H]-propranolol, [^{3}H]-digoxin (with and without 5 µM elacridar) and [^{3}H]-cimetidine were added to the apical side. 150 µL of transport medium were added to the basolateral side. The plate was then incubated at 37ºC and 5% CO_2, for 2 hours. Transport was measured from the apical to the basolateral side (A→B). Samples of 50 µL were collected from the basal side every 30 minutes and, after every sample collection, the same volume of fresh transport media was added to the basolateral side. After 2

hours, samples were collected from both the apical and basal sides. Compound concentration was determined by liquid scintillation counting.

[^{14}C]-mannitol was used as a leakage marker and was added to each well. Only wells that showed mannitol $P_{app} < 3.0 \times 10^{-6}$ cm·s^{-1} were taken into consideration in the study[80].

The P_{app} (cm·s^{-1}) of each compound was calculated according to *Equation 3* where V_r is the volume of the basolateral compartment (mL), $\Delta C_r/\Delta t$ is the change in substance concentration over time in the basolateral compartment (dpm·mL^{-1}·s^{-1}), A is the surface area of the insert (cm^2) and C_0 is the initial compound concentration in the apical compartment (dpm·mL^{-1}).

II.10. Statistical analysis

Results are reported as mean ± standard deviation. The statistical analysis was performed using GraphPad Prism 9.0.0 (San Diego, CA, USA). The Shapiro-Wilk test was used to verify if the data followed a normal distribution. The *p* values were determined using a two-tailed Student's t-test and a one-way or two-way analysis of variance (ANOVA) followed by Tukey's, Sídák's or Bonferroni's multiple comparison post-test. The *p* values were reported with asterisks: $^{*,\#}p \leq 0.05$; $^{**,\#\#}p \leq 0.01$; $^{***,\#\#\#}p \leq 0.001$.

CHAPTER III. RESULTS AND DISCUSSION

Modelling the intestinal epithelium is essential to improve our understanding of the cellular mechanisms underlying the pathophysiology of IBD, as well as the processes of drug absorption and transport. Traditionally, the Caco-2 cell line has been used as the standard *in vitro* model due to its high proliferation rate[81]. However, having been isolated from a human colorectal adenocarcinoma, these immortalised cells exhibit an altered phenotype characterised by the absence of critical signalling pathways, receptors, and transporters[82]. Preclinical animal models are biologically more complex, but there is often a lack of translation of data from these models into humans, likely due to species-specific differences. Besides, animal models are not amenable to high-throughput studies.

Recently, human intestinal organoids have been considered more physiologically relevant than traditional models due to their ability to closely mimic the molecular and cellular phenotype of human tissue[83]. By bridging the gap between scalability and translatability, human intestinal organoids can provide value insights into the mechanisms governing the onset of IBD.

Given the ultimate goal of studying anti-inflammatory effects and drug transport across a model of IBD that is physiologically relevant, human intestinal organoid cultures were established. Specifically, human colonoid cultures were chosen due to their relevance to both CD and UC.

III.1. Establishment of human colonoid cultures

III.1.1. Optimization of culture conditions

Initially, colonic crypts isolated from biopsies of healthy patients were embedded in a 50% (v/v) mixture of either Matrigel® or Cultrex™ combined with ice-cold Advanced DMEM/F12, 1x P/S, and 1% (w/v) BSA. However, Matrigel® has been shown to provide superior support for colonoid development. To further improve colonoid expansion, the amount of Matrigel® was increased to 70% (v/v). In addition, improvements in colonoid formation were observed when Matrigel® was mixed directly with medium instead of seeding crypts in Advanced DMEM/F12 with 1x P/S and 1% (w/v) BSA.

Another aspect that was optimized was the colonoid expansion medium, necessary to ensure propagation. Starting from the recipe based on Pleguezuelos-Manzano *et al.*, 2020[84], different compositions were tested and the one that led to cultures with the highest yield of colonoids is shown in **Table 3**. The three proteins chosen for optimization were Wnt-3A, R-spondin1 (R-spo1), and noggin, essential growth factors critical for maintaining stemness and promoting stem cell propagation[85]. Initially, R-spo1-conditioned media produced in-house by Cultrex® HA-R-Spondin1-Fc 293T cells and noggin recombinant protein or noggin-conditioned medium were used at different concentrations and combinations. After various attempts, to limit the experimental variables and despite the higher costs associated, it was decided to use only commercial R-spo1 recombinant protein instead of the conditioned media produced in-house. On the contrary, the commercial noggin-conditioned medium and Wnt-3A-conditioned medium produced in-house were considered suitable to produce sufficient growth of colonoids (data not shown). Wnt-3A-conditioned media was used as fresh as possible and not older than two months.

However, even after the optimization attempts, the colonoid expansion medium showed not to provide sufficient support for recovery after colonoid passage. The use of the in-house medium was discontinued and, instead, IntestiCult™ Organoid Growth Medium (OGM) provided by STEMCELL™ Technologies was used from

there onwards (**Fig. 13**). Several human colonoid lines were successfully established from freshly isolated crypts which proves the reproducibility of the methodologies used.

Table 3. Composition of colonoid expansion medium produced in-house (based on Pleguezuelos-Manzano *et al.*, 2020[84]).

Components	Final Concentration	Supplier
Adv. DMEM^{+++} (+ 1x GlutaMAX + 10 mM HEPES + 1x Anti-Anti)	-	Gibco (Walthalm, MA, USA)
Wnt-3A conditioned medium produced in-house	50% (v/v)	L Wnt-3A (ATCC® CRL-2647™) cell line
R-spondin1	1 µg·mL^{-1}	Peprotech (London, UK)
Noggin-Fc fusion protein conditioned medium	2% (v/v)	ImmunoPrecise (Utrecht, Netherlands)
N-2 supplement (100x)	1x	Gibco (Walthalm, MA, USA)
B-27™ supplement (50x)	1x	Gibco (Walthalm, MA, USA)
N-Acetyl-L-cysteine	1 mM	Sigma-Aldrich (St. Louis, MO, USA)
Nicotinamide	10 mM	Sigma-Aldrich (St. Louis, MO, USA)
Human epidermal growth factor (EGF)	50 µg·mL^{-1}	Sigma-Aldrich (St. Louis, MO, USA)
Human gastrin I	10 nM	Bachem (Bubendorf, Switzerland)
Prostaglandin E2 (PGE2)	10 nM	MedChemExpress (NJ, USA)
Galunisertib (LY2157299)	0.5 µM	MedChemExpress (NJ, USA)
SB202190	10 µM	MedChemExpress (NJ, USA)
Rho-KI (Y-27632) **only added at the time of seeding*	10 µM	MedChemExpress (NJ, USA)

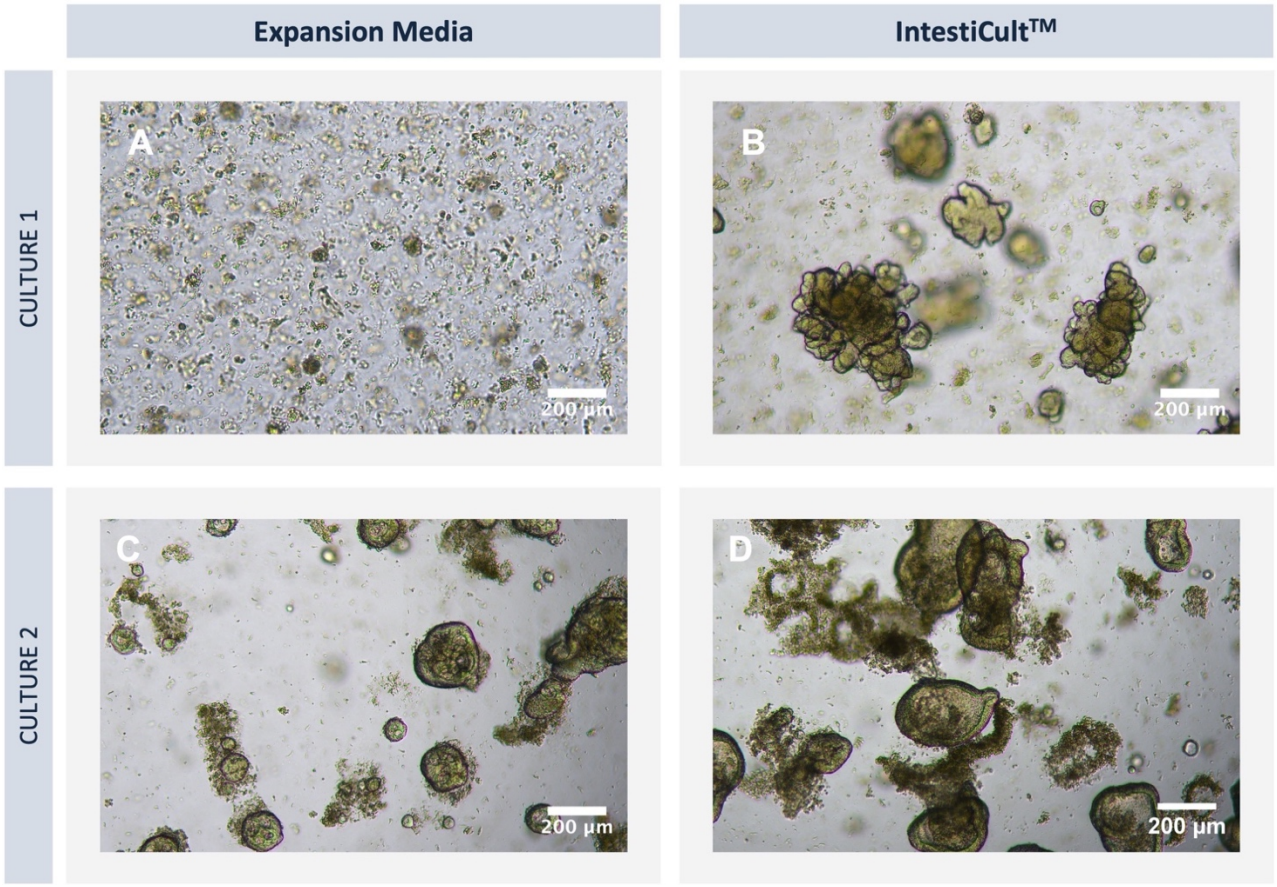

Figure 13. Optical microscopy images of colonoids obtained from single cells (A, B) and crypt fragments (C, D) in expansion media produced in-house and IntestiCult™ Organoid Growth Medium (OGM). Colonoid yield is higher with IntestiCult™ OGM.

III.1.2. Human colonoid culture

Human colonoids were established from adult stem cells located at the bottom of intestinal crypts. Briefly, colonic biopsies were collected from the descending colon of 6 healthy patients. Details related to patient's demographics and sample characteristics can be found in **Table 2**. Human intestinal crypts were isolated from freshly collected biopsies both mechanically, by shaking them vigorously in the buffer, and chemically, by using a dissociation buffer containing a chelating agent (EDTA) and a reducing agent (DTT). The isolated crypts were resuspended in 70% (v/v) Matrigel® and 30% (v/v) ice-cold complete IntestiCult™ OGM and dome cultures were established, as shown in **Fig. 14B**. Once seeded, human colonic crypts start to swell (**Fig. 14C**) and after a few days, colonoids with mixed morphologies were generated: colonoids with crypt-like structures (**Fig. 14D, E**) and cystic-like colonoids (**Fig. 14D**).

Complete IntestiCult™ OGM promotes the growth of adult stem cells found at the base of intestinal crypts seeded in Matrigel®. However, in addition to stem cells, crypts are composed of several other cell types. The development of crypt-like protrusions is thought to result from the incorporation of terminally differentiated cells that contribute to the formation of differentiated-type colonoids. Notably, these crypt-like structures tend to diminish with successive passages, resulting in a predominance of cystic-like colonoids, as seen in **Fig. 15**.

In **Fig. 14D**, colonoids are notably darker when compared to **Fig. 14C.** Over time, debris, possibly including cellular metabolic by-products and apoptotic cells, accumulate in the core, darkening the colonoids. This is a reliable indicator that they require passaging[86].

ICC has provided further insights into the cellular organisation. Colonoids were stained for F-actin (phalloidin, green) and nucleus (DAPI, blue). Proliferative cells were marked with anti-Ki67 (red). **Fig. 16** shows that F-actin had a stronger signal in the centre of colonoids. F-actin is the most abundant component of the cytoskeleton and, therefore, F-actin staining shows the delimitation of cells. Consequently, the signal intensifies on the side where microvilli are present[87]. The enhanced signal within the colonoid inner side suggests that cells are oriented inwards, leading to the conclusion that the generated colonoids exhibit a basal-out polarity. ICC images also showed that colonoids were mainly delimited by proliferative cells and that their centre was depleted of cells.

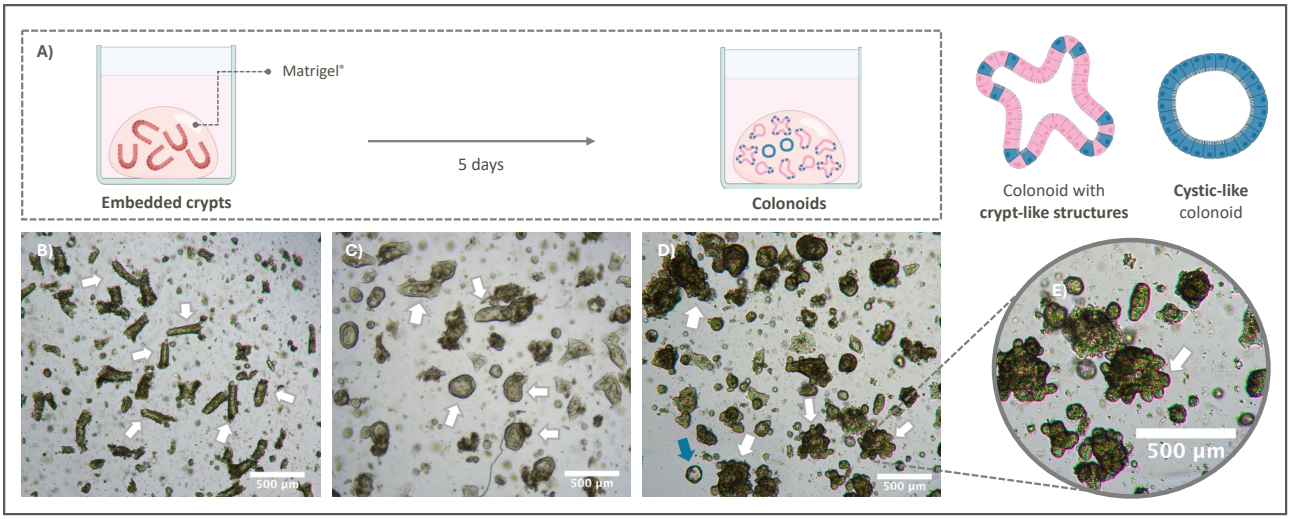

Figure 14. Establishment of human colonoids in dome cultures. A) Schematic representation of the establishment of dome cultures. **B)** Crypts isolated from human colonic biopsies #43 (HCB43) embedded in Matrigel®, at day 0. **C)** Swollen crypts, at day 2. **D)** Human colonoids with mixed morphologies, at day 5. Colonoids with crypt-like structures highlighted with white arrows and a cystic-like colonoid highlighted with a blue arrow. **E)** Colonoid with crypt-like structures in detail.

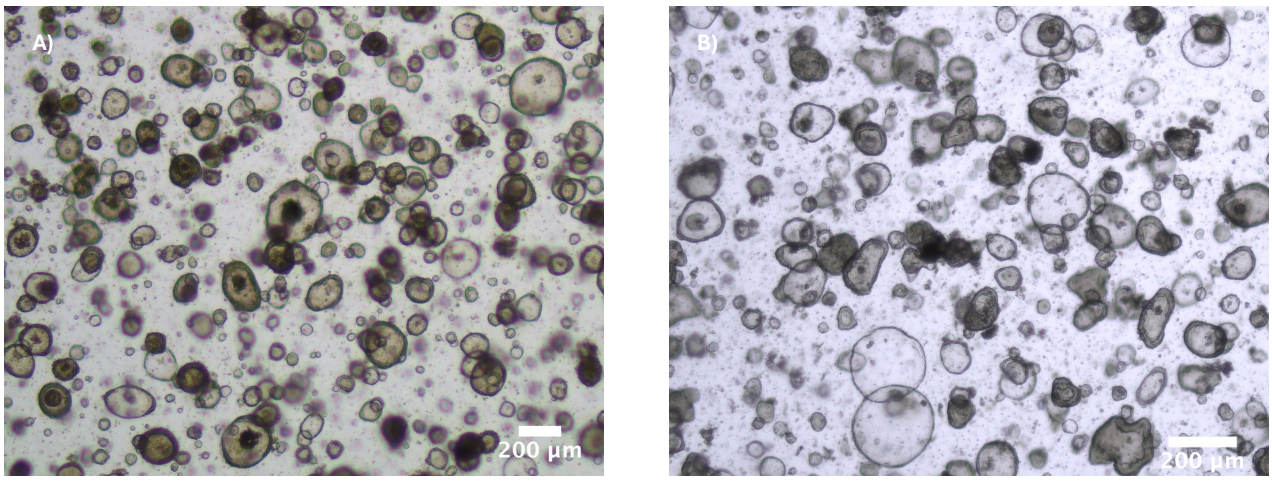

Figure 15. Optical microscopy images of cystic-like colonoids derived from human colonic biopsies #43 (HCB43). **A)** Colonoids at passage 2 after 7 days in culture. **B)** Colonoids at passage 4 after 7 days in culture.

Expansion in Matrigel® domes presents some technical challenges that can hinder long-term expansion and scalability. Colonoid growth in domes is constrained by oxygen and nutrient delivery as well as stress accumulation[88]. Consequently, frequent passaging is required to maintain the cultures. This is particularly problematic due to culture-associated epigenetic and phenotypic changes that may occur, including DNA methylation and cell senescence[89]. Additionally, the preparation and handling of solid matrices increases the complexity of colonoid cultures, hampering high-throughput applications.

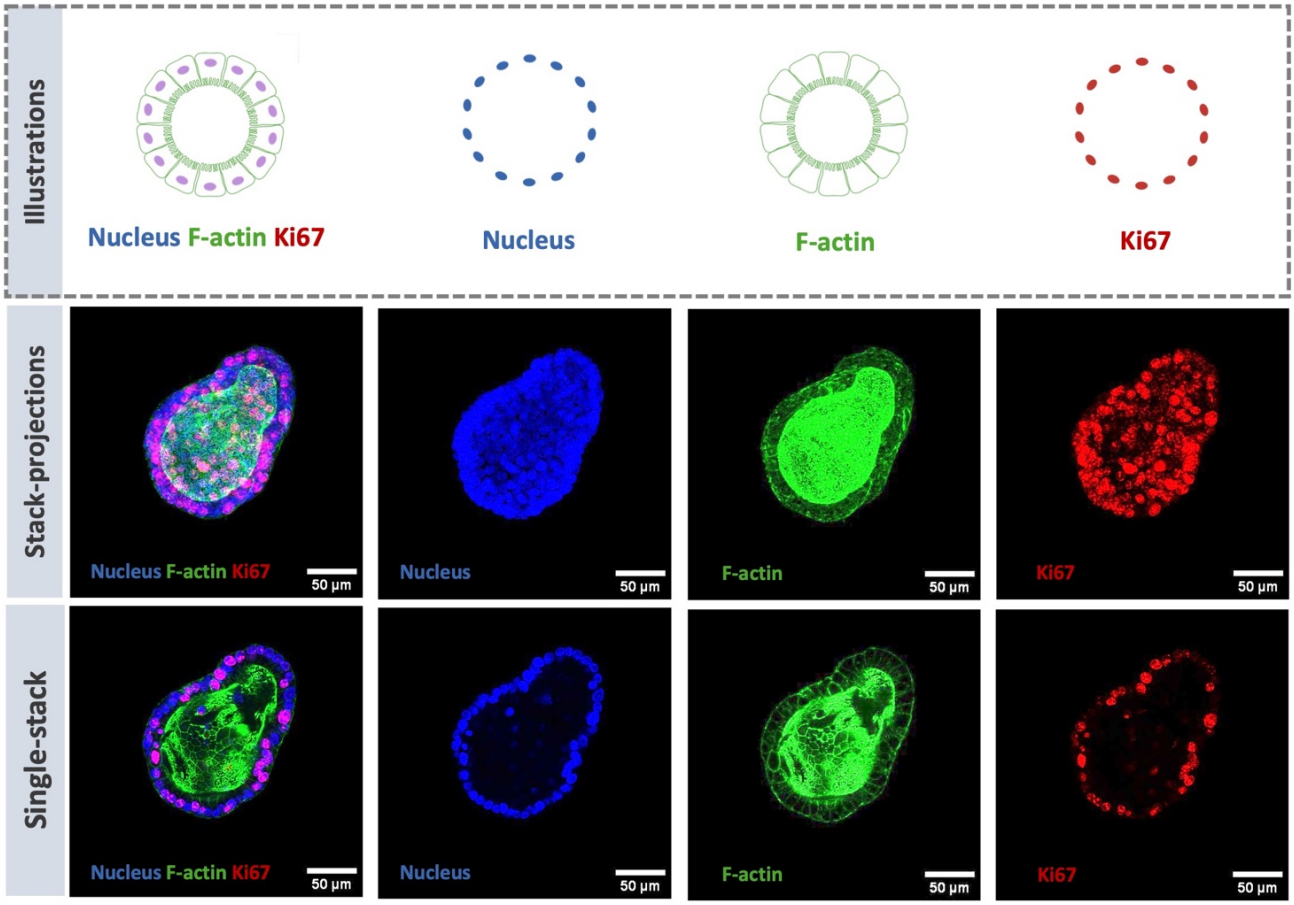

Figure 16. Confocal images of a cystic-like human colonoid. Cells were stained for F-actin (phalloidin, green) and nucleus (DAPI, blue). Proliferative cells were marked with anti-Ki67 (red). Images show the overall 3D structure of colonoids and their basal-out polarity. Colonoids were mainly delimited by proliferative cells and their centre was depleted of cells.

A novel culture technique, first described by STEMCELL™ Technologies, facilitated the expansion scale-up. Colonoids were grown in a Matrigel® cloud suspended on 3 mL of complete IntestiCult™ OGM. In **Fig. 17**, colonoids grown in dome (**A**) were compared to suspension cultures (**B**), illustrating that suspension cultures were more effective for colonoid expansion. This method enhances accessibility to oxygen and nutrients, prevents the accumulation of stress, and extends the duration between passages.

Following confirmation of this technique's reproducibility, suspension cultures became the standard method for expanding human colonoids throughout the project.

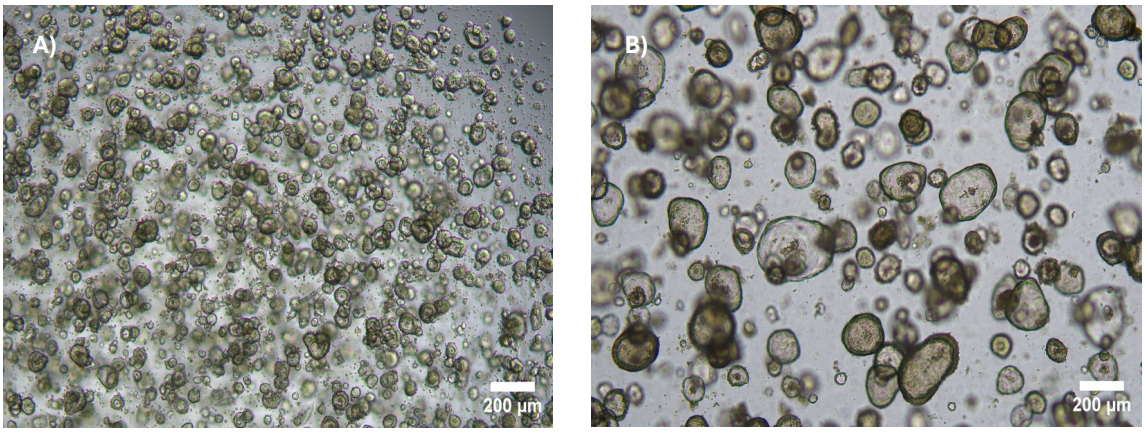

Figure 17. Dome vs Suspension culture. Human colonoids derived from human colonic biopsies #37 (HCB37) culture in (**A**) dome and (**B**) suspension.

III.2. Establishment of human colonoid-derived monolayers

One of the key features of organoids is their ability to replicate the structural complexity of an organ. However, their 3D confined geometry limits access to the apical side of the cells, making them unsuitable for transport studies across epithelial barriers[90]. Organoid microinjection or cell polarity reversal protocols have been used to access the luminal side or to expose the apical side to culture conditions, respectively[87,91]. Yet, these approaches are technically demanding and difficult to reproduce consistently, limiting their practical application.

Alternatively, organoid-derived cells can be seeded onto permeable supports (inserts), allowing monolayers to be formed and providing straightforward access to both apical and basolateral compartments. Within this setup, cells can be further differentiated into various epithelial populations, thereby recreating physiologically relevant phenotypes. To develop a relevant IBD *in vitro* model, suited for drug screening and transport studies, colonoid-derived monolayers (CDMs) were first established. Several culture conditions were tested to optimize cell proliferation and differentiation (**Suppl. Fig. 4)**. Inserts were coated with collagen 10 $\mu g \cdot cm^{-2}$, Matrigel® 1:50 and Cultrex 1:50. Uncoated inserts were used as controls. While uncoated inserts were unsuitable to establish monolayers, tight epithelial barriers were formed on coated inserts, regardless of the coating type (**Suppl. Fig. 4A**). As demonstrated previously, colonoids are predominantly composed of proliferative cells. Since the goal was to obtain a physiologically relevant epithelial population, cell differentiation had to be supported. To this end, monolayers were cultured in a) IntestiCult™ OGM switching to ODM upon confluence or b) IntestiCult™ ODM only. TEER values for monolayers cultured in ODM alone were significantly higher than those cultured in both OGM and ODM, as shown in **Suppl. Fig. 4B**. However, these values exceed physiological levels, which may lead to an underestimation of paracellular transport. Air-liquid interfaces (ALI) have been suggested to promote cell proliferation and differentiation[92]. ICC images showed in **Suppl. Fig. 4C and D** confirmed that exposing epithelial cells to air increases cell differentiation and mucus production. Still, this rise in the number of differentiated cells may have led to a weakening of the tight junctions, explaining the observed decrease in TEER values.

Ultimately, colonoids were enzymatically and mechanically dissociated into single cells and seeded at $7.5x10^5$ $cells \cdot cm^{-2}$ onto 24-well inserts coated with Matrigel®. The epithelial barrier integrity was monitored by TEER measurements. CDMs were successfully established from six colonoid lines, identified by the ID of the biopsies from which they were derived, as reported in **Table 4**. Colonoids were dissociated and seeded between passages 4 and 15 and confluence was reached between day 4 and 9. Optical microscopy images from monolayers derived from HCB25 are shown in **Fig. 18** as an illustration of the establishment of CDMs.

Table 4. Properties of human colonoid-derived monolayers (CDMs) later exposed to inflammatory conditions. 6 colonoid lines were used to established CDMs and identified by the ID biopsies from which they were derived (HCB). Monolayers were seeded between passages 4 and 15, and confluence was reached between day 4 and 9.

Biopsies ID	Passage #	Confluence
HCB25	Passage 15	Day 4
HCB29	Passage 9	Day 7
HCB31	Passage 11	Day 7
HCB37	Passage 7	Day 9
HCB43	Passage 4	Day 4
HCB48	Passage 5	Day 4

HCB: Human colonic biopsy.

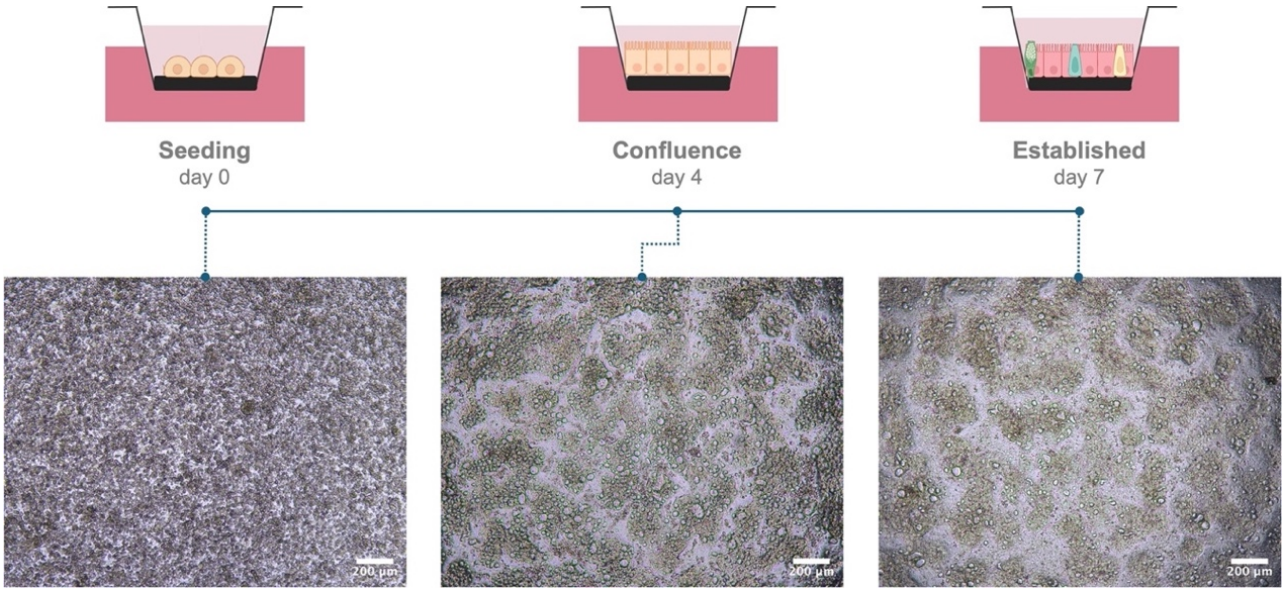

Figure 18. Optical microscopy images throughout the establishment of colonoid-derived monolayers (CDMs) from human colonic biopsies #25 (HCB25).

IntestiCult™ OGM was switched to ODM at confluence, typically when TEER values were higher than 100 Ω·cm^2: this moment varied from donor to donor and ranged from day 4 to day 9.

Figure 19 shows that CDMs developed into robust epithelial barriers, with TEER values increasing over time, indicating that tight junctions were formed, and cells were polarized[93]. TEER values reached an average of 459.69 ± 85.19 Ω·cm^2, on the last day of culture. These values are well within the range reported in the literature, which spans from 209 to 1100 Ω·cm^2 for colonoid-derived monolayers from the ascending and sigmoid regions[55,64,94]. When compared to the TEER values of *ex vivo* colonic tissues, obtained from Üssing chambers, which range from 300 to 400 Ω·cm^2 and are considered to be the most physiologically relevant, the established monolayers effectively mimicked a tight epithelial barrier[95].

Human CDMs not only developed into relevant epithelial barriers, but also captured donor-to-donor variability as evidenced by the different growth profiles obtained from patient to patient. Having confirmed the suitability of this model, the CDMs were characterised under inflammatory conditions.

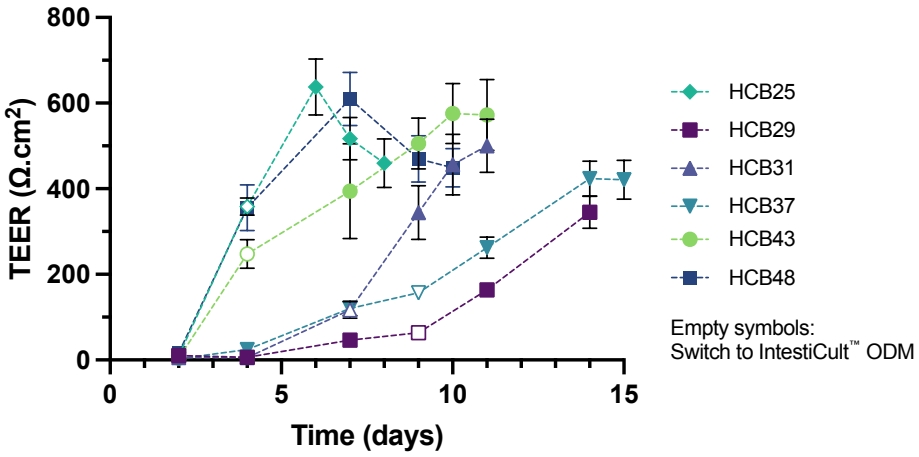

Figure 19. **Growth profile of colonoid-derived monolayers (CDMs).** Transepithelial electrical resistance (TEER) values increased over time. The days in which monolayers reached confluence (TEER ≥ 100 Ω·cm^2), and consequently medium was switched from IntestiCult™ organoid growth media (OGM) to organoid differentiation media (ODM), is highlighted by empty symbols. Values show mean ± standard deviation. HCB: human colonic biopsies.

III.3. Functional and morphological characterization of colonoid-derived monolayers exposed to TNF-α and IFN-γ

IBDs are chronic, relapsing diseases characterised by intestinal inflammation and epithelial injury. While it remains uncertain whether it is a cause or a consequence in IBD pathogenesis, the disruption of tight junctions leads to loss of mucosal barrier integrity. This breach, in turn, allows luminal contents to infiltrate, subsequently triggering a sustained immune response mediated by the activation of immune cells[96].

Two approaches are commonly used to mimic intestinal inflammation *in vitro*: (i) co-culturing intestinal epithelial cells with mucosal immune cells or (ii) exposing intestinal epithelial cells to pro-inflammatory mediators[97]. Despite providing valuable insights into epithelial-immune cell crosstalk, the first approach is technically challenging and adds variability to an already complex system. The second strategy focuses on the effect of immune cell-derived cytokines or immunostimulatory microbial components on cell survival and behaviour.

In order to establish reproducible inflammatory conditions, human CDMs were exposed to 25 ng·mL^{-1} TNF-α and 25 ng·mL^{-1} IFN-γ for 24 hours, in the apical and basolateral sides. The cytokine concentrations selected were in the mid-range based on values reported in the literature[49,50,53–55,58–60,62–64,66,98]. CDMs in the absence of cytokines were used as a control.

Increased levels of cytokines, including TNF and IFNs, are a common feature of the chronic immune response in IBD[99]. TNF levels are markedly increased in the serum and inflamed tissue of IBD patients[100]. The pro-inflammatory effects of TNF are thought to be initiated by its binding to the TNFR1 and TNFR2 receptors, which subsequently activates NF-κB intracellularly. TNF signalling may cause cell death, increased angiogenesis, production of matrix metalloproteases and the activation of macrophages and effector T cells[96]. Type II IFN (or IFN-γ) is a multifunctional cytokine also highly up-regulated in the mucosa of IBD patients. IFN-γ may sustain inflammation through its immunoregulatory function in the differentiation and activation of macrophages and effector T cells[101].

Human CDMs under inflammatory conditions were extensively characterised both morphologically and functionally prior to transepithelial drug transport studies.

III.3.1. Cell differentiation and morphology

CDMs exposed to TNF-α and IFN-γ were fixed and stained for F-actin with fluorescent-conjugated phalloidin and the nucleus with DAPI. Microvilli were marked with anti-villin. Villin is a cytoskeletal protein that is predominantly found in the microvilli of intestinal epithelial cells. Mature epithelial cells develop a well-defined brush border fundamental for absorption[102]. Goblet cells and mucus were stained with anti-MUC2. MUC2 is secreted by goblet cells and is the major component of the colonic mucus layer[103]. Confocal microscopy images of CDMs obtained from HCB43 are shown in **Fig. 20** as an illustrative example. Images of one of the remaining CDMs can be found in the **Suppl. Fig. 5**.

Under control conditions, images showed that a well-organized epithelial barrier was formed. Staining for villin and F-actin highlighted the formation of the brush border, demonstrating that the cells were both polarised and differentiated (**Fig. 20A**). Exposure to cytokines reduced the thickness of the monolayers in some areas. The lower villin levels in CDMs under inflammatory conditions suggest that cell polarisation and differentiation were adversely affected (**Fig. 20B**). MUC2 was less expressed compared to control conditions, suggesting a reduction in mucus production and subsequent depletion of goblet cells (**Fig. 20C, D**). Cytokines also appeared to have an effect on cell survival, as higher numbers of apoptotic cells were found near the basolateral side of

the monolayers, as evidenced by chromosome condensation and fragmentation with DAPI staining (white arrows in **Fig. 20B, D**).

The decrease in villin and MUC2 expression[58], the changes in cell morphology[49] and the depletion of goblet cells[60,61] have been previously described for human *in vitro* models of IBD. However, to the best of our knowledge, these findings have not been demonstrated in human CDMs. The changes in cell morphology and differentiation, namely barrier dysfunction and reduction of goblet cells and mucus production, caused by cytokine exposure, are consistent with the changes seen in endoscopic and histological images of tissue from patients with IBD[35].

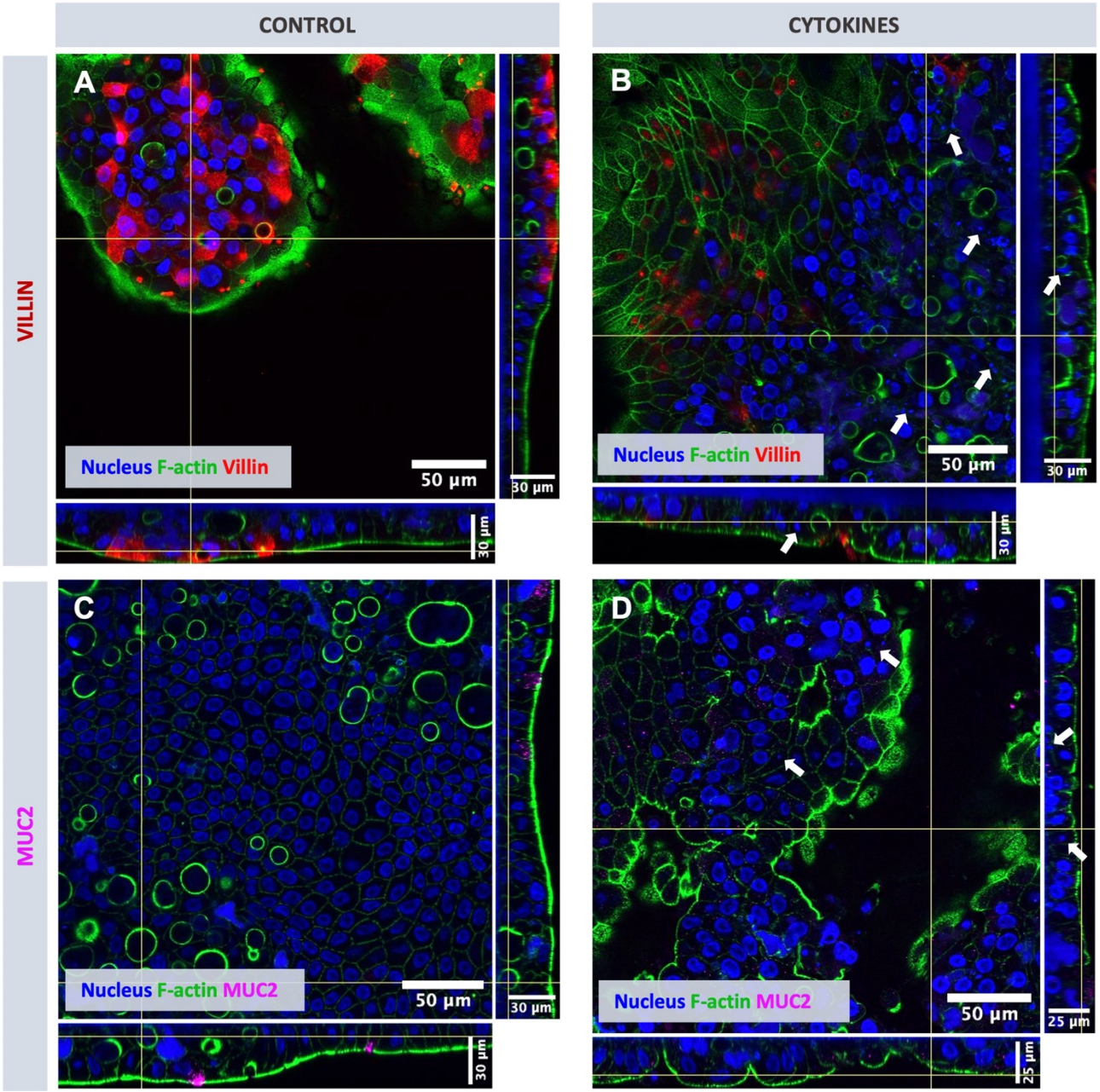

Figure 20. Confocal microscopy images of colonoid-derived monolayers (CDMs) in the absence (control) (A, C) and presence of 25 ng·mL^{-1} TNF-α and 25 ng·mL^{-1} IFN-γ (cytokines) (B, D) on the apical and basolateral sides for 24h. Cells were stained for F-actin (Phalloidin, green) and the nucleus (DAPI, blue). Microvilli were marked with anti-Villin (red). Goblet cells and mucus were stained with anti-MUC2 (magenta). White arrows show examples of chromosome condensation and fragmentation. CDMs obtained from human colonic biopsies #43 (HCB43).

III.3.2. Barrier integrity

The integrity of the gut epithelial barrier was assessed through TEER measurements and as changes of FITC-D4 permeability. The TEER of CDMs was monitored at timepoint 0 and after 24 hours of exposure to cytokines. In the absence of cytokines, TEER values did not significantly change during this interval, except for monolayers obtained from HCB29, in which case there was a significant increase (**Fig. 21A**). In **Fig. 21B,** TEER values at 24h were normalized with respect to TEER values at 0 hours and showed that cytokine exposure impaired significantly the barrier integrity except for monolayers obtained from HCB31.

Regarding the changes in FITC-D4 permeability (**Fig. 22**), Papp values of FITC-D4 for CDMs obtained from HCB25 and HCB37 under inflammatory and non-inflammatory conditions were lower than $3.5x10^{-6}$ cm·s^{-1} (**Fig. 22**). This confirms that the monolayers maintained their barrier function and were not leaky[80]. On the contrary, for CDMs obtained from HCB43, Papp values were higher than $3.5x10^{-6}$ cm·s^{-1} even in the absence of cytokines, which could have indicated that monolayers were leaky. This was contradicted by the high TEER values (478.61± 79.11 cm·s^{-1}), measured at the end of the transport study in control conditions, suggesting that the epithelial barrier was maintained. On the other hand, cytokine exposure led to a significant increase of FITC-D4 Papp, demonstrating the disrupting action of inflammatory mediators on the epithelial integrity (**Fig. 22**).

Despite the significant difference in TEER values between inflamed and non-inflamed conditions, there was no difference in Papp values of FITC-D4 for CDMs obtained from HCB25 and HCB37, contrary to what was expected. This may be due to a higher sensitivity of the TEER monitoring technique compared to the FITC-D4 assay, and to the fact that TEER values reflect the permeability to ions while the permeability to FITC-D4 mirrors the passage of non-charged molecules.

The negative impact of cytokine exposure on epithelial barrier integrity, either as a function of TEER or paracellular permeability measurements, is well described in the literature[54,55,59,60,63,64]. However, the lack of standardised protocols for establishing *in vitro* models based on organoids and reproducing intestinal inflammation limits direct comparisons. A similar study in which colonoid-derived monolayers were also exposed to a combination of TNF-α and IFN-γ (25 ng·mL^{-1}), for 48 hours and only in the basolateral compartment, showed no significant effect of cytokine exposure on the barrier integrity expressed as TEER changes[54].

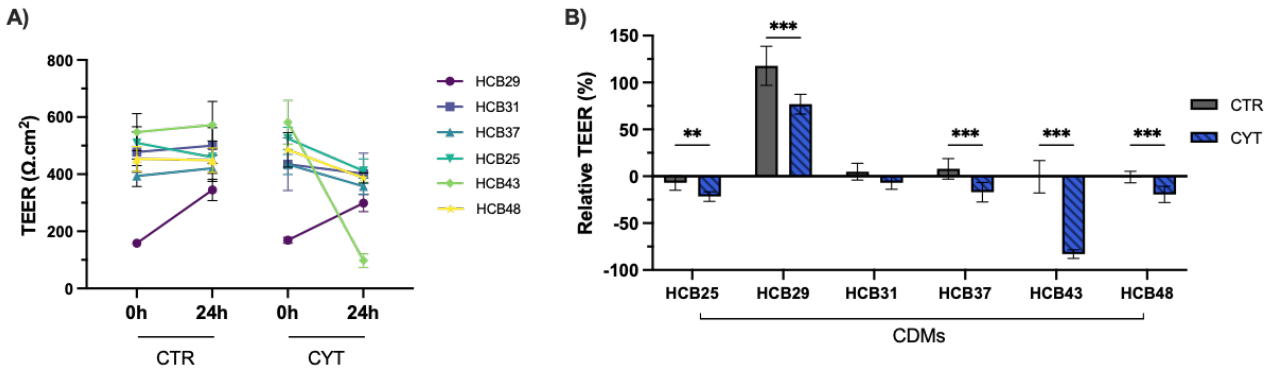

Figure 21. Transepithelial electrical resistance (TEER) values of colonoid-derived monolayers (CDMs) after 24h exposure to vehicle (CTR) or to 25 ng·mL^{-1} TNF-α and 25 ng·mL^{-1} IFN-γ (CYT). **A)** TEER values (Ω·cm^2) at 0h and 24h. **B)** TEER relative (%) to the timepoint 0h. Values are reported as mean ± standard deviation. The Shapiro-Wilk test was used to verify if the data followed a normal distribution. *p* values were determined using a two-way analysis of variance (ANOVA) followed by Sídák's multiple comparison post-test (**$p \leq 0.01$; ***$p \leq 0.001$). HCB: human colonic biopsies.

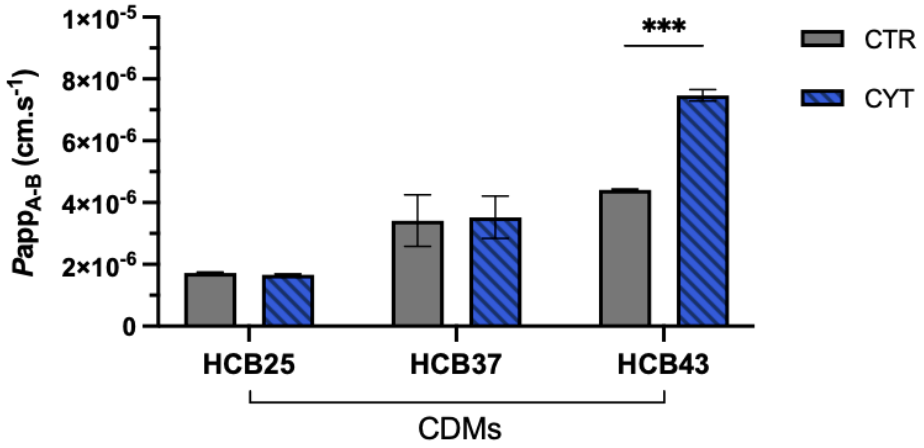

Figure 22. FITC-D4 apparent permeability of colonoid-derived monolayers (CDMs) in the absence (CTR) and presence of 25 ng·mL^{-1} TNF-α and 25 ng·mL^{-1} IFN-γ, for 24h (CYT). Results are reported as mean ± standard deviation. The Shapiro-Wilk test was used to verify if the data followed a normal distribution. *p* values were determined using a two-way analysis of variance (ANOVA) followed by Bonferroni's multiple comparison post-test (***$p \leq 0.001$). HCB: human colonic biopsies.

III.3.3. Cytotoxicity and cell metabolic activity

To better understand the potential adverse effects of inflammatory cytokines on gut epithelial cells, LDH and MTT assays were performed. In **Fig. 23**, LDH released from CDMs under inflammatory conditions was normalised to the LDH release from lysed cells (100%) and corrected for the spontaneous LDH production. The threshold level of cytotoxicity was set at 20%, given that, according to ISO 10993-5, the percentage of cell viability considered acceptable is above 80%. Cytokine exposure was cytotoxic only for CDMs derived from HCB43, consistent with previous results showing severe damage to barrier integrity.

Fig. 24 shows the changes in cellular metabolic activity of CDMs exposed to the combination of TNF-α and IFN-γ. CDMs in the absence of cytokines were used as control (100% metabolic activity). Except for CDMs obtained from HCB43, there was no significant impact of cytokine exposure on cellular metabolic activity and, consequently, on cell viability, which goes in line with the results obtained for cytotoxicity (LDH release) and barrier damage (TEER and FITC-D4 Papp).

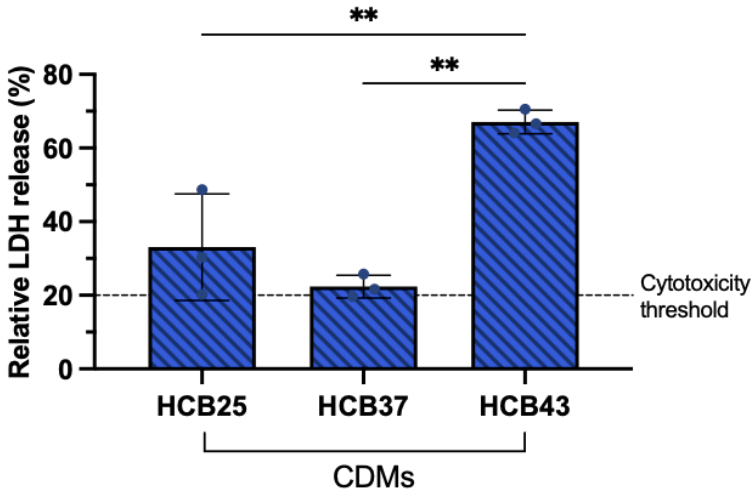

Figure 23. Lactate dehydrogenase (LDH) release (%) of colonoid-derived monolayers (CDMs) when exposed to 25 ng·mL^{-1} TNF-α and 25 ng·mL^{-1} IFN-γ, for 24h. Values obtained in the absence of cytokines were used as a baseline while 100% represents the LDH release after cell lysis. The cytotoxic threshold was set at 20%. Values are reported as mean ± standard deviation. The Shapiro-Wilk test was used to verify if the data followed a normal distribution. *p* values were determined using one-way analysis of variance (ANOVA) followed by Tukey's multiple comparison post-test (**$p \leq 0.01$). HCB: human colonic biopsies.

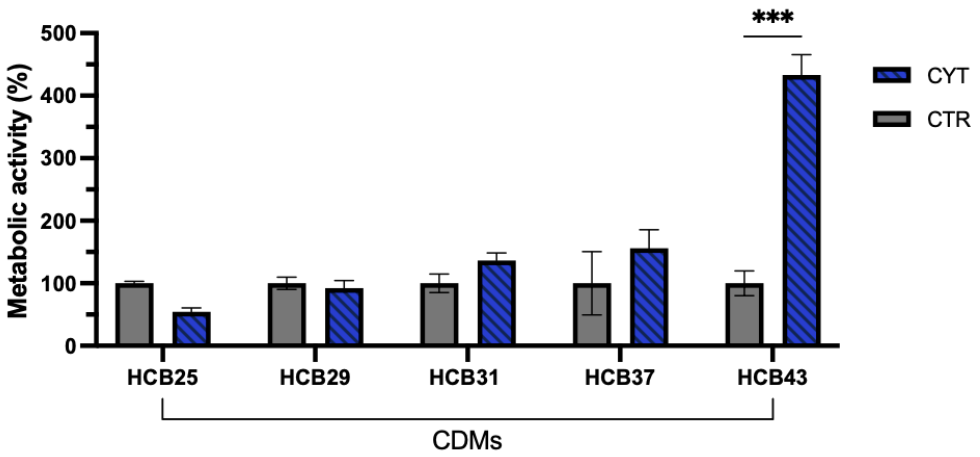

Figure 24. **Cellular metabolic activity** (%) of colonoid-derived monolayers (CDMs) exposed to vehicle (CTR) or to 25 ng·mL^{-1} TNF-α and 25 ng·mL^{-1} IFN-γ, for 24h (CYT). Values are reported as mean ± standard deviation. The Shapiro-Wilk test was used to verify if the data followed a normal distribution. *p* values were determined using two-way analysis of variance (ANOVA) followed by Sídák's multiple comparison post-test (***$p \leq 0.001$). HCB: human colonic biopsies.

III.3.4. NF-κB p65 activation

The IκB kinase/NF-κB signalling pathway plays a critical role in the pathogenesis of several inflammatory disease, including IBD. The NF-κB family of transcription factors consists of five members: p65/RelA, c-Rel and RelB, and the p50 and p52 proteins. In unstimulated cells, NF-κB subunits are restricted to the cytoplasm. Upon activation, the IκB kinase phosphorylates IκB proteins, leading to their ubiquitination and subsequent proteasomal degradation. This process releases NF-κB dimers to accumulate in the nucleus and initiate gene transcription. The canonical NF-κB pathway, primarily induced by pro-inflammatory cytokine receptors and pattern recognition receptors, allows nuclear translocation of p50, p65 and c-Rel containing dimers. These dimers then activate the transcription of pro-inflammatory genes[104]. This signalling pathway can be activated by multiple inflammatory stimuli, including free radicals, ultraviolet irradiation, TNF, IL-1β, or pathogen-associated molecular patterns[105].

Fig. 25 shows the fold change in phosphorylated NF-κB p65 levels after 24 hours of exposure to cytokines. The levels of the dimer tend to increase, but not significantly, probably due to the late time point. The quantification of NF-κB p65 should have been done immediately after the stimulus, probably 6 hours or less after exposure[106].

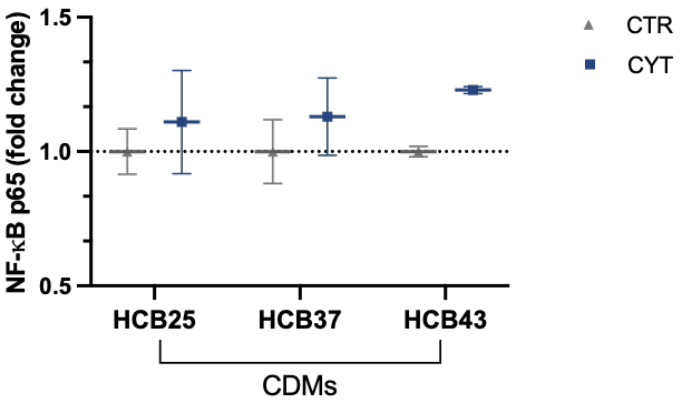

Figure 25. NF-κB p65 levels of colonoid-derived monolayers (CDMs) in the absence (CTR) and in the presence of 25 ng·mL^{-1} TNF-α and 25 ng·mL^{-1} IFN-γ, for 24h (CYT). Values are reported as mean ± standard deviation. The Shapiro-Wilk test was used to verify if the data followed a normal distribution. *p* values were determined using two-way analysis of variance (ANOVA) followed by Sídák's multiple comparison post-test. HCB: human colonic biopsies.

III.3.5. Cytokine and chemokine secretion

Not only does the intestinal epithelium respond to cytokines produced by immune cells, but it is also a rich source of its own cytokines and chemokines, which could in turn attenuate or promote inflammation[107].

IL-6 is an inflammatory cytokine and its expression by intestinal epithelial cells has been shown to be induced by TNF-α[108]. However, IL-6 was not detected in the samples collected from the basolateral side of CDMs exposed to TNF-α and IFN-γ for 24 hours.

IL-8 and C-C motif chemokine ligand CCL20, chemoattractant cytokines secreted by intestinal epithelial cells in response to inflammatory stimuli, are key players involved in immune cell trafficking. Specifically, IL-8 recruits neutrophils, Th2 and Treg, while CCL20 recruits Th17 cells and dendritic cells. These chemokines can therefore promote the migration of immune cells into the inflamed mucosa, contributing in the immune system activation. The levels of human IL-8 (**Fig. 26A**) and CCL20 (**Fig. 26B**) secreted into the basolateral side increased significantly after cytokine exposure. Under control conditions, chemokine levels were close to nil, except for CDMs obtained from HCB25 (4.94 ± 1.09 ng·mL^{-1} for IL-8 and 0.34 ± 0.09 ng·mL^{-1} for CCL20). Notably, there was no strict correlation between the level of epithelial barrier damage and chemokine production, in the sense that there was a significant increase even when the barrier integrity was not significantly impaired (as in the case of CDMs obtained from HCB31, whose TEER values were not markedly modified by inflammation, but IL-8 levels clearly augmented). Additionally, there were remarkable differences between the levels released by the CDMs obtained from different patients, confirming the ability of CDMs to mimic *in vitro* the heterogeneous responses of various subjects.

Reports in the literature are quite inconsistent: IL-8 mRNA was overexpressed by colonoids after exposure to 10 ng·mL^{-1} IL-1β, IL-6 and TNF-α for 7 days[49], while, in contrast, colonoid-derived monolayers exposed to 25 ng·mL^{-1} TNF-α and IFN-γ, an experimental set-up similar to the one used here, showed no IL-8 mRNA overexpression after 48 hours[54].

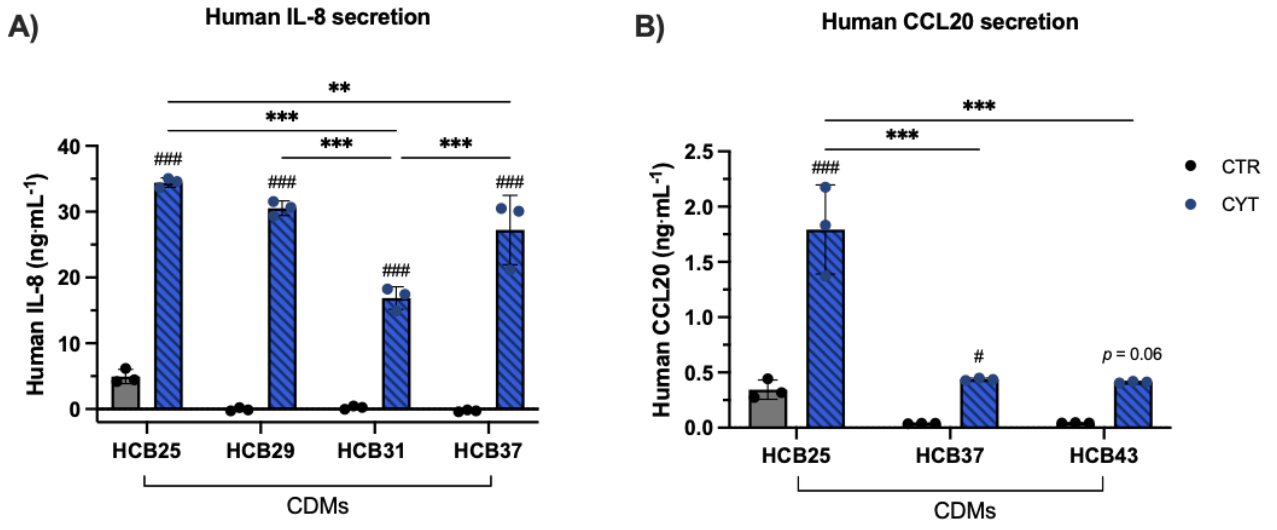

Figure 26. Secretion of human (A) IL-8 and **(B) CCL20** by colonoid-derived monolayers (CDMs) after 24h exposure to vehicle (CTR) or to 25 ng·mL^{-1} TNF-α and 25 ng·mL^{-1} IFN-γ, for 24h (CYT). Values are reported as mean ± standard deviation. The Shapiro-Wilk test was used to verify if the data followed a normal distribution. *p* values were determined using two-way analysis of variance (ANOVA) followed by Tukey's multiple comparison post-test for the comparison between patients (**$p \leq 0.01$; ***$p \leq 0.001$), and by Sídák's multiple comparison post-test for the comparison between CTR and CYT ($^{\#}p \leq 0.05$; $^{\#\#\#}p \leq 0.001$). HCB: human colonic biopsies.

Human colonoids derived from healthy tissue and treated with 0.1 μg·mL^{-1} TNF alone or with 20 μg·mL^{-1} Poly(I:C) for 24 hours showed an overexpression of CCL20 mRNA. Furthermore, there was a significant increase in CCL20 secretion compared to untreated colonoids (3.16 ± 2.96 ng·mL^{-1} for untreated *vs* 63.60 ± 32.79 ng·mL^{-1} for TNF *vs* 49.15 ± 29.16 ng·mL^{-1} for TNF+Poly(I:C)). Notably, the authors also highlighted considerable inter-individual variations in the response of colonoids, including variations in CCL20 expression[109].

III.3.6. Drug permeability studies

Transepithelial transport of reference compounds across CDMs exposed to TNF-α and IFN-γ was assessed from the apical to basolateral direction (A→B) (**Fig. 27**). The compounds selected were endowed with different permeability values and spanned several Biopharmaceutics Classification System (BCS) classes. Propranolol is a BCS class I compound commonly used as a high permeability standard. Atenolol, on the other hand, is a BCS class III compound used as a low/moderate permeability standard[110]. Budesonide, a BCS class II compound, is a glucocorticoid currently used in the treatment of Crohn's disease and ulcerative colitis[111]. Celecoxib, another BCS class II, is a non-steroidal anti-inflammatory drug (NSAID) that selectively inhibits cyclooxygenase-2 (COX-2)[112].

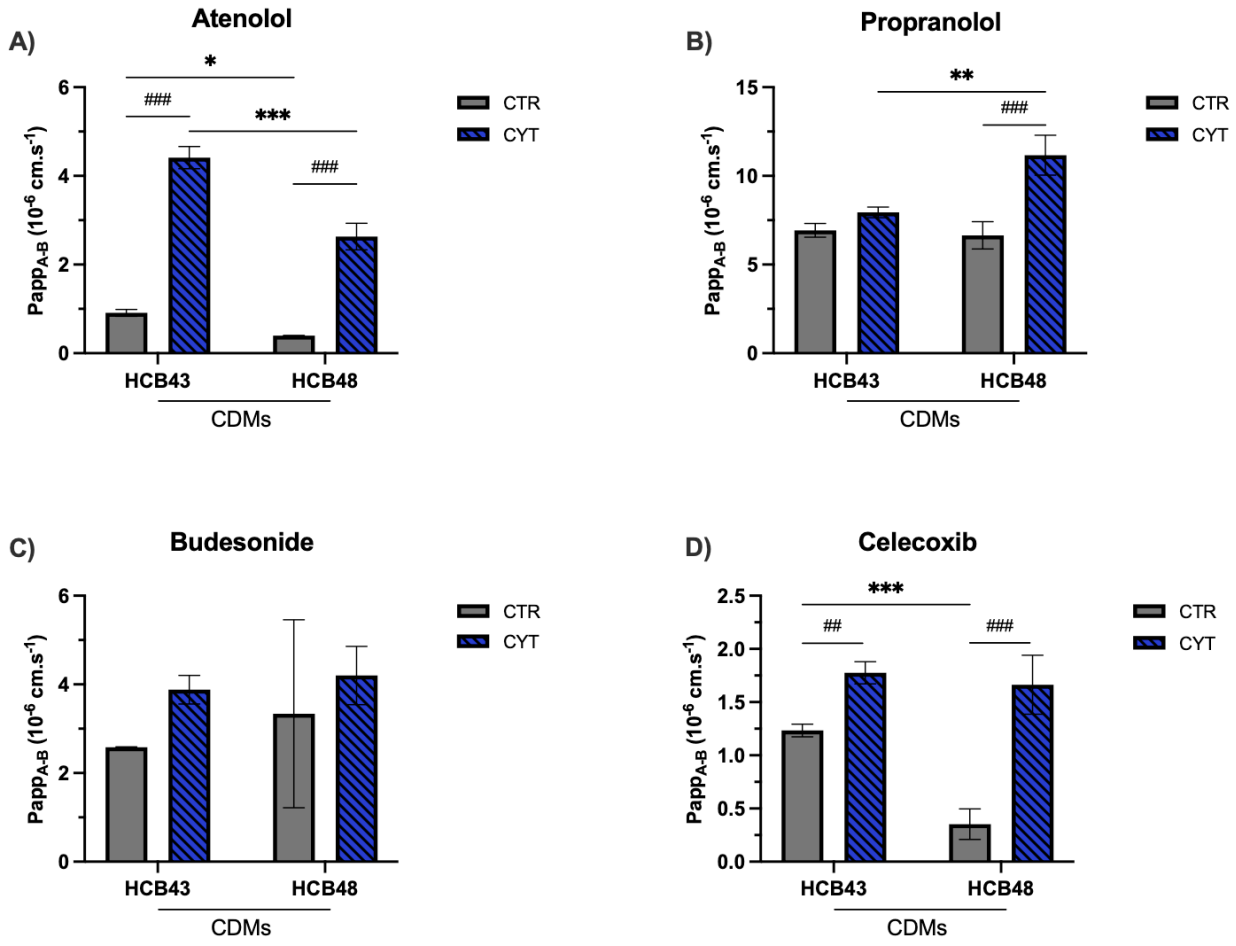

Figure 27. Transepithelial transport of (A) atenolol, (B) propranolol, (C) budesonide and (D) celecoxib across colonoid-derived monolayers (CDMs) exposed to vehicle (CTR) or to 25 ng·mL^{-1} TNF-α and 25 ng·mL^{-1} IFN-γ for 24h (CYT). Apparent permeability (Papp) was determined from the apical to the basolateral direction (A→B). Results are reported as mean ± standard deviation. The Shapiro-Wilk test was used to verify if the data followed a normal distribution. *p* values were determined by means of two-way analysis of variance (ANOVA) followed by Sídák's multiple comparison post-test ((*$p \leq 0.05$; **,##$p \leq 0.01$; ***,###$p \leq 0.001$). HCB: human colonic biopsies.

Papp values determined under control conditions for both propranolol and atenolol were in line with values reported in the literature for duodenal-derived monolayers[113].

Inflammatory conditions damage the integrity of the mucosal barrier, as previously demonstrated in section III.3.2. This could affect drug transport, especially for low permeable compounds. In our study, the transport of atenolol increased significantly under inflamed conditions. Papp values increased 5-fold for CDMs derived from HCB43 and 7-fold for HCB48 (p<0.001), confirming that paracellular transepithelial transport of this molecule was strongly affected by cytokine exposure (**Fig. 27A**).

The transport of propranolol was not affected by cytokine exposure in HCB43 (**Fig. 27B**). Nevertheless, HCB48 Papp values increased significantly when compared to control conditions (p<0.001), although this was a 2-fold increase.

After cytokine exposure, budesonide's Papp values were not significantly different compared to the control condition, as expected for a high permeable compound (**Fig. 27C**).

Despite being considered a high permeable compound, Papp values of celecoxib showed a significant increase under inflammatory conditions, irrespective of the donor (**Fig. 27D**). Celecoxib is a lipophilic compound that exhibits a propensity to become entrapped within cell membranes or accumulate intracellularly[114]. In our study, the recovery of celecoxib was remarkably low, approximately 20%, impacting the determination of Papp values, possibly due to its intracellular accumulation.

Notably, there was also a significant inter-variability between Papp values obtained from CDMs of different patients.

III.4. Transepithelial transport across colonoid-derived monolayers exposed to IFN-γ

In this section, the work performed during the secondment at Johnson & Johnson Innovative Medicine (Beerse, Belgium) will be discussed. Human colonoids provided by HUB organoids (Utrecht, Nederland) and derived from two different colonic regions (ascending and sigmoid colon), each one obtained from a different patient, as reported in **Table 2**, were used to assess the impact of inflammation, represented in this case by IFN-γ exposure, on drug transepithelial transport. Colonoids were enzymatically and mechanically dissociated into single cells between passages 12 and 17 and seeded at 3.57 x 10^5 cells·cm^{-2} on Matrigel®-coated 96-well inserts. The epithelial barrier integrity was monitored by TEER measurements (**Fig. 28**).

After 15 days in culture, TEER values reached 1006.01 ± 99.33 Ω·cm^2 in CDMs derived from the ascending colon (**Fig. 28A**), and 648.95 ± 71.87 Ω·cm^2 in CDMs derived from the sigmoid colon (**Fig. 28B**). The TEER values were consistent with those reported in literature[55,64,94]. **Fig. 28C** shows that exposure of CDMs to 25 ng·mL^{-1} IFN-γ impaired significantly the barrier integrity for the ascending colon (1006.01 ± 99.03 Ω·cm^2 *vs* 898.18 ± 82,61 Ω·cm^2, p < 0.01, Student's t-test), whereas no relevant changes were induced in the sigmoid colon (648.95 ± 71.87 Ω·cm^2 vs 666.03 ± 64.69 Ω·cm^2).

Using the established CDMs setup, the effect of IFN-γ exposure was assessed and the transepithelial transport of reference compounds was determined. Similar to the previous study, propranolol and atenolol were selected, respectively, as high and low permeability compounds, while cimetidine was selected as low permeability molecule, digoxin was chosen as a substrate of P-gp efflux, and mannitol was used as a leakage marker.

Unlike the combination of TNF-α and IFN-γ exposure to IFN-γ alone did not result in severe barrier damage. This finding is consistent with the results described by Jelinsky *et al*.,2021 which reported only a mild, dose-dependent effect of IFN-γ on TEER loss [55].

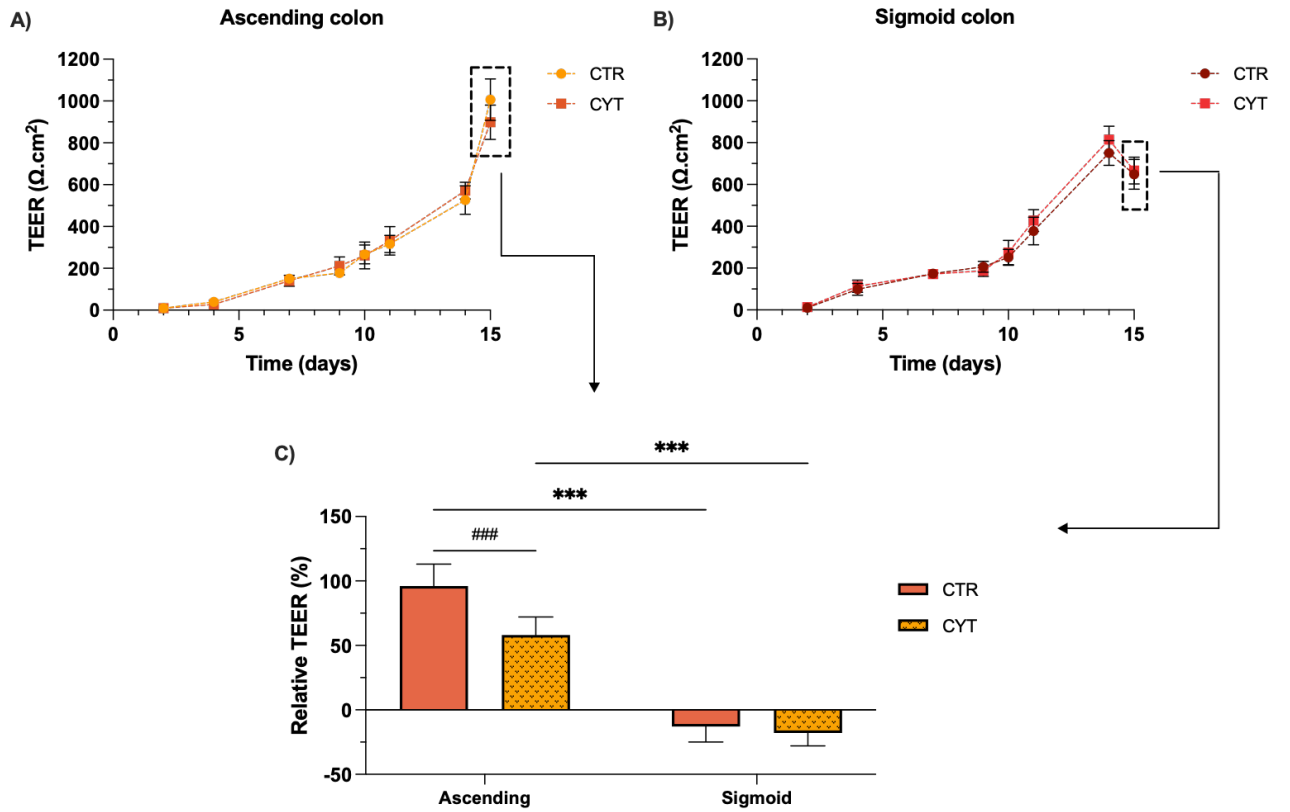

Figure 28. Transepithelial electrical resistance (TEER) **of colonoid-derived monolayers** (CDMs) **throughout growth and 24h after exposure to 25 ng·mL^{-1} IFN-γ**. Monolayers were derived from commercial organoid lines of the ascending colon (A) and sigmoid colon (B). C) TEER values relative (%) to the timepoint 0h. Results are reported as mean ± standard deviation. The Shapiro-Wilk test was used to verify if the data followed a normal distribution. *p* values were determined using a two-tailed Student's t-test (***$p \leq 0.001$).

It is well known that intestinal epithelial injury caused by IFN-γ exposure is often enhanced by its synergistic interaction with TNF-α [115]. The distinct responses observed in the two different experimental setups in this work support this hypothesis and suggest that TNF-α plays a predominant role in damaging barrier integrity. Recently, it has been reported that TNF-α synergises with IFN-γ in a dose-dependent manner to induce caspase-8-JAK1/2-STAT1 dependent death of intestinal epithelial cells. This effect was confirmed in both human colonic cell lines and primary organoids[115].

Mannitol Papp values (< 2x10^{-6} cm.s^{-1}) indicated that monolayers were not leaky, as shown in **Fig. 29A**[80]. Propranolol, atenolol, digoxin, and cimetidine Papp values under control conditions were in line with those reported in the literature for duodenal-derived monolayers[113]. **Figure 29** shows that IFN-γ exposure had no significant effect on drug transport across colonoid-derived monolayers, confirming that, in the absence of TNF-α, IFN-γ alone does not really affect the continuity of the intestinal barrier. Papp values obtained for digoxin in the presence of elacridar 5 μM (a P-gp inhibitor) were significantly higher than those obtained in its absence, both under control and inflammatory conditions. This suggests that the P-gp efflux pump is likely to be expressed and functional in CDMs. However, the determination of efflux ratios is necessary to confirm this hypothesis.

Interestingly, monolayers derived from different colonic regions showed very similar results, comparable to those reported in the literature for duodenal-derived monolayers[113]. Compared to the previously described setup and the results in section III.3.6 (**Fig. 27**), the Papp values for propranolol and atenolol are slightly lower.

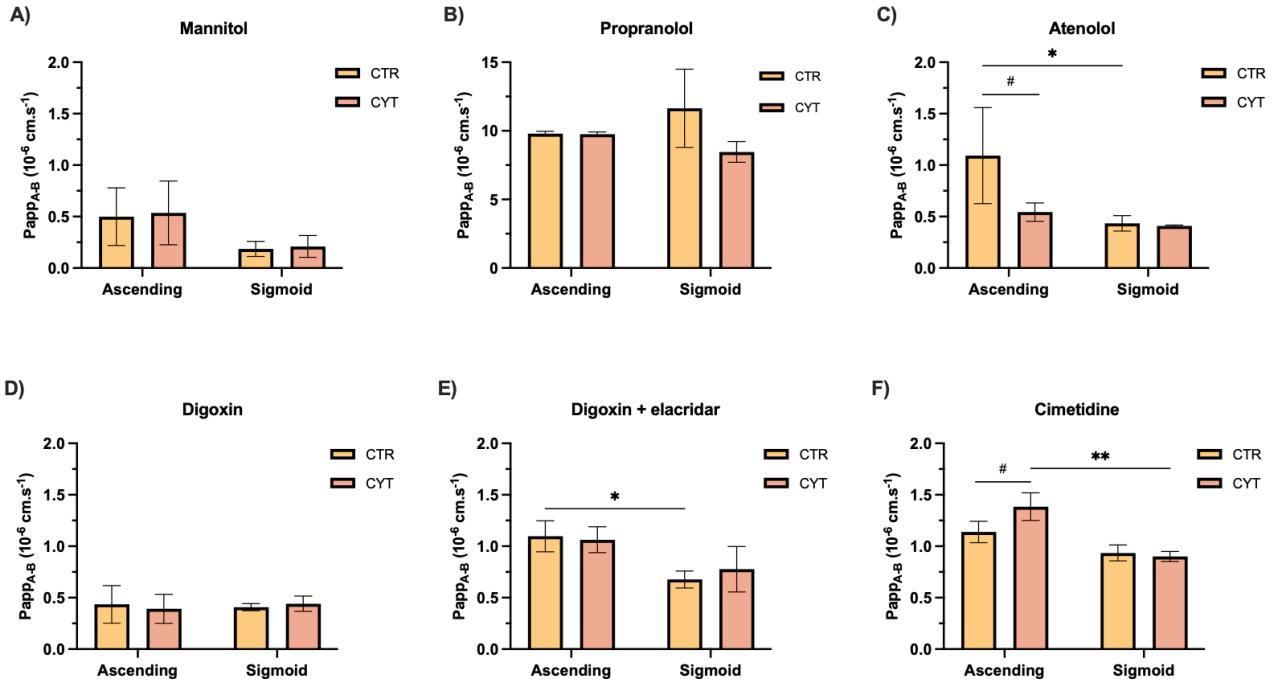

Figure 29. Transepithelial transport of (B) **propranolol,** (C) **atenolol,** (D, E) **digoxin, and** (F) **cimetidine across colonoid-derived monolayers** (CDMs) **from the ascending and sigmoid colon treated with 25 ng·mL^{-1} IFN-γ** for 24h (CYT). Vehicle-treated CDMs were used as controls (CTR). Apparent permeability (Papp) was determined from the apical to basolateral direction. (D) 5 μM elacridar was used as a P-gp inhibitor. (A) Mannitol was used as a leakage marker. Results are reported as mean ± standard deviation. The Shapiro-Wilk test was used to verify if the data followed a normal distribution. *p* values were determined using a using two-way analysis of variance (ANOVA) with Sídák's multiple comparison test (*,#$p \leq 0.05$; **$p \leq 0.01$).

CHAPTER IV. CONCLUSIONS AND FUTURE PERSPECTIVES

Over the years, the importance of *in vitro* models as a tool to further comprehend the onset of IBD has been demonstrated. Several models with varying cell sources and complexity have been used according to the needs of specific research questions, as extensively discussed elsewhere.

Organoid-based models, often derived from patient samples, offer the potential for a deeper understanding of human pathologies. The physiological relevance of PDOs depends on their ability to replicate the changes observed in primary tissues from diseased patients when cultured *in vitro*. However, somewhat conflicting results have emerged regarding PDOs derived from IBD patients. Some studies have shown that PDOs retain the transcriptional signature of primary inflamed tissue, with altered gene expression related to secretory and absorptive functions[47,116]. Other studies have shown that inflammation negatively affects the expansion rate of IBD organoids[48,51,52,117,118], and over a period of approximately four weeks in culture, they appear to lose their transcriptional inflammatory phenotype[53]. For this reason, human colonoid cultures were established from biopsies of non-IBD patients and inflammation was later induced. Colonoid-derived monolayers were then used with the end goal of conducting drug transepithelial transport studies.

This study successfully established colonoid-derived monolayers from various donors, demonstrating the feasibility of using these models for investigating epithelial barrier functions and inflammatory responses. The findings reveal significant variability in growth profiles among the monolayers derived from different individuals, underscoring the influence of genetic diversity on intestinal epithelial behaviour.

Upon exposure to TNF-α and IFN-γ, CDMs displayed heterogeneous responses that were critical in understanding the dynamics of IBD at the cellular level. Key observations included compromised epithelial barrier integrity and notable changes in cell morphology. Specifically, there was a decrease in mucus and villin production, alongside evidence of chromosome condensation and cellular damage. These morphological changes suggest a profound disruption of the epithelial structure and function, which is crucial in the pathogenesis of IBD. Furthermore, the inflammatory stimuli led to an increased secretion of IL-8 and CCL20, chemoattractant agents that *in vivo* would enhance immune cell recruitment. The upregulation of NF-κB p65 and increased FITC-D4 permeability when the epithelial damage was severe further supported that the inflammatory cascade was activated, and that the barrier integrity was damaged. This was corroborated by the significantly increased paracellular transepithelial transport, as evidenced by the increase of Papp of atenolol. These results indicate not only a breakdown in the physical barrier but also an alteration in the transport properties of the epithelium, which are crucial for its protective function.

IFN-γ alone was not sufficient to induce inflammatory conditions and changes in drug transport across colonoid-derived monolayers. Additionally, monolayers derived from different colonic regions showed very similar results, comparable to those reported in the literature for duodenal-derived monolayers.

The variation in responses to cytokine exposure and the subsequent effects on barrier integrity and cellular function highlight the complexity of IBD and the need for personalized approaches in its treatment. The insights gained from this study not only advance our understanding of the cellular mechanisms underpinning IBD but also reinforce the potential of colonoid-derived monolayers as a valuable model for further research into the disease's pathobiology and for testing therapeutic interventions.

The model developed has a considerable potential for future research and applications. One of the immediate next steps could be to conduct further transepithelial transport studies with a variety of compounds, ranging from those with low to high permeability. These studies would aim to establish robust *in vitro-in vivo* correlations to assess the relevance and predictive power of this model compared to those currently in use.

Extending the scope of the model to include colonoid cultures derived from both inflamed and non-inflamed tissue of IBD patients could provide valuable comparative insights. Such an approach would allow a direct evaluation of the model's applicability in representing the pathology of IBD, thereby enhancing its utility in disease-specific research.

Additionally, incorporating immune cells as an alternative inflammatory stimulus offers another avenue for advancing the model. By co-culturing colonoids with immune cells and inducing inflammation through this interaction, we could better simulate the complex immune-epithelial crosstalk inherent in IBD. Comparing these inflammatory responses with those observed in the current model could lead to the development of a more sophisticated and relevant system, potentially improving our understanding of IBD mechanisms and aiding in the discovery of targeted treatments.

Overall, the continued refinement and diversification of this colonoid-based model promises to provide deeper insight into epithelial biology and disease, facilitating the development of more effective therapeutic strategies for IBD and related disorders.

REFERENCES

1. Allaire, J. M. *et al.* The Intestinal Epithelium: Central Coordinator of Mucosal Immunity. *Trends Immunol* **39**, 677–696 (2018).

2. Peterson, L. W. & Artis, D. Intestinal epithelial cells: Regulators of barrier function and immune homeostasis. *Nat Rev Immunol* **14**, 141–153 (2014).

3. Delacour, D., Salomon, J., Robine, S. & Louvard, D. Plasticity of the brush border — the yin and yang of intestinal homeostasis. *Nature Reviews Gastroenterology & Hepatology 2016 13:3* **13**, 161–174 (2016).

4. Cani, P. D. *et al.* Microbial regulation of organismal energy homeostasis. *Nat Metab* **1**, 34–46 (2019).

5. Nicholson, J. K. *et al.* Host-gut microbiota metabolic interactions. *Science (1979)* **336**, 1262–1267 (2012).

6. Schroeder, B. O. Fight them or feed them: how the intestinal mucus layer manages the gut microbiota. *Gastroenterol Rep (Oxf)* **7**, 3–12 (2019).

7. Bonis, V., Rossell, C. & Gehart, H. The Intestinal Epithelium – Fluid Fate and Rigid Structure From Crypt Bottom to Villus Tip. *Front Cell Dev Biol* **9**, 661931 (2021).

8. Beumer, J. & Clevers, H. Cell fate specification and differentiation in the adult mammalian intestine. *Nature Reviews Molecular Cell Biology 2020 22:1* **22**, 39–53 (2020).

9. Gehart, H. & Clevers, H. Tales from the crypt: new insights into intestinal stem cells. *Nature Reviews Gastroenterology & Hepatology 2018 16:1* **16**, 19–34 (2018).

10. Baulies, A., Angelis, N. & Li, V. S. W. Hallmarks of intestinal stem cells. *Development (Cambridge)* **147**, (2020).

11. Barker, N. *et al.* Identification of stem cells in small intestine and colon by marker gene Lgr5. *Nature* **449**, 1003–1008 (2007).

12. Sato, T. *et al.* Single Lgr5 stem cells build crypt – villus structures in vitro without a mesenchymal niche. *Nature* **459**, 262–266 (2009).

13. Sato, T. & Clevers, H. Growing self-organizing mini-guts from a single intestinal stem cell: Mechanism and applications. *Science (1979)* **340**, 1190–1194 (2013).

14. Valatas, V., Kitamura, K., Ward, S. G. & Kolios, G. Editorial: Stromal and immune cell interactions in intestinal inflammation and fibrosis. *Front Immunol* **14**, 1152140 (2023).

15. Sun, H., Tan, J., Chen, H., Wu, N. & Su, B. Immune niches orchestrated by intestinal mesenchymal stromal cells lining the crypt-villus. *Front Immunol* **13**, 1057932 (2022).

16. Chang, J. T. Pathophysiology of Inflammatory Bowel Diseases. *New England Journal of Medicine* **383**, 2652–2664 (2020).

17. Baumgart, D. C. & Sandborn, W. J. Inflammatory bowel disease: clinical aspects and established and evolving therapies. *The Lancet* **369**, 1641–1657 (2007).

18. Kaplan, G. G. The global burden of IBD: From 2015 to 2025. *Nat Rev Gastroenterol Hepatol* **12**, 720–727 (2015).

19. Zhao, M., Gönczi, L., Lakatos, P. L. & Burisch, J. The Burden of Inflammatory Bowel Disease in Europe in 2020. *J Crohns Colitis* **15**, 1573–1587 (2021).

20. Blumenstein, I. & Sonnenberg, E. Sex- and gender-related differences in inflammatory bowel diseases. *Frontiers in Gastroenterology* **2**, 1199687 (2023).

21. Kaplan, G. G. & Windsor, J. W. The four epidemiological stages in the global evolution of inflammatory bowel disease. *Nature Reviews Gastroenterology & Hepatology 2020 18:1* **18**, 56–66 (2020).

22. Baumgart, D. C. & Carding, S. R. Inflammatory bowel disease: cause and immunobiology. *The Lancet* **369**, 1627–1640 (2007).

23. Lu, Y., Li, X., Liu, S., Zhang, Y. & Zhang, D. Toll-like receptors and inflammatory bowel disease. *Front Immunol* **9**, 326971 (2018).

24. Choo, J., Glisovic, N. & Vignjevic, D. M. Gut homeostasis at a glance. *J Cell Sci* **135**, (2022).

25. Friedrich, M., Pohin, M. & Powrie, F. Cytokine Networks in the Pathophysiology of Inflammatory Bowel Disease. *Immunity* **50**, 992–1006 (2019).

26. Choy, M. C., Visvanathan, K. & De Cruz, P. An Overview of the Innate and Adaptive Immune System in Inflammatory Bowel Disease. *Inflamm Bowel Dis* **23**, 2–13 (2017).

27. Magro, F. *et al.* ECCO Position on Harmonisation of Crohn's Disease Mucosal Histopathology. *J Crohns Colitis* **16**, 876–883 (2022).

28. Magro, F. *et al.* ECCO Position Paper: Harmonization of the Approach to Ulcerative Colitis Histopathology. *J Crohns Colitis* **14**, 1503–1511 (2020).

29. Schnur, S. *et al.* Inflammatory bowel disease addressed by Caco-2 and monocyte-derived macrophages: an opportunity for an in vitro drug screening assay. *In vitro models 2022 1:4* **1**, 365–383 (2022).

30. Veloso, P. M., Machado, R. & Nobre, C. Mesalazine and inflammatory bowel disease – From well-established therapies to progress beyond the state of the art. *European Journal of Pharmaceutics and Biopharmaceutics* **167**, 89–103 (2021).

31. Dorrington, A. M. *et al.* The Historical Role and Contemporary Use of Corticosteroids in Inflammatory Bowel Disease. *J Crohns Colitis* **14**, 1316–1329 (2020).

32. Neurath, M. F. Current and emerging therapeutic targets for IBD. *Nature Reviews Gastroenterology & Hepatology 2017 14:5* **14**, 269–278 (2017).

33. Neurath, M. F. Targeting immune cell circuits and trafficking in inflammatory bowel disease. *Nature Immunology 2019 20:8* **20**, 970–979 (2019).

34. Pizarro, T. T. *et al.* Challenges in IBD Research: Preclinical Human IBD Mechanisms. *Inflamm Bowel Dis* **25**, S5–S12 (2019).

35. Martini, E., Krug, S. M., Siegmund, B., Neurath, M. F. & Becker, C. Mend Your Fences: The Epithelial Barrier and its Relationship With Mucosal Immunity in Inflammatory Bowel Disease. *Cell Mol Gastroenterol Hepatol* **4**, 33–46 (2017).

36. Joshi, A., Soni, A. & Acharya, S. In vitro models and ex vivo systems used in inflammatory bowel disease. *In vitro models 2022 1:3* **1**, 213–227 (2022).

37. Macedo, M. H., Dias Neto, M., Pastrana, L., Gonçalves, C. & Xavier, M. Recent Advances in Cell-Based In Vitro Models to Recreate Human Intestinal Inflammation. *Advanced Science* **10**, 2301391 (2023).

38. Zhao, Z. *et al.* Organoids. *Nature Reviews Methods Primers 2022 2:1* **2**, 1–21 (2022).

39. Park, C. S., Nguyen, L. P. & Yong, D. Development of Colonic Organoids Containing Enteric Nerves or Blood Vessels from Human Embryonic Stem Cells. *Cells 2020, Vol. 9, Page 2209* **9**, 2209 (2020).

40. Workman, M. J. *et al.* Engineered human pluripotent-stem-cell-derived intestinal tissues with a functional enteric nervous system. *Nature Medicine 2016 23:1* **23**, 49–59 (2016).

41. Palikuqi, B. *et al.* Adaptable haemodynamic endothelial cells for organogenesis and tumorigenesis. *Nature 2020 585:7825* **585**, 426–432 (2020).

42. Takahashi, Y. *et al.* Reciprocal Inflammatory Signaling Between Intestinal Epithelial Cells and Adipocytes in the Absence of Immune Cells. *EBioMedicine* **23**, 34–45 (2017).

43. Rahmani, S., Breyner, N. M., Su, H. M., Verdu, E. F. & Didar, T. F. Intestinal organoids: A new paradigm for engineering intestinal epithelium in vitro. *Biomaterials* vol. 194 195–214 Preprint at https://doi.org/10.1016/j.biomaterials.2018.12.006 (2019).

44. European Parliament. *Regulation (EU) 2016/679 of the European Parliament and of the Council of 27 April 2016 on the Protection of Natural Persons with Regard to the Processing of Personal Data and on the Free Movement of Such Data, and Repealing Directive 95/46/EC (General Data Protection Regulation)*. (2016).

45. European Parliament. Directive 2004/23/EC of the European Parliament and of the Council of 31 March 2004 on setting standards of quality and safety for the donation, procurement, testing, processing, preservation, storage and distribution of human tissues and cells. https://eur-lex.europa.eu/eli/dir/2004/23/oj/eng (2004).

46. European Parliament. New EU rules on substances of human origin. https://health.ec.europa.eu/blood-tissues-cells-and-organs/overview/new-eu-rules-substances-human-origin_en (2024).

47. Noben, M. *et al.* Epithelial organoid cultures from patients with ulcerative colitis and Crohn's disease: a truly long-term model to study the molecular basis for inflammatory bowel disease? *Gut* **66**, 2193–2195 (2017).

48. Dotti, I., Mayorgas, A. & Salas, A. Generation of human colon organoids from healthy and inflammatory bowel disease mucosa. *PLoS One* **17**, (2022).

49. d'Aldebert, E. *et al.* Characterization of Human Colon Organoids From Inflammatory Bowel Disease Patients. *Front Cell Dev Biol* **8**, (2020).

50. Singh, V. *et al.* Chronic Inflammation in Ulcerative Colitis Causes Long-Term Changes in Goblet Cell Function. *CMGH* **13**, 219–232 (2022).

51. Kelsen, J. R. *et al.* Colonoids From Patients With Pediatric Inflammatory Bowel Disease Exhibit Decreased Growth Associated With Inflammation Severity and Durable Upregulation of Antigen Presentation Genes. *Inflamm Bowel Dis* **27**, 256–267 (2021).

52. Meir, M. *et al.* Enteroids Generated from Patients with Severe Inflammation in Crohn's Disease Maintain Alterations of Junctional Proteins. *J Crohns Colitis* **14**, 1473–1487 (2020).

53. Arnauts, K. *et al.* Ex Vivo Mimicking of Inflammation in Organoids Derived From Patients With Ulcerative Colitis. *Gastroenterology* **159**, 1564–1567 (2020).

54. Vancamelbeke, M. *et al.* Butyrate Does Not Protect Against Inflammation-induced Loss of Epithelial Barrier Function and Cytokine Production in Primary Cell Monolayers From Patients With Ulcerative Colitis. *J Crohns Colitis* **13**, 1351–1361 (2019).

55. Jelinsky, S. A. *et al.* Molecular and Functional Characterization of Human Intestinal Organoids and Monolayers for Modeling Epithelial Barrier. *Inflamm Bowel Dis* **29**, 195–206 (2023).

56. Lee, C. *et al.* TNFα Induces LGR5+ Stem Cell Dysfunction In Patients With Crohn's Disease. *Cell Mol Gastroenterol Hepatol* **13**, 789–808 (2022).

57. Co, J. Y. *et al.* Controlling Epithelial Polarity: A Human Enteroid Model for Host-Pathogen Interactions. *Cell Rep* **26**, 2509-2520.e4 (2019).

58. Onozato, D. *et al.* Application of Human Induced Pluripotent Stem Cell-Derived Intestinal Organoids as a Model of Epithelial Damage and Fibrosis in Inflammatory Bowel Disease. *Biol Pharm Bull* **43**, 1088–1095 (2020).

59. Sayoc-Becerra, A. *et al.* The JAK-Inhibitor Tofacitinib Rescues Human Intestinal Epithelial Cells and Colonoids from Cytokine-Induced Barrier Dysfunction. *Inflamm Bowel Dis* **26**, 407–422 (2020).

60. Hosic, S. *et al.* Cholinergic Activation of Primary Human Derived Intestinal Epithelium Does Not Ameliorate TNF-α Induced Injury. *Cell Mol Bioeng* **13**, 487–505 (2020).

61. Singhal, R. & Shah, Y. M. Oxygen battle in the gut: Hypoxia and hypoxia-inducible factors in metabolic and inflammatory responses in the intestine. *Journal of Biological Chemistry* **295**, 10493–10505 (2020).

62. Skovdahl, H. K. *et al.* Patient Derived Colonoids as Drug Testing Platforms–Critical Importance of Oxygen Concentration. *Front Pharmacol* **12**, 679741 (2021).

63. Deleu, S. *et al.* High Acetate Concentration Protects Intestinal Barrier and Exerts Anti-Inflammatory Effects in Organoid-Derived Epithelial Monolayer Cultures from Patients with Ulcerative Colitis. *International Journal of Molecular Sciences 2023, Vol. 24, Page 768* **24**, 768 (2023).

64. Varani, J. *et al.* A multi-mineral intervention to counter pro-inflammatory activity and to improve the barrier in human colon organoids. *Front Cell Dev Biol* **11**, 1132905 (2023).

65. Xu, P., Elizalde, M., Masclee, A., Pierik, M. & Jonkers, D. Corticosteroid enhances epithelial barrier function in intestinal organoids derived from patients with Crohn's disease. *J Mol Med* **99**, 805–815 (2021).

66. Lee, C. *et al.* Intestinal Epithelial Responses to IL-17 in Adult Stem Cell-derived Human Intestinal Organoids. *J Crohns Colitis* **16**, 1911–1923 (2022).

67. Jose, S. S. *et al.* Comparison of two human organoid models of lung and intestinal inflammation reveals Toll-like receptor signalling activation and monocyte recruitment. *Clin Transl Immunology* **9**, e1131 (2020).

68. Roh, T. T., Chen, Y., Paul, H. T., Guo, C. & Kaplan, D. L. 3D bioengineered tissue model of the large intestine to study inflammatory bowel disease. *Biomaterials* **225**, (2019).

69. Noel, G. *et al.* A primary human macrophage-enteroid co-culture model to investigate mucosal gut physiology and host-pathogen interactions. *Sci Rep* **7**, (2017).

70. Karve, S. S., Pradhan, S., Ward, D. V. & Weiss, A. A. Intestinal organoids model human responses to infection by commensal and Shiga toxin producing Escherichia coli. *PLoS One* **12**, e0178966 (2017).

71. Lemme-Dumit, J. M. *et al.* Altered Gut Microbiome and Fecal Immune Phenotype in Early Preterm Infants With Leaky Gut. *Front Immunol* **13**, 815046 (2022).

72. Staab, J. F., Lemme-Dumit, J. M., Latanich, R., Pasetti, M. F. & Zachos, N. C. Co-Culture System of Human Enteroids/Colonoids with Innate Immune Cells. *Curr Protoc Immunol* **131**, (2020).

73. Jowett, G. M. *et al.* Organoids capture tissue-specific innate lymphoid cell development in mice and humans. *Cell Rep* **40**, (2022).

74. Hammoudi, N. *et al.* Autologous organoid co-culture model reveals T cell-driven epithelial cell death in Crohn's Disease. *Front Immunol* **13**, (2022).

75. Angus, H. C. K. *et al.* An autologous colonic organoid-derived monolayer model to study immune: bacterial interactions in Crohn's disease patients. *Clin Transl Immunology* **11**, e1407 (2022).

76. Ihara, S. *et al.* Adhesive Interactions between Mononuclear Phagocytes and Intestinal Epithelium Perturb Normal Epithelial Differentiation and Serve as a Therapeutic Target in Inflammatory Bowel Disease. *J Crohns Colitis* **12**, 1219–1231 (2018).

77. Hubatsch, I., Ragnarsson, E. G. E. & Artursson, P. Determination of drug permeability and prediction of drug absorption in Caco-2 monolayers. *Nat Protoc* **2**, 2111–2119 (2007).

78. Riss, T., Niles, A., Moravec, R., Karassina, N. & Vidugiriene, J. Cytotoxicity Assays: In Vitro Methods to Measure Dead Cells. in *Assay Guidance Manual* (Eli Lilly & Company and the National Center for Advancing Translational Sciences, 2019).

79. Van Meerloo, J., Kaspers, G. J. L. & Cloos, J. Cell Sensitivity Assays: The MTT Assay. in *Cancer Cell Culture: Methods and Protocols* vol. 731 237–245 (Springer, 2011).

80. Hubatsch, I., Ragnarsson, E. G. E. & Artursson, P. Determination of drug permeability and prediction of drug absorption in Caco-2 monolayers. *Nature Protocols 2007 2:9* **2**, 2111–2119 (2007).

81. Kim, J., Koo, B. K. & Knoblich, J. A. Human organoids: model systems for human biology and medicine. *Nature Reviews Molecular Cell Biology* **21**, 571–584 (2020).

82. Costa, J. & Ahluwalia, A. Advances and Current Challenges in Intestinal in vitro Model Engineering: A Digest. *Front Bioeng Biotechnol* **7**, (2019).

83. Li, M. & Izpisua Belmonte, J. C. Organoids - Preclinical Models of Human Disease. *New England Journal of Medicine* **380**, 569–579 (2019).

84. Pleguezuelos-Manzano, C. *et al.* Establishment and Culture of Human Intestinal Organoids Derived from Adult Stem Cells. *Curr Protoc Immunol* **130**, e106 (2020).

85. Holmberg, F. E. *et al.* Culturing human intestinal stem cells for regenerative applications in the treatment of inflammatory bowel disease. *EMBO Mol Med* **9**, 558–570 (2017).

86. Clinton, J. & McWilliams-Koeppen, P. Initiation, Expansion, and Cryopreservation of Human Primary Tissue-Derived Normal and Diseased Organoids in Embedded Three-Dimensional Culture. *Curr Protoc Cell Biol* **82**, (2019).

87. Co, J. Y., Margalef-Català, M., Monack, D. M. & Amieva, M. R. Controlling the polarity of human gastrointestinal organoids to investigate epithelial biology and infectious diseases. *Nat Protoc* **16**, 5171–5192 (2021).

88. Hirokawa, Y. *et al.* Low-viscosity matrix suspension culture enables scalable analysis of patient-derived organoids and tumoroids from the large intestine. *Communications Biology* **4**, 1–17 (2021).

89. Edgar, R. D. *et al.* Culture-Associated DNA Methylation Changes Impact on Cellular Function of Human Intestinal Organoids. *CMGH* **14**, 1295–1310 (2022).

90. Zhao, Z. *et al.* Organoids. *Nature Reviews Methods Primers* **2**, 1–21 (2022).

91. Williamson, I. A. *et al.* A High-Throughput Organoid Microinjection Platform to Study Gastrointestinal Microbiota and Luminal Physiology. *Cell Mol Gastroenterol Hepatol* **6**, 301–319 (2018).

92. Sabapaty, A., Lin, P. Y. & Dunn, J. C. Y. Effect of air–liquid interface on cultured human intestinal epithelial cells. *FASEB Bioadv* **6**, 41–52 (2024).

93. Srinivasan, B. *et al.* TEER Measurement Techniques for In Vitro Barrier Model Systems. *SLAS Technol* **20**, 107–126 (2015).

94. Nickerson, K. P. *et al.* A Versatile Human Intestinal Organoid-Derived Epithelial Monolayer Model for the Study of Enteric Pathogens. *Microbiol Spectr* **9**, (2021).

95. Fleischer, D. Biological Transport Phenomena in the Gastrointestinal Tract: Cellular Mechanisms. in *Transport Processes in Pharmaceutical Systems* 163–200 (CRC Press, 1999).

96. Neurath, M. F. Cytokines in inflammatory bowel disease. *Nat Rev Immunol* **14**, 329–342 (2014).

97. Roh, T. T., Chen, Y., Rudolph, S., Gee, M. & Kaplan, D. L. In Vitro Models of Intestine Innate Immunity. *Trends Biotechnol* **39**, 274–285 (2021).

98. Hosic, S. *et al.* Cholinergic Activation of Primary Human Derived Intestinal Epithelium Does Not Ameliorate TNF-α Induced Injury. *Cell Mol Bioeng* **13**, 487–505 (2020).

99. Wallace, J. W., Constant, D. A. & Nice, T. J. Interferon Lambda in the Pathogenesis of Inflammatory Bowel Diseases. *Front Immunol* **12**, 767505 (2021).

100. Atreya, R., Neurath, M. F. & Siegmund, B. Personalizing Treatment in IBD: Hype or Reality in 2020? Can We Predict Response to Anti-TNF? *Front Med (Lausanne)* **7**, 575231 (2020).

101. Haep, L. *et al.* Interferon Gamma Counteracts the Angiogenic Switch and Induces Vascular Permeability in Dextran Sulfate Sodium Colitis in Mice. *Inflamm Bowel Dis* **21**, 2360–2371 (2015).

102. Athman, R., Louvard, D. & Robine, S. The epithelial cell cytoskeleton and intracellular trafficking III. How is villin involved in the actin cytoskeleton dynamics in intestinal cells? *Am J Physiol Gastrointest Liver Physiol* **283**, (2002).

103. MUC2 - Mucin-2 - Homo sapiens (Human) . *UniProt* https://www.uniprot.org/uniprotkb/Q02817/entry.

104. Wullaert, A., Bonnet, M. C. & Pasparakis, M. NF-κB in the regulation of epithelial homeostasis and inflammation. *Cell Research 2011 21:1* **21**, 146–158 (2010).

105. Gilmore, T. D. Introduction to NF-κB: players, pathways, perspectives. *Oncogene 2006 25:51* **25**, 6680–6684 (2006).

106. Meier-Soelch, J. *et al.* Monitoring the Levels of Cellular NF-κB Activation States. *Cancers (Basel)* **13**, (2021).

107. Andrews, C., McLean, M. H. & Durum, S. K. Cytokine tuning of intestinal epithelial function. *Front Immunol* **9**, 368738 (2018).

108. Sitaraman, S. V. *et al.* Neutrophil-epithelial crosstalk at the intestinal lumenal surface mediated by reciprocal secretion of adenosine and IL-6. *Journal of Clinical Investigation* **107**, 861–869 (2001).

109. Gopalakrishnan, S. *et al.* Comprehensive protocols for culturing and molecular biological analysis of IBD patient-derived colon epithelial organoids. *Front Immunol* **14**, 1097383 (2023).

110. Fredlund, L., Winiwarter, S. & Hilgendorf, C. In Vitro Intrinsic Permeability: A Transporter-Independent Measure of Caco-2 Cell Permeability in Drug Design and Development. *Mol Pharm* **14**, 1601–1609 (2017).

111. Budesonide: Uses, Interactions, Mechanism of Action | DrugBank Online. https://go.drugbank.com/drugs/DB01222.

112. Celecoxib: Uses, Interactions, Mechanism of Action | DrugBank Online. https://go.drugbank.com/drugs/DB00482.

113. Kourula, S. *et al.* Intestinal organoids as an in vitro platform to characterize disposition, metabolism, and safety profile of small molecules. *Eur J Pharm Sci* **188**, 106481 (2023).

114. Maier, T. J. *et al.* Cellular membranes function as a storage compartment for celecoxib. *J Mol Med (Berl)* **87**, 981–993 (2009).

115. Woznicki, J. A. *et al.* TNF-α synergises with IFN-γ to induce caspase-8-JAK1/2-STAT1-dependent death of intestinal epithelial cells. *Cell Death & Disease 2021 12:10* **12**, 1–15 (2021).

116. Dotti, I. *et al.* Alterations in the epithelial stem cell compartment could contribute to permanent changes in the mucosa of patients with ulcerative colitis. *Gut* **66**, 2069–2079 (2017).

117. d'Aldebert, E. *et al.* Characterization of Human Colon Organoids From Inflammatory Bowel Disease Patients. *Front Cell Dev Biol* **8**, (2020).

118. Singh, V. *et al.* Chronic Inflammation in Ulcerative Colitis Causes Long-Term Changes in Goblet Cell Function. *Cell Mol Gastroenterol Hepatol* **13**, 219–232 (2022).

SUPPLEMENTARY DATA

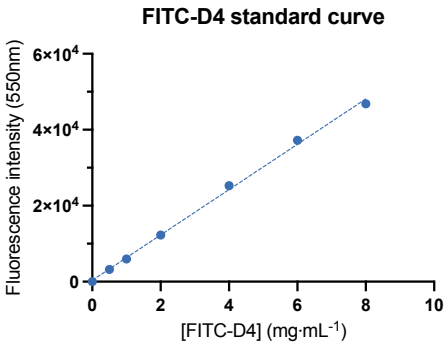

Supplementary Figure 1. Example of a fluorescein isothiocyanate-dextran 4 kDa (**FITC-D4**) **standard curve** obtained by the quantification of FITC-D4 standards in the range of 0 – 8 mg·mL^{-1}. The fluorescence intensity at 550nm for each standard was plotted against its respective concentration of FITC-D4. The results were fitted into a simple linear regression (R^2 = 0.998) to obtain the equation Fluorescence intensity (550nm) = 5970 [FITC-D4] (mg·mL^{-1}) + 351.

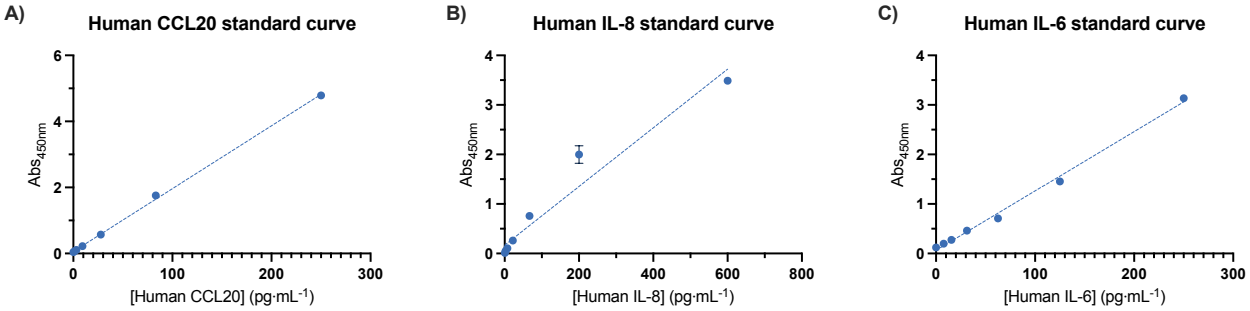

Supplementary Figure 2. Cytokine standard curves obtained by the quantification of human CCL20, human IL-8 and human IL-6 standards. The absorbance at 450 nm was plotted against the respective standard concentration (pg·mL^{-1}). The results were fitted into a simple linear regression to obtain the following equations: **A)** Abs_{450nm} = 0.019 [Human CCL20] (pg·mL^{-1}) +0.061 (R^2 = 0.999). **B)** Abs_{450nm} = 0.006 [Human IL-8] (pg·mL^{-1}) +0.168 (R^2 = 0.946). **C)** Abs_{450nm} = 0.012 [Human IL-6] (pg·mL^{-1}) +0.066 (R^2 = 0.995).

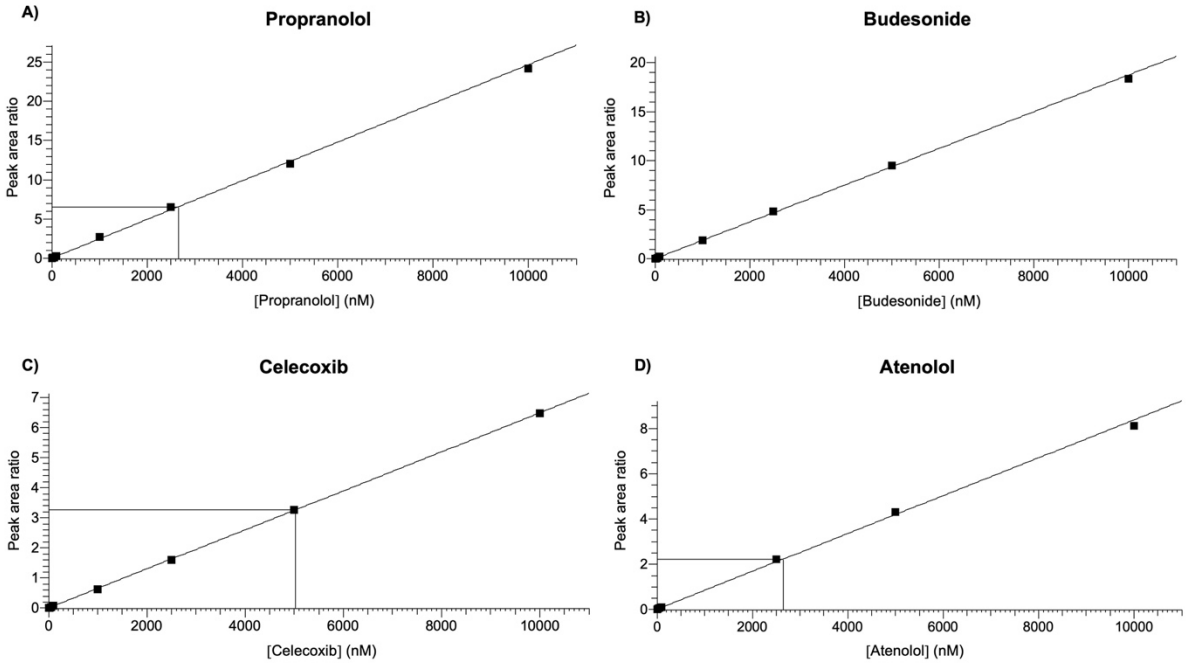

Supplementary Figure 3. Calibration curves of the compounds used in the transepithelial transport studies. Peak area ratios between the peak areas of calibration standards at different concentrations and the peak areas of internal standard are reported as a function of compound concentration in the 10000-10 nM range. **A)** Peak area ratio = 0.0025 [Propranolol] (nM) + 0.0365 (R^2 = 0.9982). **B)** Peak area ratio = 0.0019 [Budesonide] (nM) + 0.0113 (R^2 = 0.9992). **C)** Peak area ratio = 0.0006 [Celecoxib] (nM) + 0.0073 (R^2 = 0.9990). **D)** Peak area ratio = 0.0008 [Atenolol] (nM) + 0.0168 (R^2 = 0.9984).

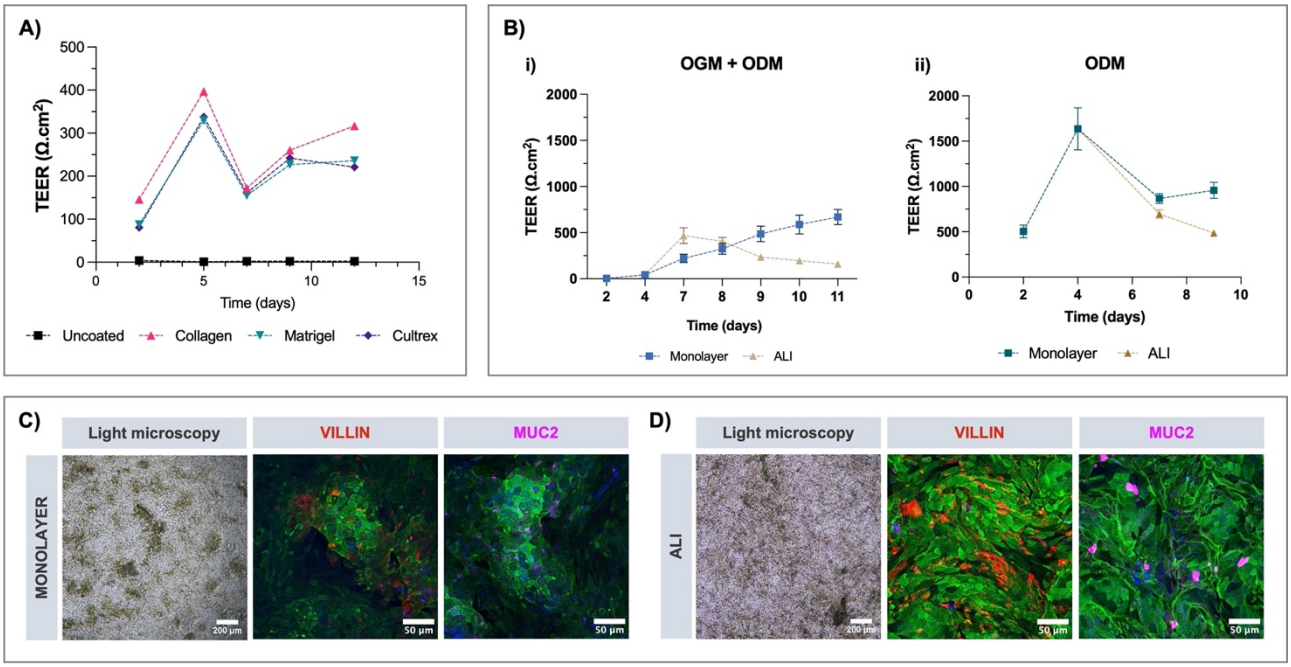

Supplementary Figure 4. Establishment of human colonoid-derived monolayers (CDMs) – **optimization of culture conditions.** A) Transepithelial electrical resistance (TEER) values of CDMs grown on inserts coated with collagen 10 µg·cm^{-2}, Matrigel® (1:50) or Cultrex™ (1:50). Uncoated inserts were used as control. B) TEER values of CDMs cultured in i) IntestiCult™ organoid growth medium (OGM) switching to organoid differentiation medium (ODM) upon confluence or ii) IntestiCult™ ODM only. Light microscopy and confocal microscopy images of CDMs cultured with media on the apical side (monolayer) (C) or without media on the apical side (air-liquid interface - ALI) (D). Cells were stained for F-actin (Phalloidin, green) and the nucleus (DAPI, blue). Microvilli were marked with anti-Villin (red). Goblet cells and mucus were stained with anti-MUC2 (magenta). CDMs obtained from human colonic biopsies #25 (HCB25).

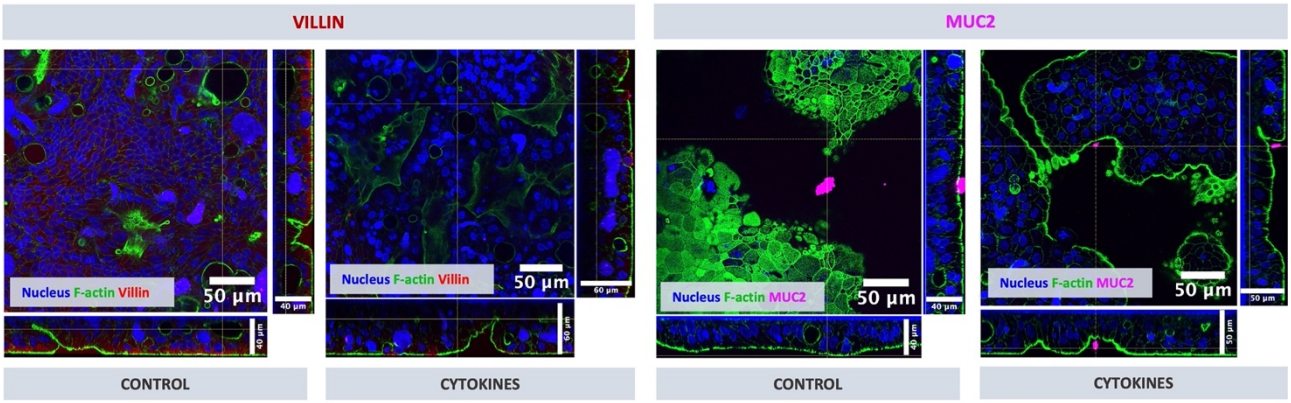

Supplementary Figure 5. Confocal microscopy images of human colonoid-derived monolayers (CDMs) **in the absence** (control) **and presence of 25 ng·mL^{-1} TNF-α and 25 ng·mL^{-1} IFN-γ** (cytokines) on the apical and basolateral sides for 24h. Cells were stained for F-actin (Phalloidin, green) and the nucleus (DAPI, blue). Microvilli were marked with anti-Villin (red). Goblet cells and mucus were stained with anti-MUC2 (magenta). CDMs obtained from human colonic biopsies #37 (HCB37).

ACKNOWLEDGEMENTS

The last three years have been an amazing journey shared with many people to whom I would like to express my deepest gratitude.

First, I would like to thank my supervisor, Professor Simona Bertoni, who trusted me with this project and supported me throughout these years. There have been many times when I have doubted, but her unwavering confidence has kept me going.

I would like to thank Professor Elisabetta Barocelli for welcoming me into her laboratory with open arms.

I am also grateful to all the members of the EU H2020 MSCA-ITN COLOTAN project for the opportunity to learn and work alongside great minds. In particular, I would like to acknowledge my fellow ESRs for sharing this adventure with me in good times and bad. Zeynep, Allen, Theo, Lea, Katha, Sebastian, Bekkah, Marco, Sydney, Alessia, Harshad, Pedro and Denny: thank you for all the incredible memories.

This project would not have been accomplished without the help of the master's students I had the privilege to supervise. Nicola, Gloria and Linda: thank you for your contribution to this work, but most importantly, thank you for the companionship. I would also like to thank my colleagues in the lab for their support when things got discouraging and for all the fun moments we shared. Among them, Francesca and Linda, you have truly welcomed me as one of your own and for that I cherish you.

On a more personal note, a very special word goes to my parents, who saw their youngest daughter move to another country in the hope that she would fulfil her dream and find a better life: to you I owe everything. I would also like to thank my family and friends back home for being my anchor and for encouraging me over the years. To my nephews Martim and Afonso, I hope I have proved to you that dreams do come true. So, dream big!

The last word, as always, goes to my life partner, my fiancé Pedro. I really could not have done this without you. I cannot thank you enough.

A todos, um muito obrigada!

This work has been carried out at the Department of Food and Drug of the University of Parma. This project has received funding from the European Union's Horizon 2020 research and innovation programme under the Marie Skłodowska-Curie Grant Agreement No. 956851.